TU Delft

QuTech
Wehner Group

MASTER THESIS

Applied Physics

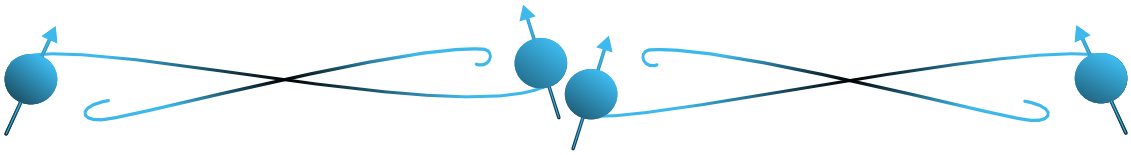

Genetic algorithm-based optimisation of entanglement distribution to minimise hardware cost

Adrià Labay Mora

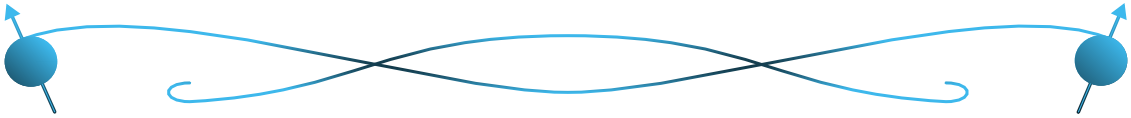

Daily Supervisor
Francisco Horta Ferreira da Silva

Supervisor
Stephanie Wehner

Year
2020/21

To my colleagues,

hitchhikers in this transitory madness

Abstract

Distribution of high-quality entanglement over long distances is a key step for the development of a future quantum internet. Exponential photon loss related to distance in optical fibres makes it impractical to connect two nodes directly. Furthermore, the impossibility of copying general quantum states forbids using the same solutions as in classical communication. Quantum repeaters can be used to extend entanglement to longer distances using teleportation; nonetheless, straightforward application still leads to an exponential decrease in the link quality. Entanglement purification probabilistically allow us to obtain few high-quality links from many low-quality ones. Several protocols combining quantum repeaters with purification have been proposed. However, the hardware quality is still lacking. Moreover, it is unclear how an improvement over a certain hardware parameter affects the final link quality or entanglement generation rate. Analytical expressions are hard to find and usually assumptions are needed, limiting their applicability. In this work, a realistic repeater chain is modelled using NetSquid, a discrete-event based quantum network simulator. A genetic algorithm-based optimisation methodology is then applied to determine what entanglement distribution protocol allows for minimal improvement over current hardware, and what these improvements must be in order to achieve a target link quality and distribution rate. In this thesis, we aim to make the path towards scalable quantum repeaters clearer, as well as understand how entanglement purification can enable this goal. We conclude that quantum repeaters are necessary to connect distances larger than 200 km. We also find that entanglement purification enables achieving target metrics with lower hardware cost when the internode distance is ≈ 100 km, where a balance is found between a low rate for longer separations and a too demanding hardware for shorter ones. Finally, we analyse the growth of the hardware cost with the distance showing that, with the best choice of protocols, it scales linearly. We believe that these results constitute a valuable stepping stone towards a blueprint for a pan-European quantum internet.

Resum

La distribució d'enllaços entrellaçats d'alta qualitat per a distàncies llargues representa un punt clau en el desenvolupament d'un futur internet Quàntic. El nombre de fotons que es perden en fibres òptiques augmenta exponencialment amb la distància i fa impracticable la connexió directa. A més, la impossibilitat de copiar informació quàntica prohibeix l'ús de les mateixes solucions que en comunicació clàssica. Les cadenes de repetidors quàntics es poden emprar per a estendre l'entrellaçament en aquestes distàncies mitjançant la teleportació quàntica; tot i això, la seva aplicació directa encara produeix una disminució exponencial en la qualitat de l'enllaç. Els protocols per a la purificació d'entrellaçament permeten generar probabilísticament uns pocs enllaços de gran qualitat a partir de molts d'altres de poca. Diversos mètodes han estat proposats combinant repetidors quàntics amb intervals de purificació, en qualsevol cas, els medis materials necessaris encara no han estat realitzats. A més, no es coneix com afecta una millora en un cert paràmetre experimental a la qualitat final o la freqüència de generació de l'enllaç. L'estudi analític de casos generals resulta difícil, normalment es requereix d'assumpcions que limiten la seva aplicabilitat. En aquest treball, una cadena de repetidors quàntics serà modelada amb el simulador de xarxes quàntiques Netsquid. Utilitzarem algorismes genètics per determinar quin protocol de distribució d'entrellaçament permet una millora mínima sobre el maquinari actual, i quines han de ser aquestes millores per tal d'aconseguir la qualitat d'enllaç i la taxa d'entrellaçament desitjada. L'objectiu final és fer el camí cap a uns repetidors quàntics escalables més clar, així com entendre en quina mesura la purificació d'entrellaçament pot ajudar-hi. Concloem que els repetidors quàntics són necessaris per a connectar distàncies superiors a 200 km. També, trobem que els protocols de purificació permeten assolir les metes proposades a un menor cost quan la distància entre nodes és ≈ 100 km, on es troba un equilibri entre una baixa taxa de generació per a separacions més llargues i un maquinari massa exigent per a més curtes. Finalment, analitzem el creixement del cost total del maquinari amb la distància, demostrant que, amb la millor elecció de protocols, aquest creix linealment. Creiem que aquests resultats constitueixen un valuós pas endavant cap a un internet quàntic a escala continental.

Acknowledgements

> Al cantar me suelo olvidar de todos los malos momentos; convertir en virtud defectos.
> Desterrar la vulgaridad aunque sólo sea un momento y sentir que no estamos muertos.
>
> — Platero y Tu, *Al cantar*

This thesis is the result of seven pandemic months of work. During this time, I have been connected with many people, and I would like to express my deepest gratitude to all of them.

First and foremost, thanks to my supervisor Prof. Stephanie Wehner, for giving me the opportunity to work in this project and for her comments and suggestions to improve the thesis.

Secondly, my thankfulness to my daily supervisor Francisco, for his initial interest in me and for all the discussions that we have had during all these months. Your feedback has been crucial to arrive at this point and I would like to wish you all the best with your PhD.

Together with Francisco, there is the great NL blueprint team formed by Ariana, David, Guus and Tim to whom I also thank their interest and willingness to help whenever I needed.

Next, my gratitude to all my colleagues, to whom I dedicate this thesis, for giving the support and distraction during all these months, sharing multidisciplinary talks and methods that certainly made us push forward and learn from each other. I wish you have enjoyed everything I shared, and thanks for reacting so well, this was motivating at some point. But specially, thanks for notifying me when the SLURM jobs finished, I wish those mails did not collapse your inbox.

During this pandemic situation, it was difficult to keep focus on writing the thesis with all the chaos going on all over the world. Being that the least of the problems, music was the safeguard to abstract me from this world that we have made and probably deserve. Hours and hours at home, alone, with my hands on the keyboard, and a white page in front waiting for inspiration to write a single sentence, have gone by peaceably with those songs.

In the end, not only was the thesis written, but enhanced thanks to the feedback and corrections received from Anna. Besides, thanks to Mercè for revising the Catalan version of the abstract.

Also, I would like to say that all of it wouldn't have been possible if it wasn't for the open source journals and websites which provide an extended database of open access scientific papers. But specially, to those altruistic scientist who publish their work for free making it available for a larger audience.

Finally, my thankfulness to my mother who designed the cover and has always been there and supported me.

ᚨᚱᛗ

Notation

We will try to use the common notation in quantum information theory, and concretely, the same as in Nielsen and Chuang [2000].

$\|\psi\rangle$	State vector or "ket" labelled by ψ
$\langle\psi\|$	Dual vector or "bra", the conjugate transpose of $\|\psi\rangle$
$\langle\psi\|\phi\rangle$	Inner product or "braket"
$\|\psi\rangle\langle\phi\|$	Outer product or "dyad"
$\mathcal{H}_n$	n-dimensional Hilbert space
ρ	Density matrix
$\otimes$	Tensor product or Kronecker product
$\rho^{\otimes n}$	Kronecker product of n times the state ρ
$A, B, \Pi, ...$	Matrix
$\mathbb{I}_n$	$n \times n$ identity matrix
$\boldsymbol{\sigma} = (\sigma_1, \sigma_2, \sigma_3)$	Vector of Pauli matrices
$A \geq 0$	A is a positive semi-definite matrix
$\|\bullet\|_1$	Trace-norm
$\|\bullet\|_2$	Euclidean norm
$\operatorname{tr} A$	Trace of A
$\hat{P}, \hat{\Pi}$	Projector, $\hat{P}^2 = \hat{P}$
$\mathscr{H}_n$	Space of $n \times n$ hermitian matrices
$\mathscr{B}$	Set with the four Bell states, basis of $\mathcal{H}_2^{\otimes 2}$
$\mathcal{E}(\rho)$	Trace preserving quantum operation on the state ρ
$\mathcal{M}$	Generalised measure
$\mathbb{P}[X = x \mid y]$	Conditional probability of finding x given y
$\mathbb{E}[X]$	Expectation value of the variable X
$\{0,1\}^n$	Space of all possible binary numbers between 0 and $2^n - 1$

Also, for the hardware parameters, we will label as $p_\alpha \in [0, 1]$ the probability that the property or operation α fails, being $p_\alpha = 0$ the perfect value. On the other hand, the symbol $\eta_\beta \in [0, 1]$ will be used to denote the efficiency of the parameter β, the probability that β succeeds, with $\eta_\beta = 1$ being the perfect value.

Glossary

BD Bell Diagonal.

CPTP Completely Positive Trace Preserving.

DC Double-Click.

EP Entanglement Purification.

EPL Extreme Photon Loss.

ES Entanglement Swap.

GA Genetic Algorithm.

LOCC Local Operations and Classical Communication.

MHEG Middle-Heralded Entanglement Generation.

NISQ Noisy Intermediate-Scale Quantum.

POVM Positive Operator Valued Measure.

QC Quantum Computer.

QEC Quantum Error Correction.

QI Quantum Internet.

QKD Quantum Key Distribution.

QM Quantum Mechanics.

QMem Quantum Memory.

QR Quantum Repeater.

SC Single-Click.

ZPL Zero Phonon Line.

Contents

1 Introduction

> Experimental science was born. But experiment is a tool. The aim remains: to understand the world. To restrict quantum mechanics to be exclusively about piddling laboratory operations is to betray the great enterprise. A serious formulation will not exclude the big world outside the laboratory.
>
> — John S. Bell, *Against Measurement*

Quantum Mechanics (QM) is squeezed into 5 mathematical postulates (e.g. see Nielsen and Chuang [2000]) that have far-reaching consequences. From these postulates, the scientific community has been able to move forward with the development of a new field in physics: quantum information. Many topics that are encountered in classical computation and communication have been brought to the quantum regime like cloning, factoring or key distribution, while new ones like teleportation or entanglement have been created. "There is a feeling that the advent of quantum information theory heralds a new way of doing physics and supports the view that information should play a more central role in our world picture" says Fuchs [2002]. This is certainly a reality. For instance, the European Union set a flagship for the next 10 years in 2016 to investigate the development of quantum technologies like quantum sensing and quantum computing.

In the context of this flagship, a Quantum Internet (QI) – an extension of the actual internet, a set of interconnected quantum devices capable of sending and storing information by using QM properties – is being developed. It aims to be more secure than the current Internet with protocols for Quantum Key Distribution (QKD) that ensure private communication between two parties [Shor and Preskill, 2000]. Other applications include secure access to remote quantum computers, more accurate clock synchronization, scientific applications such as combining light from distant telescopes to improve observations [Sidhu et al., 2021], and distributed quantum computation [Cirac et al., 1999].

Far from being simple, the QI introduces technical and intellectual difficulties due to the very nature of QM and the devices used, which fall into the category of Noisy Intermediate-Scale Quantum (NISQ) technology. The reliable transmission of a qubit – a single unit of quantum information – between distant nodes is one of the most challenging tasks. On the one hand, optical fibres suffer from photon loss increasing exponentially with distance [Ekert and Bouwmeester, 2000]. The classical solution consists of placing intermediate stations which amplify the information by encoding a single bit into multiple photons by copying its state. Unfortunately, cloning a qubit is not possible [Wootters and Zurek, 1982], so new techniques have to be found to overcome photon loss. On the other hand, even if cloning was possible, dividing the total length in arbitrary small parts may also be disadvantageous as current quantum devices realise imperfect operations increasing the total error [Briegel et al., 1998]. Moreover, the generation of these links is probabilistic, reducing the rate at which they can be realised [Barrett and Kok, 2005; Campbell and Benjamin, 2008].

A first step towards the connection of distant devices has been the development of Quantum Repeaters (QRs), devices which can, in theory, repeat quantum information faithfully [Munro et al., 2015]. Progress is being made, both experimentally and theoretically, by improving the technology and optimising connection and transmission protocols. Even so, whether a certain protocol is the

best one for a given situation depends on hardware quality and network topology, and it is not known in general.

Another drawback is that analytical solutions are in general hard to find, forcing the use of numerical techniques for more general and realistic results. Previous work along these lines has been done by da Silva et al. [2020] using NetSquid [Coopmans et al., 2020] – a software tool capable of simulating all aspects of the quantum network stack, from software to hardware specific models. There, a linear chain of N repeaters – a one dimensional quantum network – was optimised so that both end nodes share a link of sufficient quality with the least improvement over the currently available hardware. Yet, the noise introduced by NISQ devices reduces the quality of the link exponentially with the number of repeating stations.

The major contributions of this thesis are:

- The modelling of an abstract repeater chain to simplify the analysis while allowing the mapping from different physical realisations. Thus, we will **identify the working regime of the model and give a concrete mapping for one implementation**.
- The exploration of Middle-Heralded Entanglement Generation (MHEG) protocols together with Entanglement Purification (EP) protocols which, under certain conditions, can increase the quality of the links [Dür and Briegel, 2007]. Hence, we will **study the benefits and drawbacks of each protocol to understand the situations in which their use is advantageous over the others**.
- The study of the results obtained using a Genetic Algorithm (GA) together with a local search method. These, allowing us to **find a solution to the problem of what the best protocols to reduce the improvement over state-of-the-art devices are**. This is a novel approach as common techniques involve optimising over either the protocols or the hardware, separately leaving the other fixed.

Outline This work is structured as to guide the reader from the basic elements of the quantum mechanical theory to the final results acquired.

To approach this, chapter 2 introduces the required knowledge about QM and quantum information needed in follow-up chapters. General information about quantum states and measurements is given in section 2.1, which continues in section 2.2, with several measures of distinguishability between quantum states. Then, the proof of the no-cloning theorem is reproduced in section 2.3 to understand the motivation behind QRs. Finally, section 2.4 gives a brief explanation on the operations that will help us model the NISQ devices.

The next chapter 3 is devoted to the hardware and software that constitutes a quantum repeater chain. A deeper motivation for the use of QRs is given in section 3.1 and the protocol that overcomes the no-cloning restriction in section 3.2. Then, section 3.3 looks into the abstract hardware model which will be used to emulate a realistic QR chain. The following sections 3.4 and 3.5 explain two protocols that can be used to generate links between neighbouring repeaters in the former, and two protocols that can increase the quality of such links in the latter. All these protocols constitute the building blocks of the repeater chain and are put together into two network protocols in section 3.6.

Chapter 4 gives the details about the numerical simulations and the optimisation tasks. It is divided into three sections that explain the actual implementation of the aforesaid protocols (section 4.1), the characteristics of the optimisation algorithm (section 4.2), and the method used to optimise the repeater chain parameters (section 4.3).

The dissertation continues with the results obtained running the previous model. First of all, a sensitivity analysis is done in section 5.1 to validate the abstract model against a hardware specific model. Then, the solutions to the minimisation tasks are given for two different strategies in sections 5.2 and 5.3. In the end, section 5.4 presents the optimal results that allow the connection of two end nodes at a certain distance with least improvement over current hardware.

The thesis concludes in chapter 6 with a summary of the results found as well as some proposals for future work.

2. Background

> In all cases, a quantum state is specifically and only a mathematical symbol for capturing a set of beliefs or gambling commitments.
>
> — Chris Fuchs, *Quantum Mechanics as Quantum Information*

In this section, we will go through the basics of QM needed for the project and will skip other aspects, which although important are not relevant for the work. For a more detailed explanation, see the elaborate book by Nielsen and Chuang [2000] or the brief 20-paged summary on the basics of quantum information by Bennett and Shor [1998].

2.1 Formalism

Together with each physical system $\mathcal{S}$ there is an associated d-dimensional complex space $\mathcal{H}_d$, the Hilbert space. The elements of this space constitute the possible states of such system and are represented by a normalised column vector or *ket* $|\psi\rangle$ labelled by the letter ψ, which may be a tuple encapsulating properties like position, momentum, spin, among others. All the information of that system is self-contained in the state $|\psi\rangle$ but not all the information is retrievable, as we will see.

The smallest, non trivial, space is the two-dimensional Hilbert space $\mathcal{H}_2$. The space is spanned by two states labelled $\{|0\rangle, |1\rangle\}$ that form the *computational basis* $\mathcal{C}_2$. A state $|\psi\rangle \in \mathcal{H}_2$ is said to be a *qubit*, in complete analogy to the classical bit of information. A qubit can be written as a complex linear combination or *superposition* of the basis states

$$|\psi\rangle = \psi_0 |0\rangle + \psi_1 |1\rangle \qquad , \qquad |\psi_0|^2 + |\psi_1|^2 = 1 \tag{2.1}$$

where the components $\psi_j \in \mathbb{C}$ are determined through the inner product of $|\psi\rangle$ and $|j\rangle \in \mathcal{C}_2$. In Dirac notation, the inner product of a Hilbert space is represented by the product of a *bra* and a ket, the bra being the conjugate transpose of the ket, written as $\langle\psi| \equiv |\psi\rangle^\dagger$. Then, the *braket* of two states is

$$\langle\phi|\psi\rangle = \sum_{j=0}^{1} \phi_j^* \psi_j = \langle\psi|\phi\rangle^* \ . \tag{2.2}$$

The state $|\psi\rangle$, under a measurement that distinguishes the states $|0\rangle$ and $|1\rangle$, behaves like $|0\rangle$ with probability $p_0 = |\psi_0|^2$ and like $|1\rangle$ with probability $p_1 = |\psi_1|^2$. The normalisation follows from the conservation of probabilities, $p_0 + p_1 = 1$.

The study of two of more systems $\mathcal{S}_0, \ldots, \mathcal{S}_{n-1}$ is made through the *tensor product* or *Kronecker product* of the corresponding spaces $\mathcal{H}_0 \otimes \cdots \otimes \mathcal{H}_{n-1}$. When all the spaces are two-dimensional we will write $\mathcal{H}_2^{\otimes n}$, the computational basis in this big space of 2^n elements is spanned by the vectors $\mathcal{C}_n = \{|j\rangle \mid j \in \{0,1\}^n\}$ where $\{0,1\}^n$ is the space of all the combinations of n zeros and ones. Sometimes, the state $|j\rangle$ will also be written as $|j_0 j_1 \ldots j_{n-1}\rangle = |j_0\rangle \otimes |j_1\rangle \otimes \cdots \otimes |j_{n-1}\rangle$ interchangeably, although the first notation is preferable for its simplicity. If at some point there is confusion on which space $|j\rangle$ belongs to, a subscript on the ket will be written for clarification $|j\rangle_A$.

A state $|\Psi\rangle \in \mathcal{H}_0 \otimes \cdots \otimes \mathcal{H}_{n-1}$ that can be written as the tensor product of individual states for each subsystem, i.e. $|\Psi\rangle = |\psi_0\rangle \otimes |\psi_1\rangle \otimes \cdots \otimes |\psi_{n-1}\rangle$, is said to be separable. However, there exist states which cannot be expressed in the previous form and those are said to be *entangled*. The simplest example of entangled states are the Bell states $\mathscr{B}$ made out of two qubits:

$$|\Phi_+\rangle = |\Phi_{00}\rangle = \frac{1}{\sqrt{2}}\left[|00\rangle + |11\rangle\right] \ , \tag{2.3a}$$

$$|\Psi_+\rangle = |\Phi_{01}\rangle = \frac{1}{\sqrt{2}}\left[|01\rangle + |10\rangle\right] \ , \tag{2.3b}$$

$$|\Phi_-\rangle = |\Phi_{10}\rangle = \frac{1}{\sqrt{2}}\left[|00\rangle - |11\rangle\right] \text{ and} \tag{2.3c}$$

$$|\Psi_-\rangle = |\Phi_{11}\rangle = \frac{1}{\sqrt{2}}\left[|01\rangle - |10\rangle\right] \ . \tag{2.3d}$$

These states are maximally entangled, i.e. represent a situation of perfect correlation between a measurement on both qubits. Thanks to this property, they play a very important role in the context of quantum communication and constitute the building block of most protocols explored in this work.

A measurement is made by an observable $\mathcal{A}$ that has an associated Hermitian matrix or *operator* $A \in \mathscr{H}_n$ which acts on the quantum states of some Hilbert space. In the computational basis, the operator reads $A = \sum_{j,k=1}^{n} a_{jk} \, |j\rangle\langle k|$ where $|j\rangle\langle k|$ is the outer product.

The hermiticity property of all observables allows a spectral decomposition as a sum $A = \sum_\lambda a_\lambda \hat{P}_\lambda$ being $\{a_\lambda\}$ the eigenvalues of A and $\hat{P}_\lambda$ the projector onto the eigenspace spanned by the eigenvectors corresponding to a_λ obeying the orthogonality and completeness relations

$$\hat{P}_\lambda \hat{P}_\mu = \hat{P}_\lambda \delta_{\lambda\mu} \tag{2.4a}$$

$$\sum_\lambda \hat{P}_\lambda = \mathbb{I}_d \ . \tag{2.4b}$$

If $\mathcal{A}$ is a physical observable, then $\{a_\lambda\}$ are the physical values that we can observe after measuring a state $|\psi\rangle$. The probability that the result a_λ is obtained given that the state measured was $|\psi\rangle$ is

$$\mathbb{P}\left[a_\lambda|\psi\right] = \langle\psi|\hat{P}_\lambda|\psi\rangle \tag{2.5}$$

and it holds that $\sum_\lambda \mathbb{P}\left[a_\lambda|\psi\right] = 1$ on account of eq. (2.4b).

The measure is completely defined once the operators $\{\hat{P}_\lambda\}$ are given, then for each $\hat{P}_\lambda$ we associate the hypothesis that the value of the physical property $\mathcal{A}$ observed is a_λ. This measure is called projective or *von Neumann measure* because the elements are orthogonal projectors (eq. (2.4a)) [von Neumann, 1955]. The number of projectors is limited by the dimension of the space, otherwise the orthogonality condition wouldn't be satisfied. For this reason, we define a generalised measurement or Positive Operator Valued Measure (POVM) as a set of positive operators $\{\Pi_j\}_{j=1}^n$ [Kraus, 1983], with n not necessarily equal to d, satisfying the completeness and positivity conditions

$$\sum_{j=1}^{n} \Pi_j = \mathbb{I}_d \tag{2.6a}$$

$$\Pi_j \geq 0 \qquad \forall j \ . \tag{2.6b}$$

An observable of $\mathcal{H}_2$ is expressed, in the most general form, as a real linear combination of the identity matrix $\mathbb{I}_2$ and the *Pauli matrices* $\{\sigma_i\}_{i=1}^3$ which span the space of 2×2 Hermitian matrices $\mathscr{H}_2$,

$$\sigma_1 = \sigma_x = X = \begin{pmatrix} 0 & 1 \\ 1 & 0 \end{pmatrix}, \qquad \sigma_2 = \sigma_y = -iY = \begin{pmatrix} 0 & -i \\ i & 0 \end{pmatrix}, \qquad \sigma_3 = \sigma_z = Z = \begin{pmatrix} 1 & 0 \\ 0 & -1 \end{pmatrix} . \tag{2.7}$$

The elements of the computational basis are by convention the eigenvectors of the third Pauli matrix such that $\sigma_3 \, |0\rangle = + \, |0\rangle$ and $\sigma_3 \, |1\rangle = - \, |1\rangle$.

Moreover, the 3 Pauli matrices are the generators of rotations in $SU(2)$, the symmetry group of qubits. A rotation of a qubit $|\psi\rangle$ along the direction $\boldsymbol{n}$ by an angle θ is performed by the unitary operator

$$U_{\theta,\boldsymbol{n}} = \exp\left(-i\frac{\theta}{2}\boldsymbol{n}\cdot\boldsymbol{\sigma}\right) . \tag{2.8}$$

For instance, the Hadamard gate

$$H = \frac{1}{\sqrt{2}}\begin{pmatrix}1 & 1\\ 1 & -1\end{pmatrix} \tag{2.9}$$

corresponds to a $\pi/2$ rotation around the y-axis.

It is also possible to define controlled operations between two or more qubits. For two qubits, a controlled unitary CU is defined $|0\rangle\langle 0|\otimes\mathbb{I} + |1\rangle\langle 1|\otimes U$. That is, if the first (control) qubit is in the state $|0\rangle$ the second (target) is not altered. On the other hand, if the control qubit is in the state $|1\rangle$ then the unitary U is applied on the target. Typical controlled operations are the CX and CZ whose expression in the standard basis is

$$\mathrm{CX} = \begin{pmatrix}1 & 0 & 0 & 0\\ 0 & 1 & 0 & 0\\ 0 & 0 & 0 & 1\\ 0 & 0 & 1 & 0\end{pmatrix} \quad , \qquad \mathrm{CZ} = \begin{pmatrix}1 & 0 & 0 & 0\\ 0 & 1 & 0 & 0\\ 0 & 0 & 1 & 0\\ 0 & 0 & 0 & -1\end{pmatrix} . \tag{2.10}$$

Here, CX is also an entangling gate as it is used to generate the four Bell states eq. (2.3).

The states we have been talking so far are called *pure states*, they represent situation of perfect knowledge on a system. However, there may be situations in that the state of the system is not well-defined and we have to make use of *mixed states* generated by an *ensemble of pure states* $\Xi = \{\xi_k, |\psi_k\rangle\}_{k=1}^n$ with $\sum_{k=1}^n \xi_k = 1$, meaning that the we can find the state $|\psi_k\rangle$ with probability ξ_k. A mixed state is represented by a positive-semidefinite hermitian *density matrix* ρ with trace equal to one,

$$\rho = \sum_{k=1}^{n} p_k\, |\psi_k\rangle\langle\psi_k| \ . \tag{2.11}$$

The state ρ is called pure when there is only one state in the ensemble with probability 1, then $\rho = |\psi\rangle\langle\psi|$ and we return to the case above. Moreover, the ensemble of states Ξ might contain other mixed states ρ_k occurring with probability ξ_k. In any case, the probability of observing a_λ when measuring A given ρ in eq. (2.11) is

$$\mathbb{P}\left[a_\lambda|\rho\right] = \mathrm{tr}\,\hat{P}_\lambda\rho \tag{2.12}$$

which reduces to (2.5) when ρ is pure.

By construction, the density operator (2.11) is also hermitian and admits a spectral decomposition $\rho = \sum_{k=1}^n \xi_k\, |\xi_k\rangle\langle\xi_k|$ with positive eigenvalues ξ_k and corresponding eigenvector $|\xi_k\rangle$ satisfying $\sum_k \xi_k = 1$ and $\sum_k |\xi_k\rangle\langle\xi_k| = \mathbb{I}_d$. They constitute the *eigen-ensemble* $\{\xi_k, |\xi_k\rangle\}$ where the values ξ_k are interpreted as the probability that the system was in the state $|\xi_k\rangle$. An important property follows from this fact, given a density matrix ρ it is not possible to know from which ensemble Ξ it was constructed. Or equivalently, if two ensembles Ξ and Ξ' (with the same or different number of elements) lead to the same density matrix, the two systems $\mathcal{S}$ and $\mathcal{S}'$ are completely indistinguishable.

In two dimensions, a mixed state can be expressed as linear combination of the identity matrix $\mathbb{I}_2$ and the Pauli matrices as

$$\rho = \frac{\mathbb{I}_2 + \boldsymbol{r}\cdot\boldsymbol{\sigma}}{2} \tag{2.13}$$

for some real coefficients $\boldsymbol{r} = (r_1, r_2, r_3)$. The eigenvalues of (2.13) are $(1 \pm \|\boldsymbol{r}\|_2)/2$, but because ρ is positive by definition we must have $\|\boldsymbol{r}\|_2 \leq 1$, with equality in the case of pure states. The value $r = \|\boldsymbol{r}\|_2$ is known as the purity of the state and represents the radial distance from the origin. The product $\boldsymbol{r}\cdot\boldsymbol{\sigma}$ symbolises the pseudo-scalar product between a vector and a vector of matrices: $\boldsymbol{r}\cdot\boldsymbol{\sigma} = \sum_{i=1}^3 r_i\sigma_i$.

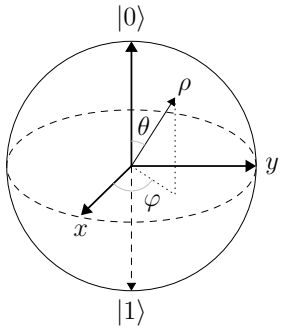

Figure 2.1: Three dimensional representation of a qubit ρ in the Bloch sphere.

From (2.13), the correspondence is clear between a qubit and a point in a 3-dimensional sphere. The state vector $\boldsymbol{r}$ can always be expressed as $\boldsymbol{r} = r(\sin\theta\cos\varphi, \sin\theta\sin\varphi, \cos\theta)$ with $r \in [0,1]$ the modulus, $\theta \in [0,\pi)$ the angle with respect the z-axis and $\varphi \in [0, 2\pi)$ the angle with respect to the x-axis. The sphere where qubits are represented is called the *Bloch sphere*, see fig. 2.1. The peculiarity is that the angle between orthogonal states is π in contrast to the usual $\pi/2$ of Euclidean space*.

2.2 Distance and fidelity

In the quantum information framework, distance is interpreted as the quantity of information shared between two quantum states. This gives us a way to compare two quantum states. First of all, it is not possible to go to the Hilbert space, put a ruler between quantum states and decide from this whether they are the same or not, just because a posterior measurement might change its nature. Despite that, we can define a distance between two general states ρ and ρ' with the metric

$$D(\rho, \rho') = \|\rho - \rho'\|_1 \tag{2.14}$$

which is the so called *trace distance* [Nielsen and Chuang, 2000], denoting by $\|A\|_1$ the *trace norm* (or norm one)

$$\|A\|_1 = \operatorname{tr}\sqrt{AA^\dagger} = \sum_\lambda |a_\lambda| \tag{2.15}$$

where $\{a_\lambda\}$ are the eigenvalues of A.

Two quantum states are said to be close to each other if the trace distance is near zero. If the states are qubits, with state vector $\boldsymbol{r}$ and $\boldsymbol{r'}$ respectively, the expression (2.14) reduces to

$$D(\rho_{\boldsymbol{r}}, \rho_{\boldsymbol{r'}}) = \frac{\|\boldsymbol{r} - \boldsymbol{r'}\|_2}{2} \tag{2.16}$$

where $\|\boldsymbol{a}\|_2 = \sum_k |a_k|^2$ is the usual vector norm (or norm two). Notice that this pseudo-distance is half the ordinary distance between two points inside a sphere.

Another measure of similarity between quantum states is the fidelity F defined as†

$$F(\rho, \sigma) = \left\|\sqrt{\rho}\sqrt{\sigma}\right\|_1^2 \tag{2.17}$$

which ranges from 0 to 1. The states ρ and σ are said to be equal when $F = 1$, they describe the same physics, even though their decomposition might be different. If $F = 0$, the two states are orthogonal.

When $\sigma = |\psi\rangle\langle\psi|$, the previous expression can be simplified to

$$F(\rho, |\psi\rangle) = \langle\psi|\rho|\psi\rangle \tag{2.18}$$

*The reason for this is a factor of two between the symmetry groups $SU(2)$ (where qubits live) and $SO(3)$ (the usual rotation group), in other words, to return to the same state one must make a rotation of 4π degrees.

†Note that, in some books, the fidelity is defined without the square.

making it clear that the fidelity is a measure of how orthogonal the two states are.

The fidelity also give us a way to quantify how entangled is a two-qubit state. That is, given a state $\rho \in \mathcal{H}_2^{\otimes 2}$, if the entanglement fidelity

$$F_{ent} = \max_{|\Phi\rangle \in \mathscr{B}} \langle \Phi | \rho | \Phi \rangle \tag{2.19}$$

is higher than $1/2$ we can ensure that the state has quantum correlations exceeding any classical strategy.

2.3 No cloning

Fundamental properties of quantum mechanics make it impossible to build a general device that copies an unknown quantum state [Wootters and Zurek, 1982].

The proof of the no-cloning theorem is straightforward and instructive to reproduce here. Suppose we want to copy a quantum state $|\psi\rangle \in \mathcal{H}$. To that purpose we build a unitary U that satisfies $|\Psi\rangle = U |\psi\rangle |0\rangle = U |\psi\rangle |\psi\rangle$. Since this machine is by definition general, we can take another quantum state $|\phi\rangle \in \mathcal{H}$ and use U to copy it in the same way as before so $|\Phi\rangle = U |\phi\rangle |0\rangle = |\phi\rangle |\phi\rangle$. Now, take the overlap of the two resulting states $|\Psi\rangle$ and $|\Phi\rangle$, on the one hand we have

$$\langle \Psi | \Phi \rangle = \langle \psi | \langle \psi | \phi \rangle | \phi \rangle = \langle \psi | \phi \rangle^2 \tag{2.20}$$

and on the other

$$\langle \Psi | \Phi \rangle = \langle 0 | \langle \psi | U^\dagger U | \phi \rangle | 0 \rangle = \langle 0 | \langle \psi | \mathbb{I} | \phi \rangle | 0 \rangle = \langle \psi | \phi \rangle \ . \tag{2.21}$$

Combining both results we obtain

$$\langle \psi | \phi \rangle^2 = \langle \psi | \phi \rangle \ , \tag{2.22}$$

thus either $\langle \psi | \phi \rangle = 0$ or $\langle \psi | \phi \rangle = 1$, either the states are orthogonal or both are the same. Thus, it is not possible to find a general U that copies arbitrary quantum states.

Note that, if cloning was possible, quantum entanglement would lead to instantaneous communication and it would be possible to perfectly distinguish two quantum states [Gisin, 1998]. In the context of QRs, this forbids the possibility of amplifying quantum information at each station as done classically. Consequently, other techniques are needed to connect two nodes with intermediate QRs that do not rely on this property.

2.4 Quantum Channels and Operations

We have defined rotations on a qubit but in general, a quantum operation acting on a quantum state $\rho \in \mathcal{H}_d$ can be defined as a map or *channel* $\mathcal{E} : \mathcal{H}_d \mapsto \mathcal{H}_d$. Not all maps are valid and in our project we will only deal with Completely Positive Trace Preserving (CPTP) maps which, as the name points out, preserve the trace so $\operatorname{tr} \rho = \operatorname{tr} \mathcal{E}(\rho)$, are convex-linear so $\mathcal{E}(\alpha\rho + \beta\sigma) = \alpha\mathcal{E}(\rho) + \beta\mathcal{E}(\sigma)$ for any $\alpha, \beta \in \mathbb{R}$ and are completely positive so $(\mathbb{I}_n \otimes \mathcal{E})(\rho) \geq 0$ for any $\rho \in \mathcal{H}_n \otimes \mathcal{H}_m$ [Nielsen and Chuang, 2000]. Any CPTP map can be expressed in terms of Kraus operators $\{E_i\}$ [Choi, 1975] such that

$$\mathcal{E}(\rho) = \sum_i E_i \rho E_i^\dagger \tag{2.23}$$

where the Kraus operators satisfy

$$\sum_i E_i^\dagger E_i = \mathbb{I} \ . \tag{2.24}$$

Concretely, if $\mathcal{E}$ acts on a single qubit, the map can be written in the form $\boldsymbol{r} \mapsto \boldsymbol{r}' = M\boldsymbol{r} + \boldsymbol{c}$ where $M \in \mathbb{R}^{3\times 3}$ and $\boldsymbol{c} \in \mathbb{R}^3$ and the Kraus operators have the form $E_i = \alpha_i \mathbb{I} + \sum_k a_{ik}\sigma_k$.

The generality of the definition of a quantum operation allow us to describe from measurements to unitary evolution but most importantly it give us a way to understand the effect of noise in quantum systems. Typical noise models are the depolarising, dephasing and amplitude damping

channel. The first describes a process for which we have no knowledge on the final state in case of failure, it is given by the expression

$$\mathcal{D}_{pol}(\rho) = (1-p)\rho + p\frac{\mathbb{I}_2}{2} \tag{2.25}$$

meaning that with probability $1-p$ the state is maintained but with probability p it is replaced by the completely mixed state. The depolarising channel is commonly used to model worst-case scenarios as it sets a upper-bound on the noise parameter p.

The second describes the process of a state losing the x, y components and focusing on the z axis, it is given by the expression

$$\mathcal{D}_{ph}(\rho) = (1-p)\rho + p\sigma_z\rho\sigma_z \tag{2.26}$$

where p is the probability of dephasing and the Kraus operators are $D_0 = \sqrt{1-p}\,\mathbb{I}$ and $D_1 = \sqrt{p}\,\sigma_z$.

The latter, describes the process of energy dissipation, that is, the relaxation of a quantum system towards its ground state, this process is characterised by the Kraus operators

$$A_0 = \begin{pmatrix} 1 & 0 \\ 0 & \sqrt{1-\gamma} \end{pmatrix} \quad , \quad A_1 = \begin{pmatrix} 0 & \sqrt{\gamma} \\ 0 & 0 \end{pmatrix} \tag{2.27}$$

being γ the probability of this decaying.

The last class of transformations that are important for future steps are Local Operations and Classical Communication (LOCC) which play an important role in the problem of entanglement transformation. In this work, entangled states are typically shared between two distant parties, each one having access to its qubit only. Operations can only be done locally, forbidding controlled operations (eq. (2.10)), but results from local measurements can be shared. The combination of the two allows to transform the combined state under certain conditions.

3. Quantum Repeater Chains

> While quantum theory can in principle describe anything, a quantum description cannot include everything. In every physical situation something must remain unanalyzed. This is not a flaw of quantum theory, but a logical necessity...
>
> — Asher Peres, *Quantum theory: concepts and methods*

In this chapter, the basic protocols used to transmit quantum information will be explored. These include entanglement swap to overcome the no-cloning theorem, entanglement generation to create EPR pairs between neighbouring repeater stations, entanglement purification to increase the quality of those pairs and the network protocol that controls the scheduling of all the previous in a repeater chain. A brief description of a general repeater hardware is sketched to account for some of the possible sources of noise that affect the states in the chain. The goal of the repeater chain is to have a robust method to generate a link between the end nodes of sufficient quality and at a required rate.

3.1 Introduction

The realisation of a quantum network composed of interconnected quantum nodes capable of transmitting and storing quantum information is the ultimate goal of the "second quantum revolution" [MacFarlane et al., 2003]. Transmission of information using photons through optical fibres represents a good candidate for quantum communication, as photons interact very little with each other or the environment. Despite that, satellite-based communication has also been explored and represents a clear alternative to ground-based communication [Sidhu et al., 2021].

Currently, no large-scale QI capable of connecting nodes at distances larger than 100 km exists [Kozlowski and Wehner, 2019]. Its development forces us to reinvent the wheel as it is impossible to use the same solutions that worked for classical networks. Those rely heavily on the ability to read and copy information, the latter of which being forbidden in QM due to the no-cloning theorem (section 2.3). Moreover, typical fibres have an exponential loss of about 0.22 dB/km at a wevelength of 1550 nm implying a transmission probability of 10^{-22} over a distance of 1000 km [Simon, 2017]. The use of intermediate stations is inevitable to cover large distances with the current hardware.

Despite the fundamental differences with classical communication, we can partially overcome photon-loss in a similar way. By dividing the total length into smaller segments and placing a QR in-between the segments, we ensure that a photon sent between adjacent nodes reaches the other one with a higher probability. The basic task of a QR is to connect and transmit information, thus requiring more modest properties than a fully-fledged Quantum Computer (QC).

Three generations of quantum repeaters, distinguished by the maximum tolerable noise and the time scaling with the total distance, have been proposed [Muralidharan et al., 2016]. The first generation of QRs makes use of two-way communication – meaning that a node can interact with both of its neighbours – at the cost of lower entanglement generation rate. Yet, more noise can be

tolerated than in the second and third generation, which make use of quantum error correction techniques and one-way communication. The necessary requirements for these lasts generations are too demanding in the NISQ era; therefore, we will stick to the first generation of QRs.

Hereafter, we consider linear repeater chain formed by N_{node} nodes, $N_{node} - 2$ repeaters, equally separated from each other. Each node is connected to its nearest neighbours by a quantum and classical channel and communication is allowed in both directions. All protocols can make use of two-way signalling between nearest repeaters, and are designed to work with noisy hardware.

3.2 Entanglement Swap

Absorption losses in optical fibres limit the capacity to transmit information over large distances. The transmission of a photon between two nodes A and B separated by a distance L can be modelled by an exponentially decreasing function $\eta(L) = \exp(-L/L_0)$ where L_0 is the attenuation distance of the fibre. Thus, the average number of attempts needed to have one photon reaching the other station is [Ekert and Bouwmeester, 2000]

$$\mathbb{E}[N] = \frac{1}{\eta(L)} = e^{L/L_0} \ , \tag{3.1}$$

leading to an exponential increase of the number of attempts as the distance grows.

Classical communication techniques overcome this issue by dividing the length into n segments with repeater stations connecting them that copy and retransmit the information. Thus, photons travel at most a distance L/n before they are amplified. The average total number of attempts in each segment is $\exp(L/nL_0)$ and correspondingly, the total number of attempts across the whole length is

$$\mathbb{E}[N_{rep}] = ne^{L/nL_0} \ , \tag{3.2}$$

which is much smaller than the brute-force method in eq. (3.1). The minimum number of transmissions is found for $n_{min} = L/L_0$ leaving $(L/L_0)e$ attempts to connect two nodes with equally spaced repeaters.

Of course, the method is not directly applicable in quantum communication as the copying of quantum information is forbidden by the no-cloning theorem (see section 2.3). Despite that, it is still possible to send a quantum state if the two parties hold an EPR pair [Einstein et al., 1935] using the teleportation protocol with only LOCC [Bennett et al., 1993], which consists of the two steps shown in protocol 1. The previous does not violate the no-cloning theorem as all information about the initial state is completely destroyed in the sending node once the protocol finishes, and the state is moved to the other party's qubit.

Protocol 1 Teleportation

Setup Two nodes A and B share the entangled state $|\Phi\rangle_{AB} \in \mathscr{B}$ and A holds the qubit $|\phi\rangle_{A'}$ to be sent.

Steps

1: A performs a $\mathrm{CX}_{A'\to A}$ followed by a H gate on A' and measures both qubits in the computational basis obtaining four possible outcomes (jk).

2: A sends measurement outcomes to B, which applies the correction operator $\sigma_z^j \sigma_x^k$ to its qubit.

A corollary of this protocol is that not only does it allow to send a quantum state, but it also effectively maps all quantum correlations of the initial state held by A to the final state held by B. It implies that if the state to teleport is part of an EPR pair, the teleportation protocol swaps the entanglement from the qubit in A to the qubit in B [Żukowski et al., 1993]. This process is called Entanglement Swap (ES) or simply *swap*. An example is illustrated in fig. 3.1. There, R holds two entangled Bell states, one with A ($|\Phi\rangle_{RA}$) and the other one with B ($|\Phi\rangle_{R'B}$), and

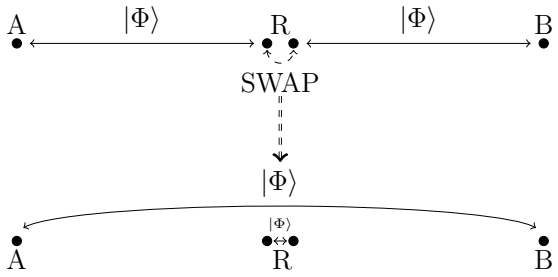

Figure 3.1: Visualisation of the entanglement swap protocol where node R performs the teleportation protocol.

performs the teleportation protocol so that A and B become entangled. The initial state of the whole system is $|\Phi\rangle_{RA}\,|\Phi\rangle_{R'B}$ and after applying the teleportation protocol on R's qubits, the final state is $|\Phi\rangle_{RR'}\,|\Phi\rangle_{AB}$, where A takes the role of R' and vice-versa.

This last procedure allow us to apply a similar repeater protocol as in classical communication. The total communication length is again divided into N segments. QRs connect those segments and a Bell state is generated between each pair of adjacent nodes. Throughout this project, this state will also be known as an *elementary link*. Then, the entanglement swap protocol is applied at each repeater until the first and last node share an entangled pair. Once the end nodes share it, they can consume their state to send a qubit using the teleportation protocol in its original form or to any other application [Wehner et al., 2018].

This straightforward use of ES is not applicable in all situations. To understand why, it is necessary to look into the hardware which is being used for the first generation of QR.

3.3 Repeater Hardware

Any physical realisation of a repeater chain must be capable of creating, manipulating and storing entangled states for as much time as necessary before a swap happens, must have a quantum channel linking them and an interface that maps the states in memory to photonic states which can be sent through the channel [Northup and Blatt, 2014].

Quantum Memory The first requirement implies that a QR needs a Quantum Memory (QMem) with as many qubits as nodes it is connected to, and a method to perform operations on those qubits. Some proposals for QMems use nitrogen-vacancy (NV) centres [Rozpedek et al., 2019], trapped-ions [Zwerger et al., 2017] or atomic ensembles [Sangouard et al., 2011]. This project does not focus on a particular implementation but simply assumes an abstract model comprised of common properties found in different physical realisations.

Thus, we consider repeaters with imperfect operations and memories with non-perfect storage fidelity. The latter is defined as the fidelity between the stored initial state and the output state after a time t. There are four different kinds of operations that can be performed on a QMem:

- Initialisation: Initialises a qubit in a state characteristic of the memory. This tends to be the ground state $|0\rangle$ but may vary. The probability that this process fails is p_{init} and it is modelled by a depolarising channel $\mathcal{D}_{\text{pol}}$. The initialisation takes a time t_{init} to complete.

- Single qubit gates: Operation on a single qubit U_1 like rotations around an axis. These gates are modelled using a depolarising channel with failure probability $p_{1,gate}$ as in eq. (3.3). The time needed to complete is $t_{1,gate}$.

$$\rho \xrightarrow{U_1^{(j)}} (1 - p_{1,gate})U_1^{(j)}\rho[U_1^{(j)}]^\dagger + p_{1,gate}\,\mathrm{tr}_j\,\rho \otimes \frac{\mathbb{I}_2^{(j)}}{2} \tag{3.3}$$

- Two qubit gates: Operation between two qubits U_2 like controlled unitaries. Modelled as

before as a depolarising noise with probability $p_{2,gate}$ (eq. (3.4)) and duration $t_{2,gate}$.

$$\rho \xrightarrow{U_1^{(jk)}} (1-p_{2,gate})U_2^{(jk)}\rho[U_2^{(jk)}]^\dagger + p_{2,gate}\,\mathrm{tr}_{jk}\,\rho \otimes \frac{\mathbb{I}_2^{(j)}}{2} \otimes \frac{\mathbb{I}_2^{(k)}}{2} \tag{3.4}$$

- Measurement: The extraction of information from qubits is usually done via a measurement in the standard basis $\mathcal{C}_2$. The faulty measurement can be described with the POVM

$$\mathcal{M} = \{M_0 = (1-\xi_0)\,|0\rangle\langle 0| + \xi_0\,|1\rangle\langle 1|\,, M_1 = (1-\xi_1)\,|0\rangle\langle 0| + \xi_1\,|1\rangle\langle 1|\} \tag{3.5}$$

  where ξ_0 (ξ_1) is the probability that a state was in $|0\rangle$ ($|1\rangle$) but the orthogonal state was measured. This operation also takes some time t_{meas} to complete.

The first three are modelled as depolarising noise to represent the worst case scenario, where all information about the original state is lost and replaced by a completely mixed state. Initialisation and single qubit gate errors are usually much smaller than two qubit errors and the same holds for their duration [Benhelm et al., 2008; Bradley et al., 2019].

Storage errors are modelled as a combination of dephasing and amplitude damping channel with time, which are defined by the relaxation time T_1 – the time needed for a state in $|1\rangle$ to decay into $|0\rangle$ – and the dephasing time T_2 – the time need for a superposed state to be lost. This decoherence process fits very well with experiments realised on different quantum systems [Ekert and Bouwmeester, 2000; Nielsen and Chuang, 2000]. Mathematically, the channel $\mathcal{T}(t)$ is defined as $\mathcal{A}[\gamma(t)] \circ \mathcal{D}_{ph}[p(t)]$ with time dependent coefficients

$$\gamma(t) = \exp\left(-\frac{t}{T_1}\right) \qquad , \qquad p(t) = \exp\left[-t\left(\frac{1}{T_2} - \frac{1}{T_1}\right)\right] \tag{3.6}$$

where it holds by definition that $T_1 > T_2$. The latter limits the maximum time a state can be reliably stored in a memory, and therefore, a quantum repeater chain must be capable of generating entanglement in less time than T_2. This time is thus a critical threshold to allow for quantum communication. As an example, NV-centers have a an intrinsic decoherence time around milliseconds that is increased to a second with dynamical decoupling [Abobeih et al., 2018] while the relaxation time is on the order of hours.

Some implementations, like NV-centers or trapped-ions, have a restricted topology which means that the interaction between qubits as well as the interaction between qubits and the outside world is limited. For instance, NVs have a single communication qubit, the electron spin, that is used to generate entanglement. The states are stored in carbon qubits which have longer coherence times but only support rotations around the z-axis. To apply other single qubit gates, the state has to be moved back and forth from the carbon to the electron where the operation is applied, thus introducing extra noise in each swap. Also, two-qubit gates are only supported between the electron and a carbon. To keep it general, these restrictions will not be taken into account.

Quantum Channel A repeater is connected to each of its neighbours via a commercial telecom fibre. The efficiency of the channel η_{fibre} depends on the internode distance L and fibre transmission loss γ expressed in units of dB/km*. It defines the probability that a single photon travels a distance L,

$$\eta_{fibre} = 10^{-\gamma L/10} \tag{3.7}$$

which decreases exponentially with the distance.

Moreover, the losses are wavelength dependent and are minimised for 1310 nm and 1550 nm [Saleh and Teich, 2019] with an average attenuation of 0.38 db/km and 0.22 db/km respectively [CISCO, 2021]. This represents an efficiency below 10^{-4} for distances larger than 100 km and 200 km respectively. The latter being more useful for large-scale communication.

Another detail is that the velocity of light in glass is reduced due the different refractive index that is found in the core, a value of approximately $n = 1.44$ is characteristic of silica glass fibres, implying a speed of light of $c_{fibre} = c_0/n \approx 208\,189.207$ km/s [Saleh and Teich, 2019].

*Related to the attenuation length L_0 in eq. (3.1) by $L_0 = 10/\gamma \ln 10$.

Light-Matter interface The last requirement for a quantum repeater is an interface mapping memory states into photonic states which can be sent through the channel. This is important to generate entangled links between nearby stations and it depends on the type of memory. We can however extract a common procedure that will help us in modelling this process.

The interface consist on two processes: the emission of light by the QMem and the detection of the photon emitted by the detector. Both processes succeed with an efficiency η_{em} and η_{det} respectively. Hence, the combined light-matter interface efficiency is

$$\eta_{lm} = \eta_{em}\eta_{det} \tag{3.8}$$

The emission process depends to a large extent on the type of memory. First of all, QMems are coupled to optical fibres that collect photons emitted by them. The efficiency of this coupling determines how well emitted photons are collected by the fibre and it can be a combination of different parameters.

For instance, in NV-centres, not all photons emitted can be used but only those falling withing the Zero Phonon Line (ZPL). This represents $3\% - 4\%$ of all emitted photons, which can be amplified to 46% using optical cavities [Riedel et al., 2017]. The ZPL is not in the transmission bandwidth of the fibre and must be converted using a non-deterministic process that has been demonstrated to succeed with a probability $> 30\%$ [Zaske et al., 2012]. Therefore, to the intrinsic collection efficiency of the fibre η^*_{col} one must add the conversion efficiency η_{conv} to determine the total collection efficiency η_{col}. Thus, the emission efficiency becomes $\eta_{em} = \eta_{zpl}\eta_{col} = \eta_{zpl}(\eta^*_{col}\eta_{conv})$.

The detection process at the other end of the fibre represents the opposite process. Single-photon detectors are extremely sensible to fluctuations. Despite that, efficiencies ranging from 80% to 90% have been demonstrated [Esmaeil Zadeh et al., 2020]. This excludes some sources of noise like dark counts, the false detection of a photon due to thermal fluctuation of the detector [Rozpedek et al., 2019].

The light matter interface hardware efficiency can be combined with the fibre transmission efficiency (3.7) to form the total transmission efficiency

$$\eta_{trans} = \eta_{fibre}\eta_{lm} = \eta_{fibre}\eta_{em}\eta_{det} \tag{3.9}$$

In general, the transmission efficiency is dominated by the fibre transitivity for long distances and by the light-matter interface efficiency for short distances. Regardless, the combined value remains small and optimal protocols are needed to generate elementary pairs.

3.4 Entanglement Generation

In the context of the 1G of QRs, the most common protocol used to generate entanglement between two nodes is the MHEG protocol that places a measurement station in between the two nodes [Muralidharan et al., 2016], where photons are sent for processing. This has the advantage that the photon travel distance is reduced by half the internode distance, increasing the transmission efficiency. The station measures the photons emitted by the nodes and it sends the outcomes to the nodes. Two types of protocols that use MHEG are Single-Click (SC) and Double-Click (DC), distinguished by the number of photons that have to be detected in the midpoint station to yield an entangled state.

Single-Click Single-Click has been investigated for NV-centers [Humphreys et al., 2018] and atomic ensembles [Sangouard et al., 2011] among other platforms. Generally, the information is encoded in the presence or absence of the photon and requires that only one photon arrives to the station [Campbell and Benjamin, 2008].

The process starts by creating the superposed state

$$|\alpha\rangle = \sqrt{\alpha}\,|0\rangle + \sqrt{1-\alpha}\,|1\rangle \tag{3.10}$$

in each of the involved nodes. A process specific to each implementation couples the matter state to the presence/absence of a photon,

$$|\alpha,\gamma\rangle = \sqrt{\alpha}\,|0\rangle\,|1\rangle_\gamma + \sqrt{1-\alpha}\,|1\rangle\,|0\rangle_\gamma \ . \tag{3.11}$$

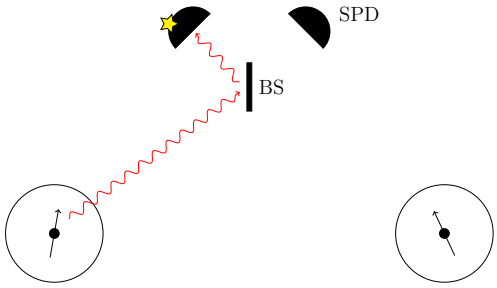

(a) Single-Click protocol. The detection of a single photon in either detector triggers the success signal.

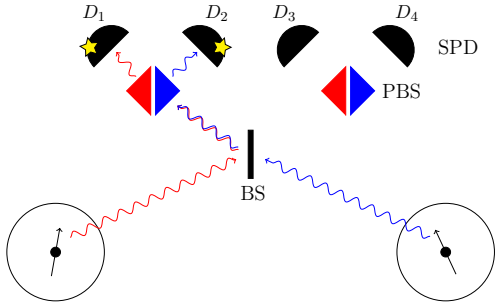

(b) Double-Click protocol. The two polarisation modes are represented with different colors. The PBS separates the two modes and the detection of two photons with different modes, D_1 & D_2 or D_3 & D_4, results in a successful entanglement generation attempt.

Figure 3.2: Non-deterministic entanglement generation using a middle-heralded station. Two nodes trigger the encoding an emission of a photon from one of their qubits, the path information is removed at the beam splitter (BS) which sends the photon(s) to the single-photon detectors (SPD) in (a) or to the polarisation beam splitter (PBS) in (b).

Protocol 2 Single-Click entanglement generation protocol

1: Each node generates the state $\sqrt{\alpha}\,|0\rangle + \sqrt{1-\alpha}\,|1\rangle$.

2: The bright state $|0\rangle$ is excited and decays emitting a photon which is collected and sent through the fibre.

3: A BS in the central station removes the which-path information and sends the photons to the SPD.

4a: If a single detector clicks, the station sends a message back to both nodes confirming the generation of an entangled state.

4b: Otherwise, repeat from step 1.

Here, α is called the bright-state population as it corresponds to the photon emission probability. This process takes a time T^*_{cycle} to complete for which the memory is busy and can not fulfil other entanglement requests.

The photon is then collected by the fibre and sent to the middle station. There, a $50\% - 50\%$ beam splitter removes the which-path information, as shown schematically in fig. 3.2a. The path information removal is imperfect due to two-photon quantum interference but the degree of indistinguishability V, or simply called *visibility*, can be estimated in a Hong-Ou-Mandel experiment. There, the ratio r of distinguishable events in which both photons emerge from the same leg of the beam splitter against the number of indistinguishable events is measured, with which the visibility can be approximated by $V = 1 - r$ [Hensen et al., 2015; Kalb et al., 2017].

The entanglement generation attempt succeeds conditional on the detection of a single photon in one of the detectors. This process is essentially non-deterministic as a single entanglement generation attempt might fail due to low detection efficiencies η_{trans} or high dark count rates. To reduce the probability of dark counts p_{dc}, the detectors only accept clicks during a small time window t_w around the photon expected arrival time.

Other noise sources that only affect the quality of the state but not the generation rate are double excitations p_d and phase-path uncertainty σ_ϕ. The former quantifies the probability that the qubit emits two photons and the latter the standard deviation on the phase difference ϕ acquired during the photon travel paths [Kalb et al., 2017]. Both effects can be modelled as a dephasing

channel with probability p_d and [Humphreys et al., 2018]

$$p_\phi = \frac{1}{2}\left(1 - e^{-\sigma_\phi^2/2}\right) \tag{3.12}$$

respectively. These errors are not general and might differ for different implementation. Thus, in order to keep it general, we define the dephasing parameter p_{ph} which reduces the quality of the state. In particular, the value of this parameter for NV-centers is

$$p_{ph} = (1-p_\phi)p_d(1-p_d) + p_\phi[(1-p_d)^2 + p_d^2] \ , \tag{3.13}$$

consisting of a dephasing channel on both qubits with probability p_d and a single channel in any of the qubits with probability p_ϕ.

The state that is generated conditional on the detection of a single photon and its success probability, assuming $\eta_{trans} \gg p_{dc}$, are [Coopmans et al., 2020]

$$\rho_{SC} = f_{SC}\,|\Psi_\pm\rangle\langle\Psi_\pm| + (1-f_{SC})\,|00\rangle\langle 00| \tag{3.14}$$

$$p_R = 2\alpha\eta_{trans} \tag{3.15}$$

where the fidelity depends on the bright-state population, the visibility and the dephasing probability as

$$f_{SC} = \frac{1}{2}(1-\alpha)(1+\sqrt{V})(1-p_{ph}) \tag{3.16}$$

There exists a clear trade-off between success probability (3.15) and fidelity (3.16) competing for higher rates or better quality states. This protocol is extremely useful for low transmission efficiencies as it only requires one photon to arrive to the middle-station which also ensures that the non Bell Diagonal (BD) term in eq. (3.14) can be made small.

Double-Click This type of MHEG protocol uses two orthogonal photonic modes to encode the information. Examples of photonic modes include their timing ('time-bin encoding') or their polarization ('polarization encoding'). For this reason, both photons have to arrive to the middle station such that a Bell-state measurement can be performed [Simon and Irvine, 2003]. This makes DC protocols less efficient than SC for large distances as transmission efficiencies are much smaller than 1. Despite that, they have been already been used to connect two NV-centers using a time-bin encoding [Hensen et al., 2015] and two rubidium-87 atoms using polarisation encoding [Hofmann et al., 2012]. The former is based on Barrett and Kok [2005] which uses two successful consecutive rounds of SC schemes, while the latter, is based on Simon and Irvine [2003] which uses two polarisation beam splitters (PBS) to separate the modes and it performs a partial bell-state measurement between the outgoing photons (see fig. 3.2b). In the end, the resulting state fidelity and the success probability is the same in both versions of the protocol.

The state in the nodes is initialised in the superposition $|+\rangle = (|0\rangle + |1\rangle)/\sqrt{2}$. This is then entangled to the two orthogonal photon modes α and α' as*

$$|\alpha,\alpha'\rangle = \frac{1}{\sqrt{2}}(|0\rangle\,|\alpha\rangle_\gamma + |1\rangle\,|\alpha'\rangle_\gamma) \ . \tag{3.17}$$

Errors might not allow to create the state above perfectly and typically it results in a light-matter superposition with fidelity $f_{lm} < 1$. This can also be used to comprise other errors like double excitations in NV-centres.

The photons from the two nodes interfere in the middle station, and the detection of two different modes (a primed and an un-primed mode) in different detectors triggers a success signal.

Staying in the limit $\eta_{trans} \gg p_{dc}$, the protocol succeeds with probability [Bernien et al., 2013]

$$p_{DC} = \frac{\eta_{trans}^2}{2} \tag{3.18}$$

*As said, the modes can correspond to horizontal ($\alpha = H$) and vertical polarisation ($\alpha = V$) in a polarisation encoding or an early (α) and late (α') bin in the time-bin encoding.

Protocol 3 Double-Click entanglement generation protocol

1: A state is generated by the two nodes in the superposition $(|0\rangle + |1\rangle)/\sqrt{2}$.

2: The bright state $|0\rangle$ is excited and decays emitting a photon which is collected and sent through the fibre.

3: A BS in the central station removes the path information and sends the photons to the PBS, in case the polarisation modes are used. The PBS sends each mode to a different detector.

4a: If two detectors for different modes click, an entangled state has been generated and replies with a success signal to the nodes.

4b: Otherwise, repeat from step 1.

and the state that is generated can be approximated by

$$\rho_{DC} = \frac{f_{lm}}{2}\left[(1 \pm V)\,|\Phi_{01}\rangle\langle\Phi_{01}| + (1 \mp V)\,|\Phi_{11}\rangle\langle\Phi_{11}|\right] + \frac{1 - f_{lm}}{2}\left[|00\rangle\langle 00| + |11\rangle\langle 11|\right] \tag{3.19}$$

where the $\pm$ sign depends on the detectors that clicked, $+$ if both detectors belong to the same arm of the beam splitter (represented as D_1D_2 or D_3D_4 in fig. 3.2b) or $-$ if they belong to different arms (D_1D4 or D_2D_3). The detection of two photons with the same mode generates states proportional to $|\Phi_{j0}\rangle$ which can not be distinguished from each other and are therefore discarded. This introduces the factor of $1/2$ in eq. (3.18), since 2 out of 4 Bell states are discarded.

The quality of the generated state decreases not only with the light-matter state fidelity but also due to the beam splitter visibility, which affects the fidelity linearly in contrast to eq. (3.16) because two photons are interfering. The major difference with SC protocols is that there is no trade-off between success probability and fidelity. Moreover, the phase uncertainty that is introduced due to different path length now becomes a global phase, having no effect on the final state. Consequently, DC protocols are better suited for higher success probabilities, in situations where $p_{DC} > p_{SC}$.

Waiting Time The waiting time T_{gen} for MHEG protocols can be understood with a geometric distribution, which determines the probability that the t-th attempt succeeds after $t-1$ failed runs, [Brand et al., 2020]

$$\mathbb{P}\left[T_{gen} = t\right] = p_{gen}(1 - p_{gen})^{t-1} \tag{3.20}$$

where p_{gen} is the MHEG protocol success probability. Then, the average waiting time to create a link is

$$\mathbb{E}[T_{gen}] = \frac{T^*_{cycle} + 2T_{com}}{p_{gen}} \tag{3.21}$$

where $T_{com} = (L/2)/c$ is the time needed for a photon to reach the detector in the middle of two nodes separated a distance L. For long distances, $T_{com} \gg T^*_{cycle}$ leading to an entanglement generation rate that decreases proportional to $\exp(-L)/L$. Implying an average waiting time of $\sim 4\,\mathrm{s}$ for a transmission efficiencies of 10^{-4}, suggesting that nodes should be placed closer together to achieve rates larger than 1 Hz.

To slightly increase the rate, Humphreys et al. [2018] proposed a variation of the SC protocol (which can be extended trivially to DC) that deterministically delivers a state after a given cut-off time even though not a single attempt succeeded. In such case the state delivered can be classically-correlated ($F_{fail} = 1/2$) or completely mixed ($F_{fail} = 1/4$). Nevertheless, the final fidelity becomes $F = p_{succ}F_{succ} + (1 - p_{succ})F_{fail}$ so for low success probabilities we might have $F < 1/2$, which makes the state impractical for communication.

Moreover, the noise present in the devices as well as the imperfect generation of entangled states between pairs of nodes reduces the efficiency of straightforward application of entanglement swap. In fact, it leads to an exponential decrease in the fidelity of the state [Briegel et al., 1998]. Thus, it is necessary to have efficient methods that increase the fidelity of entangled states in order to achieve both a high rate and fidelity of the end to end link.

3.5 Entanglement Purification

EP protocols can improve the quality of the links using LOCC. The essential idea is to create several copies of a noisy entangled state and use them to obtain fewer entangled states of higher fidelity. There exist EP protocols that work on a single copy of the state, these are classified as filtering protocols [Horodecki et al., 1997] and although optimal schemes exist for certain states [Verstraete et al., 2001] it is not in general possible to increase the fidelity of a mixed state with this method [Kent, 1998; Linden et al., 1998]. Thus, we will focus only on the so called distillation protocols that, in analogy with the distillation process in chemistry which purifies a substance from a mixture, purify a state from an ensemble of mixed states.

All the protocols that we will introduce make use of two-way classical communication meaning that both nodes involved in the purification process can exchange any necessary information between them. One-way classical EP protocols exist and those are found to be equivalent to Quantum Error Correction (QEC) techniques [Bennett et al., 1996b; Dür and Briegel, 2007] but this software requires much better hardware than what is currently available and is expected to be implemented as part of third generation of quantum repeaters [Muralidharan et al., 2016].

A distillation protocol assumes the presence of an ensemble of m two-qubit states $\Xi = \{\rho_k \in \mathcal{H}_2 \otimes \mathcal{H}_2\}_{k=1}^{m}$ with a fidelity f_k to the target Bell state $|\Psi\rangle$. From Ξ, a subset of $d < m$ states are chosen according to a particular strategy and LOCCs are used followed by a final measurement on a part of these states. This measurement serves to obtain information about the $n < d$ remaining pairs which is used to either keep them or discard them. This ensures that a pair that is kept has a final fidelity f'_k that exceeds the original one f_k. This process can be iterated to discretely increase the fidelity up to a maximum value.

Protocol 4 DEJMPS

Setup Two nodes A and B share m BD-states ρ with fidelity $F > 1/2$.

Steps

1: Pick two states $\rho_1, \rho_2 \in \Xi_{BD}$.

2: Apply two bilateral local CX operators $\mathrm{CX}_{A_1 \to A_2} \otimes \mathrm{CX}_{B_1 \to B_2}$.

3: Measure qubits A_2 and B_2 locally in the σ_z basis and share the outcomes a and b.

4a: If $a = b$, discard the second pair and keep the first pair.

4b: Otherwise, discard both pairs.

The protocols explored in this project are DEJMPS [Deutsch et al., 1996] and Extreme Photon Loss (EPL) [Dam et al., 2017]. The former, named after its authors, operates on Bell-diagonal states, and in particular Werner states, while the later works with R-states (see eq. (3.14)). Apart from this difference, their implementation is the same. Both of them are $2 \to 1$ protocols, meaning that from the original set Ξ, $d = 2$ pairs are chosen to yield a single state at the end if success. Assuming that each link connects the nodes A and B, the protocol first applies a bilateral CX gate followed by a measurement of the target pair in the z direction. The outcomes are exchanged between both nodes and the control link is kept if both outcomes are the same in the case of DEJMPS* (see protocol 4) or if both outcomes are equal to 1 in the case of EPL (see protocol 5), the target pair is discarded in any case. Otherwise, the control pair is also discarded.

The final state in the case of perfect operations is another BD state with higher fidelity in the case of DEJMPS and an ideal EPR pair in the case of EPL. This is because EPL takes advantage of the classical non BD components which are ignored by DEJMPS. The increase in fidelity in the latter case can be described in terms of the original components. A BD state can be characterised

*Deutsch et al. [1996] formulated the original version of this protocol by considering the target Bell state $|\Phi_{00}\rangle$ this implied a preliminary step to swap the components of the states $|\Phi_{00}\rangle$ and $|\Phi_{01}\rangle$ which is skipped in our case as the target state is the latter.

by its diagonal components in the Bell basis $\{\lambda_{jk}\}_{j,k=0}^{1}$ where

$$\rho_{BD} = \sum_{j,k=0}^{1} \lambda_{jk} |\Phi_{jk}\rangle\langle\Phi_{jk}| \tag{3.22}$$

and $F = \lambda_{01}$ is the fidelity of the state. For two originally equal links, the final state has components

$$\begin{pmatrix} \lambda_{00} \\ \lambda_{01} \\ \lambda_{10} \\ \lambda_{11} \end{pmatrix} \longrightarrow \begin{pmatrix} \lambda'_{00} \\ \lambda'_{01} \\ \lambda'_{10} \\ \lambda'_{11} \end{pmatrix} = \frac{1}{p_{DEJ}} \begin{pmatrix} \lambda_{00}^2 + \lambda_{10}^2 \\ \lambda_{01}^2 + \lambda_{11}^2 \\ 2\lambda_{00}\lambda_{10} \\ 2\lambda_{01}\lambda_{11} \end{pmatrix} \tag{3.23}$$

where p_{DEJ} is the probability that both outcomes are the same, given by

$$p_{DEJ} = (\lambda_{01} + \lambda_{11})^2 + (\lambda_{00} + \lambda_{10})^2 \tag{3.24}$$

It has been shown that for any $\lambda_{01} > 1/2$ it holds that $\lambda'_{01} > \lambda_{01}$, being $\lambda_{01} = 1$ an attractive fixed point of the previous map Macchiavello [1998].

Protocol 5 EPL

Setup Two nodes A and B share m R-states ρ.

Steps Same as protocol 4, except

4a: If $a = 1$ and $b = 1$, discard the second pair and keep the first pair.

We might be tempted to go for EPL since it returns a perfect Bell state and the initial fidelity is not lower-bounded but this comes at the cost of discarding two times more links than DEJMPS, reducing the success probability to

$$p_{EPL} = \frac{f^2}{2} \tag{3.25}$$

where f is the fidelity of the an R-state. The output fidelity in the noiseless case is 1.

In any case, it is not well known how these protocols perform in the presence of noise. In fig. 3.3, the difference in success probability and fidelity can be seen for both protocols. The expressions used to derive them are found in appendix A. Although EPL has no limit on the initial fidelity, the low success probability for poor quality states represents a clear drawback. However, a single iteration of DEJMPS might not be enough to achieve the target fidelity so possibly more iterations are needed and compensate the low success probability of EPL.

Also, the noise limits the maximum achievable fidelity, which is lower than one in both cases as can be seen in fig. 3.3. For DEJMPS, this maximum fidelity is still an attractive fixed point for identical initial states [Pirker et al., 2017] but the minimum initial fidelity required increases, reducing the range for which this protocol improves the fidelity [Dür and Briegel, 2007].

In practical situations, the states fed into distillation will certainly be different due to the time dephasing introduced in quantum memories. In this situation, the final fidelity depends on the components of the target state [Dür et al., 1999]. For EPL, the state returned is a general mixed state with fidelity smaller than 1 but still larger than that of DEJMPS. Moreover, the noise introduced during distillation might too high and reduce the fidelity of the state instead of increasing it. This effect is clearly seen in the DEJMPS protocol.

Considering that both initial states are Werner states with fidelity F, the relative difference in fidelity $F'/F - 1$ after a single round of DEJMPS with output fidelity $F' > F$ is shown in fig. 3.4. The region where the fidelity improves is squeezed as the two-qubit gate error increases. Therefore, the restricted regime where DEJMPS can be used as well as the small improvement on the fidelity represents the major obstacle for the applicability of this protocol.

Other distillation protocols like BBPSSW [Bennett et al., 1996a] have been discarded due to the high amount of resources needed to converge to a perfect state. In fact, DEJMPS has been

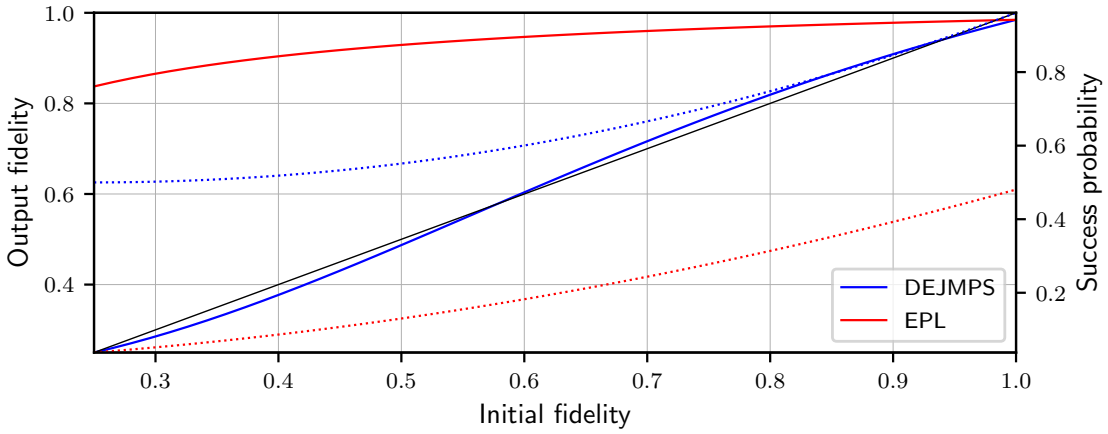

Figure 3.3: Comparison of DEJMPS and EPL protocols. Solid lines correspond to fidelity (left axis) while broken lines to success probability (right axis). The input states are identical Werner state for DEJMPS and R-states for EPL. This clearly shows the reduced success probability of EPL and the little increase over the original fidelity of DEJMPS. The error parameters used in the plot are $p_{2,gate} = 0.02$, $\xi_0 = \xi_1 = 0.99$.

proven to be optimal for BD states using numerical techniques [Rozpedek et al., 2018b] as well as machine learning methods [Wallnöfer et al., 2020]. Similarly, EPL has proven its advantage over DEJMPS with R-states [Rozpedek et al., 2018b].

3.6 Repeater Chain Network Protocol

As seen, performing consecutive entanglement swaps on a repeater chain decreases the fidelity of the links exponentially with every swap but the excessive use of distillation reduces the connection rate between the end nodes. Furthermore, EP is not useful in all cases introducing extra errors if it is not used in its working regime. We will now introduce the BDCZ protocol, named after its authors, which establishes how these two protocols can be put together to generate a final link [Briegel et al., 1998].

BDCZ uses a nesting strategy on a linear chain with $N = L^n + 1$ nodes, that is, $N - 2$ repeater

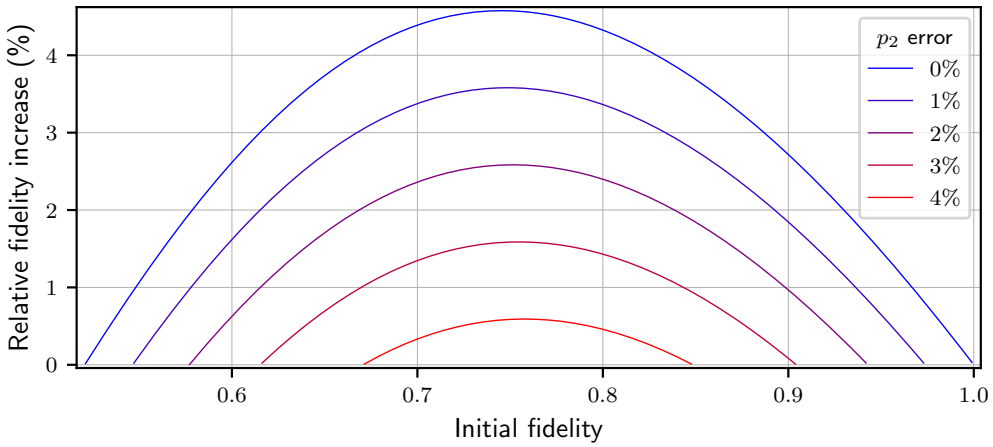

Figure 3.4: Relative improvement over the fidelity of a Werner state after one application of DEJMPS for different two-qubit gate error and fixed $\xi_0 = \xi_1 = 0.99$. The maximum tolerable error is $p_2^{max} = 4.59\%$.

stations and two end nodes. Here n identifies the number of nesting levels and L the number of links that are swapped without intermediate distillation. More concretely, a height $h = 0, \ldots, n$ is assigned to each node in the chain that depends on its relative position $j = 0, \ldots, N$ and it is determined by the relation

$$\begin{cases} j/L^{h_j} \mod L = 1 & \text{if } j > 0 \\ h_0 \equiv n \end{cases} . \tag{3.26}$$

Then, whenever two nodes with equal height are connected by an entangled pair, they can decide to swap or distill and swap. Once all links at a given height have been swapped, the level is increased and all nodes with a height smaller than the current nesting level do not interact anymore unless some step fails.

To give an example, consider the linear chain in fig. 3.5 with $N = 10$ nodes, $n = 3$ nesting levels and $L = 3$ nodes per segment. The nodes have height $h_3 = h_6 = 1$, $h_0 = h_9 = 2$ and 0 the rest. Initially, $N - 1$ elementary links are created between neighbouring stations. Then, nodes with $h = 0$ swap their links while the rest just hold them. For instance, nodes 4 and 5 swap their links connecting nodes 3 and 6. The same happens for other 0th level nodes until all nodes with height equal or larger than one are connected. At the following nesting level, nodes 3 and 6, which were before just holders, swap their links to finally connect the end nodes.

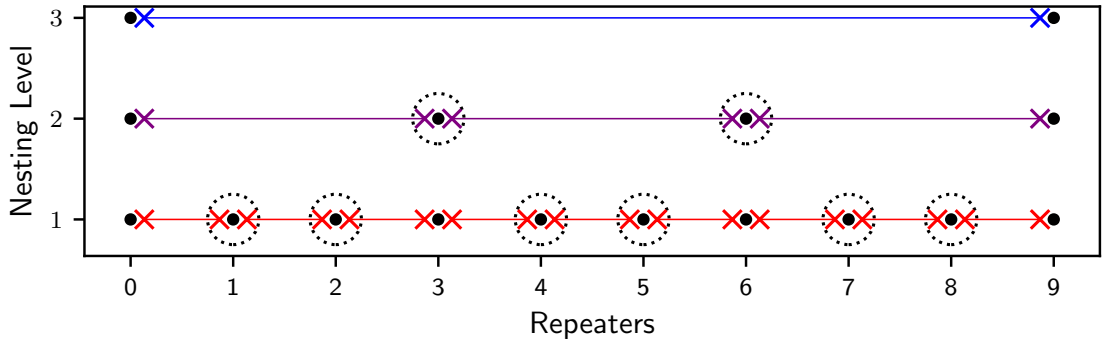

Figure 3.5: Schema of the nesting protocol for $L = 3$ and $M = 9$, N/L^k links are generated at each level k. The black circles represent the repeater stations which still hold entangled qubits (crosses), a dashed circle is drawn around the qubits that need to be swapped.

Distillation can be used at any stage before swapping. If at any level l the distillation between nodes jL^l and $(j+1)L^l$ fails, it is only necessary to recreate the links of previous levels in-between them. This reduces the amount of resources needed at the end. If M pairs are needed to purify a single one, the total amount of resources is $(LM)^n$ that results in a polynomial increase in the number of resources [Briegel et al., 1998].

In order to reduce the amount of time, the spatial resources are moved to temporal resources. That is, at a level l, instead of waiting for the M links to be generated, the distillation is done sequentially as soon as two links exist. This implies that a link is distilled M times with newly created pairs that have suffered from less dephasing. Using this temporal strategy, the expected waiting time T^l at the l-th level needed to purify a pair d times can be calculated using the iteration formula [Dür et al., 1999]

$$T^l_{k+1} = \frac{T^l_k + T^l_0}{p_{suc}(\rho_k, \rho_0)} \quad , \quad T^l_0 = T^{l-1} \tag{3.27}$$

where $p_{suc}(\rho_k, \rho_0)$ is the distillation success probability between a state ρ_k that has been purified k times and the new pair ρ_0. Here $1/p_{succ}$ takes into account the number of repetitions until a single step succeeds to which we have to accumulate the necessary time to create all previous pairs, T^l_k, as well as the new pair T^l_0. Concretely, for $l = 0$, T^l_0 corresponds to the entanglement generation waiting time in eq. (3.21).

Solving the recursion, one finds that the average waiting time to distil a pair d times is

$$\mathbb{E}[T_d^l] = \sum_{j=1}^{d} \left[\prod_{k=j}^{d} T_0^l \frac{1+\delta_{k1}}{p_{suc}(\rho_k, \rho_0)} \right] \approx \sum_{j=1}^{d} \left[\frac{2T_0^l}{p_{suc}(\rho_0, \rho_0)} \right]^{d-j} \tag{3.28}$$

where the approximation is valid when the success probabilities at the different k steps is similar.

When no distillation is used, BDCZ can be simplified to a swap as soon as possible (SWAP-ASAP) strategy which triggers the swap protocol as soon as a node has entanglement with both its neighbours [Coopmans et al., 2020]. The waiting time is thus much smaller and essentially dominated by the entanglement generation time (3.21) but the final fidelity, considering equal Werner states with fidelity F, decreases exponentially with the number of nodes [Briegel et al., 1998]

$$F_L = \frac{1}{4} + \frac{3}{4} \left[\frac{(1-p_{1,gate})^2 (1-p_{2,gate})(3+4(\xi_0\xi_1 - \xi_0 - \xi_1))}{3} \right]^{L-1} \left(\frac{4F-1}{3} \right)^L . \tag{3.29}$$

Taking all the advantages and disadvantages of the protocols explained in this chapter, it is not clear which one performs best. Furthermore, the answer might not be general but depend on the setup studied like the total distance to be covered, the number of nodes or the particular implementation used for the repeater stations. To shed some light into this problem, numerical techniques will be used in the following to find the optimal protocol and hardware parameters that allow us to achieve a certain end to end fidelity while keeping the generation rate high enough for communication.

4 Methods

> What we often forget is that a model is not a description of reality; it is a description of our assumptions about reality.
>
> — Jeremy Gunawardena, *Models in biology: 'accurate descriptions of our pathetic thinking'*

The goal of modelling a realistic repeater chain represents a hard analytical problem due to the large amount of parameters and situations that must be taken into account. It is usually necessary to assume specific scenarios or simplify the model which reduces its applicability. Here, the repeater chain will be simulated using Netsquid [Coopmans et al., 2020], the discrete-event quantum network simulator developed by QuTech. It allows for realistic hardware modelling in order to mimic state-of-the-art devices as well as its software. Using this simulation tool, GAs will be used to optimise a set of hardware and software parameters to achieve a target goal. Previous work has be done in this direction [da Silva et al., 2020] which will be extended to include EP.

4.1 Model

Coopmans et al. [2020] have worked on modelling a repeater chain in NetSquid implementing several protocols and strategies to connect two end nodes with an arbitrary number of intermediate repeaters forming a linear chain. This chain consist of N_{node} nodes separated by a distance L_{node} and connected by a classical and quantum channel between nearest neighbours. The nodes possess a quantum memory capable of storing a fixed number of qubits at the same time and a classical logic which controls the action to be done next in a queue of events. Those actions include MHEG, ES, EP and message handling occurring with different priorities according to the global network protocol in consideration. Thus, at each step a node looks for the next action in the queue and executes the corresponding tasks. The node is kept busy until all tasks finish, implying that only one action can be done at a time. Once it finishes, it repeats the process until no further action is found. The details about these actions are shown below.

Two network protocols are implemented: SWAP-ASAP and BDCZ, the first uses unordered entanglement swapping as soon as a node shares links with both its neighbours while the second performs distillation before links are swapped in a nested strategy as explained in section 3.6. The priority with which the actions are taken is ES → MESSAGE → MHEG for SWAP-ASAP and ES → EP → MESSAGE → MHEG for BDCZ. In both cases, ES is prioritised to connect end nodes as soon as possible and MHEG postponed until no other action can be done as it is the one that takes longer to complete. The major difference between both logics is the inclusion of EP before the message handling action, in which nodes process actions requested by its neighbours, as will be seen below.

The noise models implemented have been explained in section 3.3 and consist on depolarising noise for single and two qubit gates and initialisation, classical faulty measurements and time dependent memory decoherence.

To control the qubits that are in use, an entanglement tracker in each node keeps track of the links that it currently holds with information about the qubit holding the link, the Pauli correction needed to obtain the target Bell state $|\Phi_{01}\rangle$, the remote node to whom it is connected, the number of times it has been distilled and the creation time. This allows to choose the best link for each action. Also, by keeping track of the correction gates instead of applying directly, the error introduced with operations can be reduced as fewer gates are used.

At the end, the model will generate an entangled state between the end nodes for which we can compute the fidelity to the ideal Bell state $|\Phi_{01}\rangle$ and the rate at which it has been generated among other quantities. These two measures will be used the benchmark the quality of the setup considered. We must note that these measures are stochastic and therefore multiple runs have to be executed to estimate their actual value.

Entanglement Generation This action is responsible for the generation of elementary links between two neighbouring repeaters using a MHEG protocol. To that goal, the nodes have to negotiate the time at which the process starts taking into account the global network logic and the fact that only one action is allowed at a time. Hence, the agreement phase is done using the *initiator/responders* protocol used by Coopmans et al. [2020]. Odd nodes (nodes with 0 height in BDCZ) are the initiators and even or end nodes the responders. Initiators are responsible for checking if enough states are shared between each of their neighbours, if not, a message is sent to the corresponding node asking for confirmation to start the generation process. The responder will handle the message and answer back with a confirmation signal once it is ready, triggering the actual MHEG protocol.

In order to reduce the computational time, a simplified Magic Distributor [Avis et al., 2021] is used, a tool to generate entanglement without simulating every attempt. The distributor samples the successful attempt according to the geometric distribution in (3.20) with success probability p_{elem} and computes the total waiting time as in eq. (3.21). Then, the corresponding state is also sampled for each of the two possible detector outcomes (see section 3.4) and it is added to the QMem of the nodes. Finally, a message is sent to them with the outcome of the detector which allows the nodes to update their entanglement tracker and include the new link with any necessary Pauli correction.

In both MHEG protocols explained, the state can be modelled with a single parameter being the elementary link fidelity f_{elem} to the state $|\Phi_{01}\rangle$. Hence, any errors that affect the quality of the state are taken into account in this parameter, like the beam splitter visibility. Similarly, those errors that limit the generation rate have to be included in the elementary link success probability, like fibre transmitivity or detector efficiencies.

Entanglement Purification Both DEJPMS and EPL are $2 \to 1$ protocols therefore this process can only start if two nodes in the same level share two pairs. If more than two pairs are shared, then the two that have distilled the most or those that have been stored for the least amount of time are selected to be distilled. The one with least number of distillations or the older is the pair that is always discarded at the end of the protocol. Then, the first node that is available sends a request to distill to the other node and proceeds with the protocol and there is no need to wait for a confirmation signal. Once the second node processes the message, it will also execute the requested EP protocol. The outcomes of the measurements are exchanged and any necessary Pauli correction is added to the entanglement tracker if the attempt succeeded or the pair is discarded in case of failure.

Before EP starts, one must take into account that the links might not be targeting the state $|\Phi_{01}\rangle$. Thus, it is necessary that at least one node applies the necessary correction to the control link as explained by Coopmans et al. [2020].

Entanglement Swap This action is slightly different for the two network protocols. In SWAP-ASAP, a node checks if a pair is shared with any node to its left and any node to its right and executes the ES protocol if so. Instead, in the BDCZ, a node only checks if a pair is shared between both its neighbours in that nesting level and those pairs have already been distilled the necessary amount of times. Again, in the event that two or more links satisfy the conditions, the newer ones

are chosen to reduce the errors due to temporal dephasing. After the protocol finishes, the node notifies the neighbours about the swap, which include the information about the new repeater in the entanglement tracker.

Other techniques have been studied to select the best link to be swapped and distilled like cut-off strategies [Brand et al., 2020; Rozpedek et al., 2018a]. For instance, a temporal cut-off on the maximum storage time of a link can be set after which the pair is discarded. This has the potential effect of increasing the final fidelity at the cost of reducing the rate. The analysis of this technique lies out of the scope of this project but can be studied in the future projects.

Message Handling Processing of classical message sent between repeaters, which include requests to start MHEG or EP and the outcome of an ES or EP. We assume no error on classical messages, they always arrive to the receiver station, but of course the arrival is delayed by the light travel time in fibre.

4.2 Optimisation Algorithm

GAs are global optimisation algorithms based on the mechanics of natural selection and natural genetics. They combine survival of the fittest among individuals with the structured yet randomised information exchange to form a search algorithm. The combination of exploration with exploitation of extreme points makes it ideal to find the global solution on situations of major ignorance about it [Goldberg and Edward, 1989].

These algorithms also represent a clear advantage over deterministic methods like gradient descent when the optimisation function $\mathcal{F}$ is heuristic or non-differentiable since it doesn't make use of derivatives. Moreover, local methods are specialist in falling to the closest local minimum from the initial point thus failing in finding the global optimum. On the other hand, the random behaviour of GA might imply that one obtains different results for multiple runs. Therefore, a good strategy combining exploration and exploitation is needed to let the algorithm escape from local traps but converge to the best minimum found so far.

The optimisation process starts by creating an initial population with P_0 individuals, either randomly or in a latin hyper-cube structure to maximise the space covered. Each individual in the population is a collection of G parameters (genes) determined by the number of parameters to optimise. The fitness of each individual is evaluated and the best $P < P_0$ individuals are selected. Then, this population goes through the genetic operators. Typical implementations of a GA consist on four steps: selection, recombination or crossover, mutation and elitism. The first selects n_s individuals from the population, the second recombines them to form n_c children, the third mutates the gen of the $n_s + n_c$ individuals with probability p_m and finally the n_e fittest individuals are added to the new population to guarantee that the best ones are not lost during the process. The final population has $n_s + n_c + n_e \leq P$ individuals which is completed with $P - n_s - n_c - n_e$ fresh random ones. The process is repeated until the maximum number of generations n_g is reached.

The exact operators used are the roulette wheel method for selection which selects n_s parent individuals according to their fitness, i.e. better individuals have a higher change of being passed to the following generation. Concretely, the probability that an individual k is chosen is $\mathcal{F}_k / \sum_k \mathcal{F}_k$, where the sum runs over all individuals in the population. The recombination is a one-point crossover operator that generates a child by swapping two parents by a gene selected randomly. Two random numbers i_1 and i_2 sampled uniformly in the range $[0, n_s)$ determine the two parents and a third one $g \in [1, G)$ the gene. The child will have the first g genes from parent i_1 and the next $G - g$ from parent i_2. The process is repeated until n_c children are born. Mutation changes all genes of the individuals with probability p_m. The change is scaled by a factor $s_f \in [0, 1]$ that controls how much a gene should be changed from its previous value. That is, a gen $x \in [x_{min}, x_{max}]$ changes according to $x \to x + u(x_{max} - x_{min})$ where u is a random number sampled in the range $[-s_f, s_f]$. In case the final value falls outside the bounds $[x_{min}, x_{max}]$, the gen is mutated by sampling a random number x' directly in the allowed range, hence $x \to x'$. During the first generations, s_f is close to one to allow full space exploration while in later generation the factor tends to 0 to exploit any minimum found. Finally, the elitism operator ensures that the best individual is always kept

from generation to generation so n_e is typically just 1 as other *good* individuals can be selected during the selection operator.

Those same operators have been used by [da Silva et al., 2020] and proved to give good results in scenarios similar to the ones we will consider. The value of the selection, recombination and mutation parameters are not fixed but literature tells that good values for the operators are n_s $10 - 20\%$ of the initial population, n_c $60 - 70\%$ and $p_m < 0.1$ [Goldberg and Edward, 1989]. The initial population is not restricted to a fixed size but choosing a very big value can turn the GA into a brute force method. For that reason, P_0 is chosen to have twice the value of P. The last two parameters, population size and number of generations, will be selected depending on the setup in consideration and the size of the search space.

Even though the final solution returned by the GA with enough generations and population might be the global optima it can happen that it didn't converge to the exact minimum due to its inherent randomness. For this reason, we will complement the random exploration of GAs with a deterministic method. This will be executed for the best parameter set at the end to approach the solution to the minimum if necessary. The algorithm used is a variation of the iterative local search algorithm [Luke, 2013] which explores better solutions by slightly changing each parameter by a small amount h (see algorithm 1). The fitness is evaluated again with the change, in case this is smaller than the original, the mutation is accepted and the mutation with smallest cost among all parameters is finally used at the next iteration. If a parameter, after reducing its cost, does not satisfy the constraints or yields a higher cost then it is removed from the optimisation procedure. This process is repeated until there is no more parameter to optimise or the maximum number of iterations has been reached.

Algorithm 1 Iterative local search

```
I                                          ▷ Individual to optimise
P                                          ▷ Parameter set to optimise
f_best ← F
h ← 0.5
while P ⊈ ∅ do
    I_best ← I
    for p ∈ P do
        i ← REDUCE(I, p, h)                ▷ Returns a new individual with the gene p reduced by h.
        f ← F(i)
        if f < f_best then
            f_best ← f
            I_best ← I
        else
            P ← P \ {p}
        end if
    end for
    I ← I_best
    h ← h/2
end while
```

It is important to remark that there is no guarantee at first that allows us to determine whether the solution found by the GA is a global optimal and neither that the local search finds the exact local minimum. The results will have to be examined thoroughly to confirm it.

4.3 Simulations

The simulation allows to extract important information like the fidelity of the end-to-end link F and the rate at which it has been generated R. A high fidelity is needed to use the state for applications like distributed quantum computation or secret-key distribution [Wehner et al., 2018]. Similarly, high rates are needed to perform those applications within a reasonable time. Yet, a trade-off between the two quantities exist, as has been seen in some of the protocols explained,

which also depends on the quality of the hardware used. Gate errors and coherence times only affect the final fidelity but other parameters like the light-matter interface efficiency impact both quantities. Thus, the goal would be to find the set of hardware parameters that represent the least improvement over state-of-the-art hardware capable of achieving a given target fidelity F_t and rate R_t. The solution to this problem is not clear even if one considers a single protocol and thus we expect that multiple solutions exist per protocol. For this reason, GAs are used to find the optimal parameters. The abstract model consist of 22 parameters that can be distinguished into three categories: tunable hardware parameters (table 4.1), non-tunable parameters (table 4.2) and protocol parameters (table 4.3).

The collection of tunable parameters is composed of hardware properties that are part of the quantum architecture and include single and two qubit gate errors, cycle time duration or coherence times for instance. All those parameters have a baseline value, defined as the best value achieved by current technology, which can have been achieved in different experiments, and a perfect value that represents the ideal scenario. Then, we can define the cost k of improving a parameter x from its baseline x_b to the perfect value as

$$x = (x_b)^{1/k} \longrightarrow k = [\log_{x_b}(x)]^{-1} \ , \tag{4.1}$$

which models the progressive hardness of improving the quantity [Coopmans et al., 2020; da Silva et al., 2020]. The function grows monotomically in the range $[0, 1]$ and satisfies $x(k \to \infty) = 1$ showing that it is not possible to achieve a perfect value for that given parameter with finite resources.

Table 4.1: Tunable hardware parameters

Parameter	**Description**	**Ideal Range**
f_{elem}	Elementary link fidelity	$[f_{elem,b}, 1]$
p_{elem}	Elementary link success probability	$[p_{elem,b}, 1]$
$p_{1,gate}$	Single qubit gate error	$[0, p_{1,b}]$
$p_{2,gate}$	Two qubit gate error	$[0, p_{2,b}]$
$\xi_0,\ \xi_1$	Probability of measuring incorrectly the states $\|0\rangle$ and $\|1\rangle$ in the z basis	$[0, \xi_{j,b}]$
p_{init}	Qubit initialisation error	$[0, p_{init,b}]$
T_1 (ns)	Relaxation time	$[T_{1,b}, \infty)$
T_2 (ns)	Dephasing time	$[T_{2,b}, T_1)$
T^*_{cycle} (ns)	Intrinsic time needed to excite and emit a photon	$(0, T^*_{cycle,b}]$
t_1 (ns)	Single qubit gate duration	$[0, t_{1,b}]$
t_2 (ns)	Two qubit gate duration	$[0, t_{2,b}]$
t_{init} (ns)	Qubit initialisation duration	$[0, t_{init,b}]$
t_{meas} (ns)	Measurement duration in the z basis	$[0, t_{meas,b}]$
N_{qubit}	Number of qubits per node	$N_{qubit,b}, \ldots, \infty$

The parameters in table 4.1 have to be mapped to this range while satisfying that the perfect value is mapped to 1. For instance, coherence times are mapped using the relation $T \to 1 - 1/T$ which converges to 1 as T grows*. Gate error probabilities p are mapped as $1 - p$. Other parameters might be limited due to physical constraint like the cycle time in NV-centers as it depends on the relaxation time of the bright state. In those cases, the ideal value can not be reached and the range should be limited to the physically allowed range.

In any case, even if a perfect value can be achieved, the asymptotic behaviour of eq. (4.1) near the ideal value forbids this. Therefore, for computational purposes, the maximum value (after the map) will be limited to at most $1 - \epsilon$ where $\epsilon = 10^{-6}$.

*Another option would be to use eq. (3.6) but for the values of T_1 and T_2 considered this requires a higher precision than that supported by floating-point numbers in a standard computer. Thus, those expressions are approximated assuming $1/T \ll 1 \Rightarrow \exp(-1/T) \approx 1 - 1/T$, which tends slower to 0.

More details about the mapping are given in appendix B.

The non-tunable hardware parameters consist on values that are not part of the quantum architecture explicitly. Instead, they define the problem to be solved. For instance, one can pose the question of what are optimal tunable parameters to connect two end nodes at a total distance $L_{node}(N_{node}-1)$ using N_{node} repeaters given a certain value for the transmission loss in fibre γ and the speed on light in fibre. The last two depending on the material of the fibre which typically can not be chosen or modified. Similarly, the total distance between two nodes that might represent cities in a map is fixed but one could place more or less repeaters in-between. Despite that, they have an impact on the final fidelity and rate, for instance, longer distances or higher transmission losses are expected to result in a higher hardware cost.

Table 4.2: Non-tunable hardware parameters

Parameter	**Description**
γ (dB/km)	Transmission loss in fibre
c (km/s)	Velocity of light in fibre
L_{node} (km)	Internode distance
$N_{node} = N_{qr} + 2$	Number of nodes/quantum repeaters in the chain

Finally, the protocol parameters control the underlying logic of the repeater chain and do not have any cost. Despite that, they also influence the fidelity and rate and consequently a better protocol might imply a lower hardware cost. However, the answer to what is the best protocol for a particular set of hardware parameters is not known and therefore has to be optimised together with the tunable hardware parameters. For instance, EP can reduce the required elementary link fidelity but increase the elementary link success probability because more links are needed in the same time.

Table 4.3: Tunable protocol parameters

Parameter	**Description**	**Choices**
Logic	Global network logic to use	SWAP-ASAP, BDCZ
EP [a]	Entanglement purification to use per level	DEJMPS, EPL
d^a	The number of times to distill a link per level	$\mathbb{N}$

[a] BDCZ only. The number of levels is specified by N_{node}.

The question posed in this dissertation is encoded into the fitness function which consists on two terms: the parameter cost $\mathcal{C}$ and the penalty $\mathcal{P}$ for not achieving the target values. The parameter cost is the sum of all the individual costs (4.1),

$$\mathcal{C}(\{x_j\}) = \sum_j \left[\log_{x_{j,b}}(x_j)\right]^{-1} \tag{4.2}$$

and the penalty used is the squared difference between the target and the obtained value [Goldberg and Edward, 1989],

$$\mathcal{P}(\{y_k\}) = \sum_k [1 + (y_{k,t} - y_k)^2]\Theta(y_{k,t} - y_k) \tag{4.3}$$

where $y_k \equiv y_k(\{x_k\}), y_{k,t} \in [0,1]$ and Θ is the Heaviside theta function to ensure no penalty is applied when all targets are satisfied. Hence, the fitness function is

$$\mathcal{F}(\{x_j\};\{y_k\}) = \mathcal{C}(\{x_j\}) + A\mathcal{P}(\{y_k\}) \tag{4.4}$$

with a factor A is used to ensure that $C(\{x_j\}) < AP(\{y_k\})$ for any allowed parameter set $\{x_j\}$. For this reason, we add one to the penalty of each target, to ensure that $\mathcal{P} > 1$ for not satisfied

constraints, and consequently, the previous inequality holds. The form of this function forces the algorithm to find the optimal solution that achieves the targets, no matter how large the cost is. If no solution exists in this regime, the parameter set that deviates less from the targets is the one that minimises the fitness function.

The particularity of the fitness function allows to implement a local search method over the tunable hardware parameters because eq. (4.4) is a monotonically decreasing function as the parameters approach their baseline value until the penalties are no longer satisfied. Therefore, the `REDUCE` function introduced in algorithm 1 can be implemented as in algorithm 2 which changes the p-th parameter of the individual I by reducing its cost by h. Using this method, the cost of the hardware parameters can be reduced without changing the protocol parameters, that is, the same strategy is used at a smaller cost.

Algorithm 2 Cost reduction

procedure REDUCE(I, p, h)
  $k \leftarrow [\log_{p_b}(I_p)]^{-1}$ ▷ Compute the cost associated to p with baseline value p_b
  if $k - h > 1$ **then**
    $I_p \leftarrow (p_b)^{1/(k-h)}$
  else
    $I_p \leftarrow p_b$
  end if
  return I
end procedure

Even though the number of parameters that describes the model is reduced compared to a realistic hardware model, running an optimisation task with all of them becomes prohibitive as the size of the search space scales exponentially with the number of parameters. Therefore, a subset of these parameters, the ones that have a larger effect or whose quality is lower, will be selected for each particular optimisation.

Given that we want to explore the use of distillation, one parameter will be the global strategy to use, this maps integers to a particular network protocol. The GA explained only deals with floating-point numbers, but integer genes have to be treated slightly different. For them, the mutation scale factor is ignored and new integers are always sampled over the full range. This is because two consecutive integers might imply completely different strategies as seen in table 4.4. SWAP-ASAP is one of the possible strategies, together with EPL. The previous protocol generates states with close to unit fidelity after a single round so no extra iterations are considered. Instead, a maximum of 3 successful consecutive distillation rounds is limited with DEJMPS. We must remember that EP is probabilistic, and thus, it has an impact on the rate, as seen in eq. (3.28). The higher the amount of iterations, the larger the amount of links to be created, and the lower the final rate. Therefore, it might not be beneficial to iterate the protocol more times. Despite that, if at some point there is signs that more iterations could be helpful, that is, the GA converges to results using this last strategy. Then, more strategies will be included with four or more rounds of DEJMPS. Unless specified, the strategy parameter will range over these five possibilities in table 4.4. However, their actual meaning will depend on the particular situation in study.

Table 4.4: Mapping of integers to strategy, the use of an entanglement purification scheme implies BDCZ as network protocol.

Value	Strategy
0	SWAP-ASAP
1	EPL
2	DEJMPS (1 round)
3	DEJMPS (2 rounds)
4	DEJMPS (3 rounds)

Together with the strategy, we will also optimise over a subset of hardware parameters. da Silva et al. [2020] proposed to use the elementary link fidelity f_{elem}, elementary link success probability p_{elem}, relaxation time T_1, dephasing time T_2 and swap quality. The latter is defined as the depolarising error associated to a single application of protocol 1. Optimising over the elementary link parameters is necessary as their value for long distance connections is typically small [Bernien et al., 2013; Hensen et al., 2015]. Similarly, decoherence times represent a stepping stone in this process because links have to be created faster than those times to achieve high fidelities. The last parameter will be replaced by the two-qubit error noise parameter $p_{2,gate}$ that controls the depolarising noise of CX gates, the most used gate in all protocols considered and the one with a larger error (see table B.1). The way in which they will be optimised will be explained in the corresponding sections as several methods can be used depending on the protocols.

The target values correspond to the end-to-end fidelity F and generation rate R, the drawback being that those values are probabilistic. Consequently, the penalty is evaluated on the average value $\overline{F}$ and $\overline{R}$ over multiple runs. In previous work, considering only SWAP-ASAP, the target fidelity was of 0.7. Here, owing to the use of EP, we expect that better fidelities can be reached so the two pairs of target values considered will be: $(F_t = 0.8, R_t = 1\,\text{Hz})$ and $(F_t = 0.9, R_t = 0.1\,\text{Hz})$. A priori, the latter can favour the use of distillation due to its higher target fidelity, although noise might forbid to achieve such value in some cases.

Optimisation tasks will be run for a fixed combination of L_{node} and N_{node} spanning countrywide distances, so $> 100\,\text{km}$. The latter is limited to $N_{node} = 2^n + 1$ in the BDCZ protocol, where $n \in \mathbb{N}$ is the number of nesting levels.

The simulations are executed on the High Performance Computing facility in the Netherlands. The super-computer used is the Cartesius system which consist on nodes between 16 and 64 CPUs [SURFsara, 2021] in which we can parallelise the fitness evaluation of the individuals within a generation. The most common node has 24 cores so the population size will be a multiple of this number to take all the advantage from this parallelisation. Concretely, we empirically found that $5 \times 24 = 120$ individuals per generation and 250 generations was enough to converge to a solution in most situations studied. The computational time increases exponentially with the number of nodes, a single execution of the simulation for 2 nodes takes 0.5 ms, increasing to 100 ms for 9 nodes. Implying a total running time from 30 min for 2 nodes to 3 days for 9. For this reason, chains with at most 9 nodes ($n = 3$) will be considered.

The rest of the GA will be fixed in all simulations, these being $n_s = 24$, $n_c = 72$ and p_m to one over the number of parameters. The amount of parameters changes with the setup studied but ranges from 5 to 7. For the local search method, an initial value of $h = 0.1$ is used with a maximum of 10 iterations. All these values were found to give good results in practical situations. The exploration of how these values could be modified to speed up the convergence of the algorithm falls out of the scope of this thesis.

A problem that is encountered is that an individual that satisfies the targets in one generation might not do so in the next one due to the stochastic nature of the simulation. Consequently, a high cost will be assigned to the individual and might be forgotten, affecting the convergence of the algorithm. Despite that, we expect that the form of the penalty mitigates this problem. Hence, even if a good individual does not satisfy the targets in one generation, the distance from the target values might be smaller than other less optimal individuals and therefore kept for the next generation during the selection process. Furthermore, the average values will be computed with enough points as to reduce this uncertainty. Concretely, 200 points will be used for 2 and 3 nodes and 100 for 5 and 9 nodes as a balance between computational time and accuracy. This can be done for a large amount of nodes because more links are being generated and distilled so the final values represent already an average.

5. Results

> The ability to understand something before it's observed is at the heart of scientific thinking.
>
> — Carlo Rovelli, *The Order Of Time*

This chapter explores the results that have been obtained with different entanglement distillation strategies and entanglement generation protocols. The model is validated against a full hardware simulation, in particular, the platform considered during this section in based on a NV-center QR. Then, GAs are used to obtain optimal solutions to the problems posed in each section. Finally, the comparison of all the results is done as to determine the optimal setup to connect two nodes at a certain distance.

5.1 Validation

As has been mentioned throughout this work, the abstract model is designed to reduce the amount of required parameters. Nevertheless, care must be taken before disregarding some of them. To benchmark the accuracy of the fidelity and rate using our abstract model, we compare the results with those obtained running a hardware specific model simulating a NV-center repeater chain in [Coopmans et al., 2020]. There, the fidelity and entanglement generation rate were measured for a linear repeater chain with 0 (direct connection) and 3 repeaters. Entanglement generation was done using SC and the network protocol used was SWAP-ASAP. Also, a restricted topology was considered, with one qubit being the electron or communication qubit, and the others being the carbon qubits. The two types of qubits have different errors parameters and the particularity that only the electron qubit can generate entanglement with another node.

In our case, all qubits are assumed to be identical, discarding any restrictions on the topology. The properties of these abstract qubits are taken as the most pessimistic ones in case of discrepancy between the electron and carbon qubits. This choice was made to compensate part of the errors that are ignored due to the unrestricted topology.

The MHEG is modelled as the generation of an R-state (eq. (3.14)) that succeeds with probability (3.15). The fidelity of the state is evaluated using eq. (3.16), which takes into account the beam splitter visibility, and the dephasing introduced due to double excitations and phase uncertainty. To simplify the notation, all parameters that reduce the fidelity of the elementary links are condensed into the state efficiency parameter η_f, defined as $f_{SC} = (1-\alpha)\eta_f$. Such that, comparing with eq. (3.16), yields

$$\eta_f = \frac{1+\sqrt{V}}{2}(1-p_{ph}) \ . \tag{5.1}$$

A second approximation used is the one proposed in [Humphreys et al., 2018] which assumes perfect state efficiency, $\eta_f = 1$. In both cases, dark counts are disregarded and the bright-state population is fixed to $\alpha = 0.1$. The three models are compared for two parameter sets, the first uses near-term

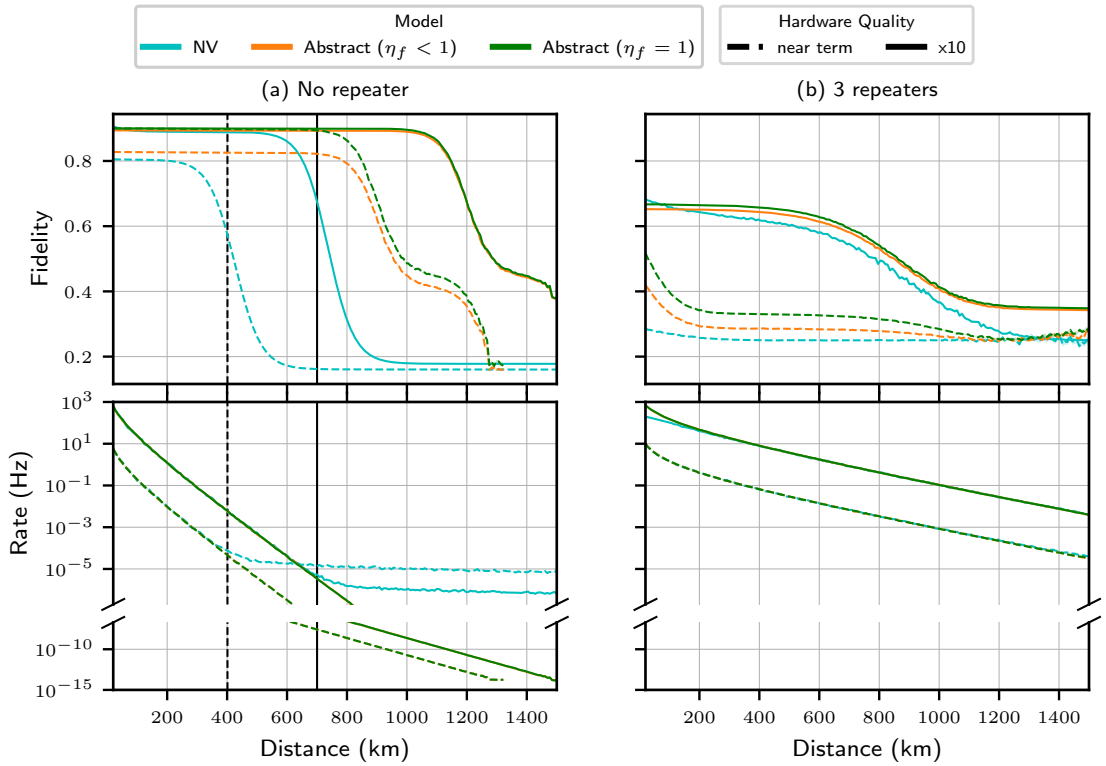

Figure 5.1: Comparison of NV-center model in [Coopmans et al., 2020] (cyan) with the abstract model using two approximations for the elementary link fidelity: in orange, with imperfect state efficiency; and in green, with perfect state efficiency. The distance is defined as the total distance between the end nodes. The vertical black lines denote the distance at which the transmission efficiency is comparable to the dark count probability. For 5 nodes, this occurs at a distance larger than the ones considered.

hardware values and the second an improved set of parameters from the near-term ones. The exact parameters used are shown in table B.1.

Another noise parameter that is neglected is the induced dephasing T_2^* for each entanglement generation attempt [Kalb et al., 2017, 2018]. Hence, we just consider the memory dephasing T_2 which is several orders of magnitude larger. Still, we expect that it does not have a large effect on the results, specially when EP is used as other noise sources will become more important. Despite that, the comparison will help us determine whether this can also be done with SWAP-ASAP.

The fidelity and rate obtained with near-term and improved parameters compared to the original data (NV) in [Coopmans et al., 2020] can be seen in fig. 5.1. We remark that the two abstract models only differ in the value of η_f, which only affects the elementary link fidelity, so no difference is expected on the rate between them.

Starting with the no repeater scenario, we can appreciate good agreement in the rate when $\eta_{trans} > p_{dc}$. After this point, the rate in the abstract model continues to decrease exponentially, whereas the NV model stabilises, showing that the absence of presence of photons is balanced by random dark counts. The most important difference occurs in the fidelity, even in this regime. The NV model always gives a lower value, as expected, but for near-term hardware, the abstract model with perfect state efficiency deviates by more than a 10%. The more realistic model ($\eta_f < 1$) does give a better approximation when $\eta_{trans} \ll p_{dc}$, but we can see that the fidelity decreases much after $\eta_{trans} \approx p_{dc}$, showing that dark counts have a larger effect on the fidelity than on the rate. Despite that, for distances where the achieved rate is higher than 0.1 Hz, the difference between the expected fidelity is $< 3\%$ with imperfect state efficiency. With improved hardware, both abstract models give accurate values for the target metrics in the regime where dark counts can be neglected.

Going to the three repeaters case, we see that the rate is almost identical for all the distances considered because the internode distance is never large enough to have to take into account dark counts. On the contrary, similar to the previous scenario, the fidelity achieved is slightly higher than the NV model, being the abstract model with $\eta_f < 1$ the one that reaches a closer value. Nevertheless, the difference is much smaller than in the previous case due to the higher amount of operations and storage time needed, which take a much more important role than the errors introduced during the creation of elementary links. However, there is one region with improved hardware where the fidelity in both abstract models falls below the NV one. The same region shows the largest deviation from the expected rate. This can be due to the choice of parameters made, the nodes considered combine the most pessimistic properties of electron and carbon qubits but also the unrestricted topology. At such short distances, the time spend mapping electron to carbon states becomes important as to give a lower rate. Even though this is neglected in the abstract models, the higher noise that is introduced in each operation, in spite of having less operations, does reduce the fidelity as compared to the NV model.

Of course, part of the disagreement in the fidelity can be a consequence of neglecting the induced dephasing in the carbon qubits. There is, however, no clear reason to include the extra parameter in the model, since the agreement between the NV and the most realistic abstract model is below 3% when the rate is above 0.1 Hz.

All in all, it is possible to conclude that the abstract model does give an accurate description of the rate in the regime $\eta_{trans} > p_{dc}$, showing that it is possible to disregard any restriction on the topology. The fidelity is better approximated with eq. (3.16), although the difference between the two abstract models is reduced if three repeaters are used. During the optimisation task, assuming $\eta_f = 1$ can lead to more optimistic results, specially in the no repeated case, but the amount of parameters to consider is also smaller. Both characterisations should be considered in an optimisation task to decide which one is better suited to describe the abstract repeater chain.

5.2 Uniform Distillation Strategy

The first strategy that will be explored is inspired in the proposal made by Briegel et al. [1998] which considered a uniform distillation strategy across all levels, that is, all links are distilled with the same protocol at all nesting levels. Originally, only DEJMPS was considered with BD states and EP was iterated until the fidelity of the state exceeded a fixed threshold. In our case, the fidelity of the state is not known, and therefore, we propose a fixed number of distillations M, equal for all levels. Another difference is that we also allow for EPL to be used. Hence, the optimisation will let the algorithm explore the five network protocols in table 4.4, where each one gives the protocol to use at all nesting levels. For instance, the second strategy corresponds to a choice of BDCZ for the network protocol and two successful distillations using DEJMPS before a link can be swapped.

The baseline values for the parameters are show in tables B.1 and B.2. These do not include the elementary link success probability and fidelity as they are not primary hardware quantities, but they are derived from others. Moreover, they depend on the MHEG protocol used. In this section, SC is investigated so these two parameters can be evaluated from eq. (3.15) and eq. (3.16), respectively. Despite that, the choice of the optimal bright-state population α is uncertain. Optimal solutions exist for single-repeater scenarios but those do not include EP schemes [Rozpedek et al., 2019]. Therefore, three methods are proposed to deal with this problem.

The first uses an unrestricted strategy, as explained by da Silva et al. [2020], the baseline fidelity and success probability are estimated by sweeping over all $\alpha \in [0, \frac{1}{2}]$. Then, the highest ones are chosen, independently from each other. Those values depend on the inter-node distance and are computed including dark counts. Given that a symmetric linear repeater chain is considered, the same value of α can be used in all segments. The optimisation then runs directly over these parameters, thereby no trade-off is imposed between the two quantities. The potential problem of this method is that both parameters can be made high at the same time without any constraints, leading to results that might be unphysical.

The other two methods use a restricted strategy. In both, the bright-state population is considered as a tunable parameter and included during the optimisation. Hence, the trade-off between the two quantities is considered. The difference between them is in the fidelity estimation,

just like fig. 5.1. The first model takes the errors during the generation of the link into account in the state efficiency, and therefore, it provides a better approximation to the fidelity. This parameter η_f will also be included during the optimisation, the baseline value can be calculated from other quantities in table B.2 using eq. (5.1). The second model disregards errors that affect the elementary link fidelity, $\eta_f = 1$. It gives good results with improved hardware or three repeaters and reduces the amount of parameters to consider. In both cases, the light-matter interface efficiency η_{lm} will be optimised, whose baseline is derived from other NV-hardware specific parameters as explained in section 3.4. As seen during the validation, setting $\eta_f = 1$ gives more optimistic results than the full model but the benefit of reducing the amount of parameters is clear. Despite that, the addition of a hardware parameter does not increase the difficulty of the problem to a large extend, as the solution is expected to behave continuously for a fixed combination of protocol parameters.

In the three methods, the hardware parameters discussed in section 4.3 will be optimised. These being the relaxation time T_1, the dephasing time T_2 and the two-qubit gate error $p_{2,gate}$.

The optimisation results will certainly allow us to decide which is the best method to use in follow-up sections, but most importantly, we would like to see the consequences of using entanglement distillation with quantum repeaters. Thus, it will be interesting to see in what cases does exist a solution that outperforms SWAP-ASAP, but also analyse those for which there is no solution in order to surpass any limitation with better strategies.

The optimisation task will be run for 3 different end-to-end distances ranging from 200 km to 800 km, and 4 different numbers of repeaters, including the no repeater scenario. The target values considered are $F_t = 0.8$ and $R_t = 1\,\text{Hz}$. The results for all three methods are shown in fig. 5.2 where the optimal strategy* is marked for each pair of number of nodes and total distance. All pairs have been executed, but only those for which the GA has found a solution are plotted. The complete set of results can be seen in appendix C.

Before going into the details, we already note that the more realistic the method is, the fewer the amount of convergent simulations. Clearly, the trade-off between fidelity and success probability represents the major drawback because it is not possible to attain both high quality links and rates for large distances. In fact, no solution is found for 800 km in any of the two restricted methods, and just one for 400 km with perfect state efficiency. This clearly reduces the applicability of the unrestricted method and forces the use of the more complex situation in which the bright-state population is also optimised.

In all cases, we see that at least one of the final values – fidelity or rate – is almost equal to the desired target. Thus, proving the successful convergence of the GA to a solution conditioned by the target values. The other value that is further away from the target might be because, either the state-of-the-art hardware is already good enough, or there is no gain in reducing the quality of the parameters as the penalty function considered (eq. (4.3)) does not take into account the distance from the targets if the threshold values are reached.

The parameter cost, specially in the unrestricted method, follows an expected behaviour that we will see hereafter. The total hardware improvement grows exponentially with the distance and number of nodes, which is expected on account of the form of the cost function (4.1). The distance directly affects the elementary link properties, therefore the hardware that creates those links has to be better. Also, they have to be maintained for a larger amount of time due to the larger communication time between stations, so higher dephasing times are needed. Despite that, we see that T_1 is not improved from the baseline, showing that the current value of 1 h is already large enough. The number of nodes has a larger effect on the two-qubit gate, as more operations are done.

The cost and its distribution among the different parameters is directly correlated with the strategy used. For instance, in the case of direct connection, no EP, the only parameters improved are f_{elem} and p_{elem} because the number of operations and storage time are negligible. With one repeater, the two restricted methods converge to a solution using EPL which is the optimal EP protocol for R-states. The parameter that is improved the most is the light-matter interface, to increase the elementary link success probability, mainly because links have to be regenerated in case the EP fails, but it allows to keep the state efficiency at its baseline value. For larger distances, it is necessary to use three repeaters, but a solution only exists in the method that assumes perfect

*There is some abuse in the notation as a network protocol is compared with two EP protocols. Of course, the use of EP implies using BDCZ as the network protocol.

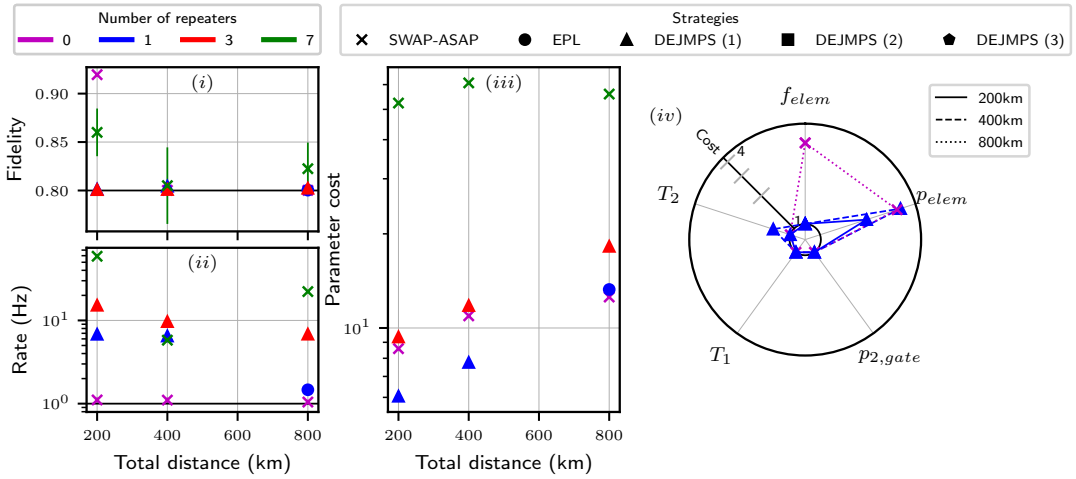

(a) Unrestricted method.

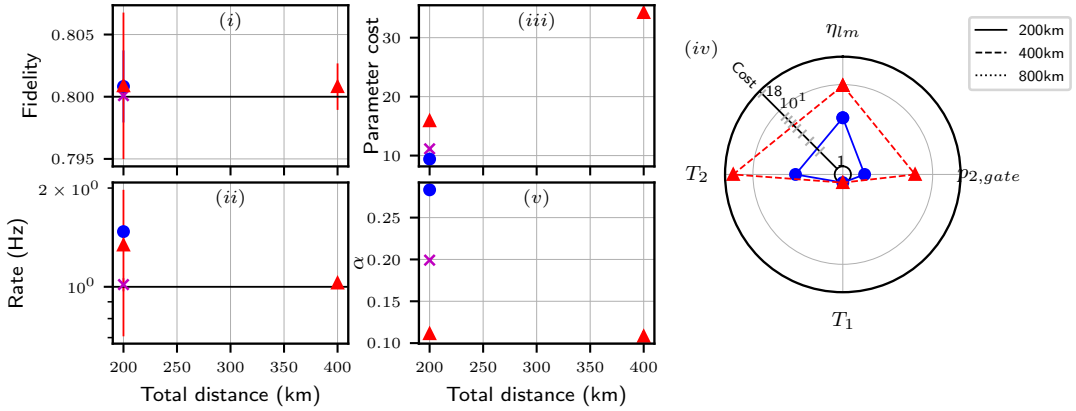

(b) Restricted method with $\eta_f = 1$.

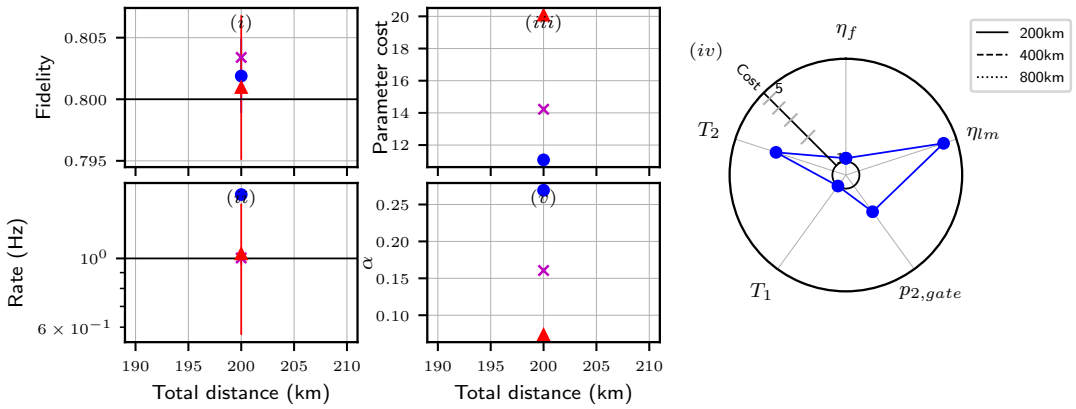

(c) Restricted method optimising over η_f too.

Figure 5.2: Optimal solutions with an uniform distillation strategy satisfying the targets $F_t = 0.8$ and $R_t = 1\,\text{Hz}$. Each point shows the optimal protocol used (markers) for each of the 12 combinations of number of repeaters (colours) and total distance between end nodes (x axis/line styles). All simulations have been run but only those that converged are shown. $(i - ii)$ the end to end fidelity and entanglement generation rate respectively. (iii) the total parameter cost. (iv) the cost associated to each of the tunable hardware parameters individually, only the optimal solution per distance is shown. (v) (for the restricted methods) the optimal bright-state population.

state efficiency. In this case, the EP protocol used is DEJMPS, which is not optimal in terms of fidelity but can achieve higher rates due to its higher success probability (see fig. 3.3). This can help us explain why no solution is found with imperfect state efficiency. In such case, the lower elementary link fidelity might forbid to achieve the target fidelity unless EPL is used but the reduction in success probability forbids to achieve the target rate. Besides, we can see that the total parameter cost is smaller with perfect state efficiency. Hence, the small difference that was accounted in fig. 5.1 has a huge impact during the optimisation procedure.

Therefore, in order to give realistic results, it is necessary to include the bright-state population during the optimisation, when working with SC. Furthermore, because the convergence of the algorithm was not affected by the addition of an extra hardware parameter, we will use the last method, that optimises over the state efficiency, in following sections. Using the most realistic method (fig. 5.2c), we already see a situation in which BDCZ with EP outperforms SWAP-ASAP. At a distance of 200 km, we see that the optimal solution corresponds to one QR with EPL. The improvement over hardware parameters is distributed among η_{lm}, $p_{2,gate}$ and T_2, being the light-matter interface efficiency the one that has to be increased the most, from 0.46% to 30.57%. The chain can tolerate two-qubit errors of $\sim 1\%$ and requires a dephasing time of $\sim 3\,\mathrm{s}$.

Despite that, no other solution is found for larger distance which suggest that a uniform distillation strategy is not optimal. In fact, we can deduce that a better strategy would be to use EPL in the lowest level, where the states are R-states, and DEJMPS in upper levels since the output of EPL is approximately BD. We will look deeply into improved strategies in the next section.

5.3 Level Dependent Strategy

As said, the best strategy might be a combination of both EP protocols. Hence, during this section, we will let the algorithm decide the optimal strategy per level, without any restriction on the protocol. That is, for each nesting level, the five strategies in table 4.4 are allowed, implying a total of 5^n global strategies S on a chain with n nesting levels, $2^n + 1$ nodes. Then, the strategy in the l-th level s_l ($0 \leq l < n$) is given by $s_l = S5^{-l} \mod 5$ where $S \in [0, 5^n)$ and $s_l \in [0, 5)$ maps to the five strategies mentioned before. A level with $s_l = 0$ means that links are directly swapped without going through a distillation procedure. By giving full freedom on the network strategy, we expect the GA to find more situations in which the use of EP reduces the hardware cost needed to generate the end-to-end link. Nevertheless, the increased amount of strategies has been seen to decrease the convergence rate of the GA when $n > 1$ due to the non-linearity of this parameter. For this reason, optimisation tasks with 3 and 7 repeaters will be run for two times more generations, $n_g = 500$.

In this case, we will also study DC, as well as SC. The elementary link parameters differ between the two MHEG protocols, and for this reason, it is not possible to include the choice of MHEG directly into the GA, but we will have to optimise them independently. The exact details are found in the corresponding sections below.

The analysis will be done for the same pairs of number of nodes and total distance between as before. Two pairs of target values will be considered: ($F_t = 0.8$, $R_t = 1\,\mathrm{Hz}$) and ($F_t = 0.9$, $R_t = 0.1\,\mathrm{Hz}$); where we expect that the latter will favour EP due to its higher fidelity threshold and its reduced rate, thus allowing the protocol to fail more times.

5.3.1 Single-Click

The study of SC will be done using the most realistic method in section 5.2, which includes the bright-state population and the state efficiency in the optimisation. The seven parameters to be optimised can be found in table C.5.

Figure 5.3 shows the results obtained for the two pairs of target values. Clearly, letting full freedom on the strategy gives many more solutions. In fact, in all cases with at least one repeater, the optimal solution found use an EP protocol. Moreover, the strategies only use this protocol in the lowest level ($l = 0$) while in upper nesting levels, for chains with 3 and 7 QRs only, links are directly swapped. For this reason, the protocol shown in the plots corresponds to the one used when $l = 0$.

In general, the solutions found have a tight fidelity threshold whereas the rate is, in some situations, one order of magnitude above the target one.The limiting factor thus corresponds to the end-to-end fidelity. Looking at the protocol, we see that in all situations the optimal solution found uses EPL in the lowest level, except one with 7 repeaters at 800 km in fig. 5.3a which uses two rounds of DEJMPS.

Focusing on the first set of solutions, the convergence to EPL reflects the optimallity of this protocol with the elementary links generated by SC. In those cases, almost no improvement is needed on the state efficiency when the target fidelity 0.8. Nonetheless, because no other purification step is done in upper levels, the other noise parameters, T_2 and $p_{2,gate}$, have to be improved. In contrast, when the target fidelity is 0.9, it is not enough to improve the noise parameters alone, but the state efficiency has to be larger than the baseline too. A proposed solution that could reduce

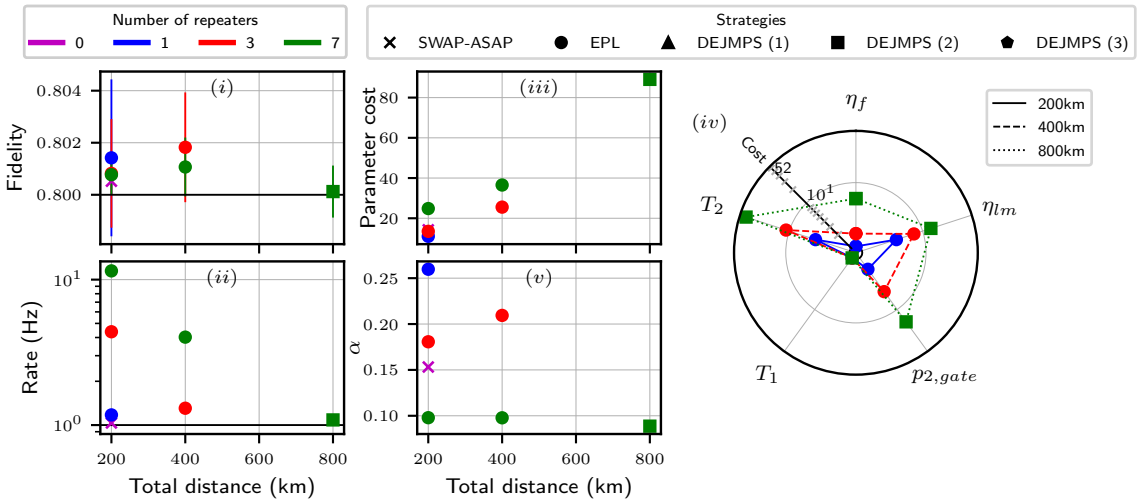

(a) $F_t = 0.8$ and $R_t = 1\,\text{Hz}$

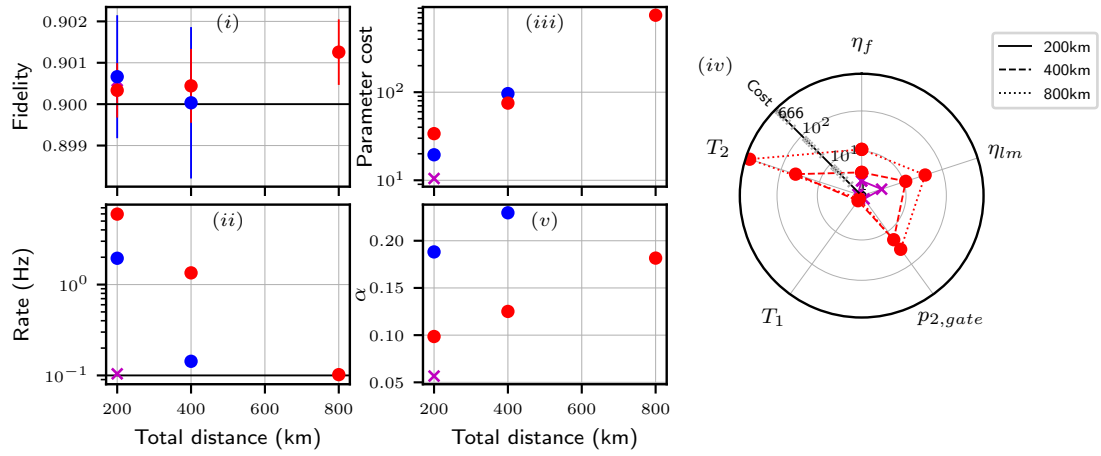

(b) $F_t = 0.9$ and $R_t = 0.1\,\text{Hz}$

Figure 5.3: Optimal solutions with a level dependent distillation strategy and single-click MHEG protocol. Each point shows the optimal protocol used in the lowest level (markers) for each of the 12 combinations of number of repeaters (colours) and total distance between end nodes (x axis/line styles). Note that the EP protocol corresponds to the one used at the lowest level since no solution was found using distillation in upper levels. $(i - ii)$ the end to end fidelity and entanglement generation rate respectively. (iii) the total parameter cost. (iv) the cost associated to each of the tunable hardware parameters individually, only the optimal solution per distance is shown. (v) (for the restricted case) the optimal bright-state population.

the requirements on the noise parameters was to use DEJMPS is upper levels, but the algorithm found this strategy less optimal. On the one hand, the probabilistic nature of EP has an impact on the rate as links have to be recreated if the protocol fails. Therefore, performing a purification step in upper levels might imply that no solution exists for the studied rates, similar to what happened in fig. 5.2. On the other hand, the number of two-qubit operations will grow, so more noise will be introduced in the system. Furthermore, if the initial fidelity does not fall within the distillation range, as seen in fig. 3.4, then DEJMPS could decrease the fidelity of the state and forbid any solution satisfying the target. This can help us understand why the solutions found use EP only at the lowest level.

An exception is encountered for 800 km with target values $F_t = 0.8$ and 1 Hz. The solution there employs two rounds of DEJMPS in the lowest level, that is, an elementary link has to be successfully distilled with two other elementary links before it can be swapped. It is remarkable that it does not make use of EPL like all the other setups considered. The reason has to lay in the target rate, which we see that is already tight to the desired value. This implies that the success probability of two iterations of DEJMPS has to be larger than a single step with EPL. Otherwise, there should exist a lower cost solution with EPL that the GA could not find. The optimal parameters for this solution can be seen in table C.6c, combining the bright-state population with the state efficiency gives an $f_{elem} \approx 0.8978$. The two-qubit gate error found is 0.12% and, if we ignore other errors, we can approximate the success probability of DEJMPS and EPL with eq. (3.24) and eq. (3.25) respectively, giving $p_{DEJ} = 0.8158$ and $p_{EPL} = 0.4030$. Indeed, two iterations of DEJMPS have a success probability of $p_{DEJ}^2 = 0.6654$ larger than p_{EPL}, showing that the latter protocol cannot achieve the target rate with less than or equal cost. Despite that, the use of DEJMPS forces the state efficiency to be improved from 91.96% to 98.52% to compensate the small increase in the fidelity.

The other hardware parameters follow the expected behaviour, their value increases with the number of nodes and the distance, except T_1 which remains at the baseline value. In particular, it is interesting to see that both solutions with three QRs in fig. 5.3b converge to a similar value of $p_{2,gate}$, 0.11% for 400 km and 0.06% for 800 km. Neither the number of nodes or the strategy changes, showing that the value of this parameter does not depend, to a large extend, on the distance covered.

In any case, we can see that the use of EP outperforms SWAP-ASAP, thus proving that it helps at lowering the hardware requirements. In only one case, at 200 km for the second pair of targets, the optimal solution is the no repeater scenario.

Finally, we note that there are no solutions with 7 repeaters for the second pair of targets. Yet, there exist solutions satisfying the much more demanding rate in fig. 5.3a. Hence, the constraint that is not satisfied must be the minimum fidelity of 0.9. In fact, we can estimate the end-to-end fidelity for the simplest strategy, that is SWAP-ASAP, using eq. (3.29). Assuming perfect two-qubit gate and elementary link fidelity, we arrive at a final fidelity of $F_8 = 0.883$, below the target value. Hence, the noise introduced in measurements and single-qubit gates becomes significant in this situation.

To overcome this limitation, simulations have also been done considering other operational errors during the optimisation, but without increasing the search space. The parameter $p_{2,gate}$ is replaced by $k_{gates} \in [1, 10^4]$, which determines the cost of individually improving the single and two qubit gate, initialisation and measurement errors. Therefore, the total cost is five times k_{gates}. The maximum value is chosen such that the search space for the two-qubit gate error is the same as before. Also, the strategy will be limited to the lowest level only and swap is enforced in upper levels. This change is motivated by the previous results found, and helps at removing the exponential increase in the search space with the number of repeaters. Thus, we can fix the number of generations to $n_g = 250$.

The optimisation results can be seen in fig. 5.4 with several points of interest in the two plots.

Firstly, the strategies found in fig. 5.3a are the same as in fig. 5.4a except for the solution at 800 km. The cost distribution among the parameters of these shared results is similar, the two that are improved the most are η_{lm} and T_2 whereas η_f and T_1 remain at their baseline value. There are of course small differences, we must remember that the total cost of improving the two-qubit gate is higher here than before because four other gates are also enhanced. Thus, the optimal solution for 200 km, which uses just one repeater, does not improve those gates. Consequently, T_2 and η_{lm} are

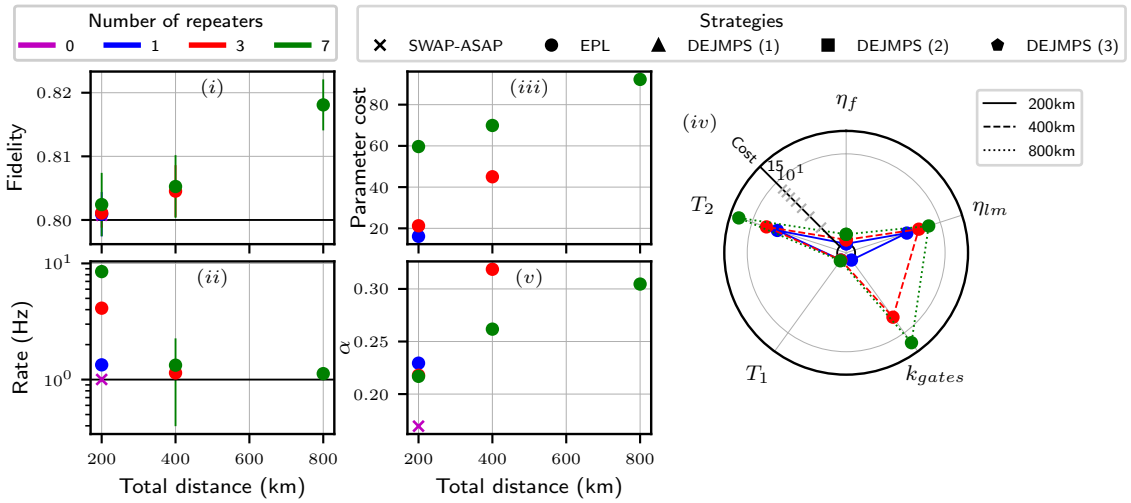

(a) $F_t = 0.8$ and $R_t = 1\,\mathrm{Hz}$

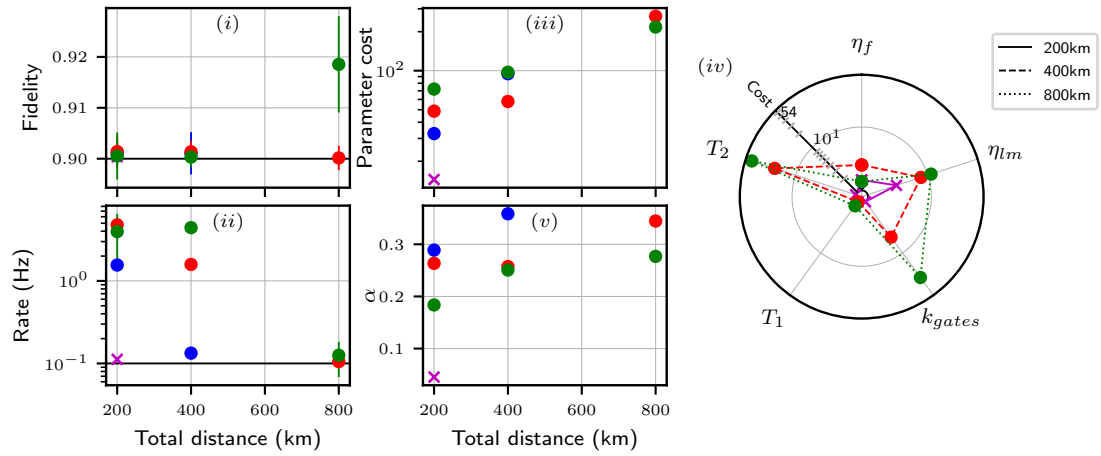

(b) $F_t = 0.9$ and $R_t = 0.1\,\mathrm{Hz}$

Figure 5.4: Optimal solutions with a level dependent distillation strategy and single-click MHEG protocol optimising over all gate errors. Each point shows the optimal protocol used in the lowest level (markers) for each of the 12 combinations of number of repeaters (colours) and total distance between end nodes (x axis/line styles). Note that the EP protocol corresponds to the one used at the lowest level since no solution was found using distillation in upper levels. $(i - ii)$ the end to end fidelity and entanglement generation rate respectively. (iii) the total parameter cost. (iv) the cost associated to each of the tunable hardware parameters individually, only the optimal solution per distance is shown. (v) (for the restricted case) the optimal bright-state population.

increased more than before. This is in contrast to the optimal solution for 400 km, which consist on three repeaters. In this case, $p_{2,gate}$ has to be upgraded anyhow, arriving at a similar value with both methods. However, on account of the reduced noise that is introduced by the other gates in this second method, the cost of T_2 and η_{lm} can be decreased.

The important difference is in the solution for the largest separation. Previously, we discussed the viability of the strategy using two iterations of DEJMPS in favour of EPL. Despite that, the GA has found a solution in this case using the latter EP protocol. This is remarkable but in no case presents a contradiction. It is important to recall the difference between both protocols, see protocol 4 and protocol 5, appearing only in the post selection of the states. DEJMPS succeeds if both outcomes are equal – no matter their value – while in EPL they both have to be equal to 1. When measurement errors are high, the protocol that is penalised the most is the latter, in the

former, two consecutive errors still lead to a successful distillation round. Therefore, in fig. 5.3a, the high error in measurements favoured DEJMPS. On the contrary, with improved measurements, a solution was found using EPL, which allowed to keep the state efficiency at the baseline value. Furthermore, the bright-state population is substantially larger now, increasing from ≈ 0.1 to ≈ 0.3, which also increases the elementary link success probability as to favour this distillation procedure.

Secondly, for the targets $F_t = 0.9$ and $R_t = 0.1\,\text{Hz}$, it is particularly interesting to see that not only do solutions exist with 7 repeaters, but also, this represents the optimal setup for 800 km. There, the protocol found to minimise the parameter cost is EPL with a final entanglement generation rate right above the target value of 0.1 Hz. It is instructive to analyse the other optimal solutions for 200 km and 400 km. In the former, the optimal solution still corresponds to direct connection with a total parameter cost of 10.48 in fig. 5.3b and 14.46 in fig. 5.4b. The latter is bigger only because 4 more gates are optimised, if we substract the cost associated with the extra gates we arrive at 10.46, almost equal to the first case, proving that the gate errors do not influence the solution. In the latter, the optimal solution uses 3 QRs but the cost drops from 75.19 to 70.96. In fact, the solutions seem to correspond to two different minimums, despite the combined cost of all parameters is similar. This can be seen clearly in the value found for the bright-state population, which is 0.1251 in the former, and 0.3167 in the latter, implying that a higher value for η_{lm} is needed in the first place to reach the target rate. Nevertheless, the maximum two-qubit gate error tolerated reached a close value, 0.11% and 0.21% respectively, the latter being slightly larger. This is reasonable as other gates are also improved so the requirements for this particular operation can be reduced. Yet, the small difference seems to indicate that the baseline value of the single-qubit and measurement is already good enough for a chain with 3 repeaters.

In both figs. 5.3 and 5.4, there exists a maximum distance, that depends on the amount of QRs, after which the creation of an entangled state is not possible due to the target values. Usually, the bound that cannot be satisfied is the rate due to the exponential decrease in the elementary link success probability, as well as the longer communication time. It is possible to give an upper bound on this distance D_{total} by considering the ideal case scenario of perfect QMem and photon detectors, hence the waiting time of a single elementary link can be estimated assuming only photon loss using eq. (3.21). The total waiting time to generate the end-to-end link with repeaters is at least $2\mathbb{E}[T_{gen}]$ because they can only perform one action at a time, as explained in section 4.1. Then, by finding the root of the function

$$R(L_{node}) = \frac{1}{2\mathbb{E}[T_{gen}(L_{node})]} - R_t = \frac{1}{2}\frac{\eta_{fibre}(L_{node}/2)}{T^*_{cycle} + L_{node}/c} - R_t \ , \tag{5.2}$$

where $L_{node} = D_{total}/(N_{node} - 1)$ and we assumed $\alpha = 0.5$, we can give an upper bound on the maximum distance.

The previous does not consider the target fidelity, as it depends on the strategy used, but for SWAP-ASAP we can give an upper bound using eq. (3.29). Hence, we can find the roots of the system of equations

$$\frac{\alpha\eta_{fibre}(L_{node}/2)}{T^*_{cycle} + L_{node}/c} - R_t = 0 \tag{5.3a}$$

$$\frac{1}{4} + \frac{3}{4}\left[\frac{4(1-\alpha)-1}{3}\right]^{N_{node}-1} - F_t = 0 \tag{5.3b}$$

in terms of α and D_{total}. This method will gives us a much more restricted bound because the trade-off between fidelity and rate is taken into account, similar to what was found in fig. 5.2. Despite that, the previous solution, which only takes into account the rate, can be seen as a bound to a EP protocol that acts on one pair and yields a perfect bell pair at the end. A much more accurate bound to a $2 \to 1$ EP can be found by considering the average waiting time to create two elementary links and the maximum success probability of the distillation protocol. Tighter bounds to the waiting time have also been studied [Brand et al., 2020; Coopmans et al., 2021]. Still, we can already extract conclusions from the simplest cases above.

The roots for the two methods are found using numerical methods, concretely the `hybr` algorithm implemented in the `scipy` python library. These are shown in table 5.1 for the two pairs of target values studied. Essentially, the first method gives the maximum possible distance while the

Table 5.1: Upper bounds on the maximum end-to-end distance that allows the creation of an entangled state within the target rate using single-click MHEG. Only photon loss is considered, assuming perfect quantum memories. The solutions correspond to the roots of eq. (5.2) and eq. (5.3) for the rate only and SWAP-ASAP respectively.

(a) $F_t = 0.8$ and $R_t = 1\,\text{Hz}$

Number of repeaters	**Rate only** ($\alpha = 0.5$) Distance (km)	**SWAP-ASAP** Distance (km)	α
0	263	231	0.2
1	479	377	0.10774
3	958	669	0.05596
7	1917	1168	0.02852
(b) $F_t = 0.9$ and $R_t = 0.1\,\text{Hz}$			
0	343	285	0.1
1	638	481	0.05179
3	1277	872	0.02636
7	2554	1563	0.01330

second gives the maximum distance considering the trade-off typical of SC, but only applicable to SWAP-ASAP, this second distance is always smaller than the former.

Clearly, the direct connection method can only be used to connect nodes at a distance $< 343\,\text{km}$ in the most optimistic case. Correspondingly, the only solution without repeaters was found at 200 km. In those situations, the optimal value of α is around 0.05 smaller than the ideal value, which can be a consequence of the approximation used to evaluate the end-to-end fidelity as eq. (3.29) is derived for Werner states and not R-states.

The use of at least one repeater allows solutions for 400 km, but to connect end nodes at a distance of 800 km, at least 3 are needed. At this larger distance, SWAP-ASAP can only be used with the second pair of targets which have a smaller target rate. Nevertheless, the vicinity of the ideal bound found at 872 km suggest that the cost of using SWAP-ASAP is much higher than the one required for a strategy with EP. The same applies to one QR with the same targets, whose bound is at 481 km, close to 400 km. Solutions with 7 repeaters are always possible in terms of rate for the distances considered, but as has been seen, the imperfect QMem have a huge impact on the fidelity as to forbid solutions with target fidelity equal to 0.9. This fact is not reflected in table 5.1 as perfect devices are considered.

One can note that, the important parameter in the rate only case is not the total distance but the internode length. In fact, dividing the distances in table 5.1a by $N_{qr} + 1$ gives a maximum internode distance of 240 km and 319 km for the two pairs of targets, respectively. The analysis was done with the total distance in order to compare them easily with the figures in this section.

All in all, it is possible to conclude that the trade-off between elementary link fidelity and success probability limits the applicability of SWAP-ASAP with SC. Furthermore, the no repeater scenario can only connect nodes separated a maximum distance of 263 km at a rate of 1 Hz, this is extended to 479 km with one QR and to almost 1000 km with three.

5.3.2 Double-Click

DC entanglement generation protocols have the benefit that the elementary link fidelity and success probability are independent from each other. Consequently, the unrestricted method proposed in section 5.2 is better suited for them. Hence, the elementary link fidelity f_{elem} will be considered as an optimisation parameter but we will replace the elementary link success probability by the light-matter interface efficiency η_{lm}. In this way, p_{elem} can be evaluated from eq. (3.18) and it remains limited by the fibre efficiency.

The baseline value for f_{elem} can be determined from eq. (3.17), giving

$$f_{DC} = f_{lm}\frac{1+V}{2} \ , \tag{5.4}$$

where the light-matter interface fidelity has been demonstrated experimentally to be approximately $f_{lm} = 0.99$ [Hensen et al., 2015]. The baseline visibility is the same as in the previous simulations, $V = 0.9$ (table B.1). This corresponds to an elementary link fidelity $f_{DC} = 0.92$, which matches with the measured state fidelity in the aforesaid reference. Also, the state that is generated can be simplified, since the component proportional to $(1-V)/2$ in eq. (3.19) is small for the baseline visibility considered. Thus, the state that is generated will be approximated by (taking the + sign)

$$\rho_{DC} \approx f_{DC}\,|\Phi_{01}\rangle\langle\Phi_{01}| + \frac{1-f_{DC}}{2}\left(|00\rangle\langle 00| + |11\rangle\langle 11|\right) \ . \tag{5.5}$$

The other parameters are the same as in section 5.3.1, those are T_1, T_2 and the global strategy S. Also, we will optimise over $p_{2,gate}$, in the first place, and over k_{gates}, after that. The strategy will be limited to the lowest level only, motivated by the results found with SC. No result is expected to be found that uses EP in upper levels as the elementary link success probability of DC is quadratically smaller than SC, and this restriction allows us to keep the number of generations constant for all numbers of repeaters.

Furthermore, to reduce the amount of simulations, we will start by determining those setups for which there can exist a solution in the ideal scenario. Because the fidelity and waiting time are independent from each other, it is possible to give an analytical expression for the lower bound on the elementary link fidelity. Thus, from eq. (3.29) we find

$$F_{lower} = \frac{1}{4} + \frac{3}{4}\left(\frac{4F_t - 1}{3}\right)^{\frac{1}{N_{node}-1}} \ . \tag{5.6}$$

The maximum distance has to be determined numerically as in eq. (5.2) with the elementary link success probability defined in eq. (3.18), hence

$$\frac{1}{4}\frac{[\eta_{fibre}(L_{node}/2)]^2}{T^*_{cycle} + L_{node}/c} - R_t = 0 \ . \tag{5.7}$$

The solutions for the 4 number of repeaters considered are presented in table 5.2. The quadratic decrease on the elementary link success probability reduces the maximum distance by around half as compared to the rate only case in table 5.1. This implies that direct connection can not be used in any situation, a minimum internode distance of 129 km and 171 km is needed to achieve rates of 1 Hz and 0.1 Hz respectively. Therefore, we are forced to use at least one repeater with this MHEG protocol. Yet, this solution can only exist at a distance of 200 km. Three QRs are needed for 400 km and seven for 800 km. Therefore, only six possible scenarios have to be considered.

The lower bound on the elementary link fidelity can be used to restrict the search space. However, this information is only useful with the SWAP-ASAP network protocol and so the same baseline value will be used in all situations. This is lower than the minimal value required by SWAP-ASAP in most situations, but it is expected that EP can reduce this requirement. Nevertheless, we should take into account that eq. (5.5) is BD because $|00\rangle\langle 00| + |11\rangle\langle 11| = |\Phi_{00}\rangle\langle\Phi_{00}| + |\Phi_{10}\rangle\langle\Phi_{10}|$, implying that the optimal EP protocol is DEJMPS. Therefore, we expect it to be the distillation protocol selected, if any, although this is not enforced. Moreover, by looking at fig. 5.2a, we can anticipate that there will be situations in which SWAP-ASAP outperforms any distillation strategy.

The results for the six possible setups are shown in fig. 5.5, those simulations for which no solution was found are excluded. In general, we can see fewer solutions than in fig. 5.3 and the ones found look very different. These either converged to SWAP-ASAP or to one iteration of DEJMPS. Let us go into the details for each of the three figures.

The first set of solutions (fig. 5.5a) corresponds to the target values $F_t = 0.8$ and $R_t = 1$ Hz with optimisation over $p_{2,gate}$ only. Looking at figure (ii), we note that the entanglement generation rates are well above the desired target when the internode distance is ≤ 50 km, in spite of using a MHEG protocol which scales proportional to η^2_{fibre}. The effect of this scaling is seen in the

Table 5.2: Upper bounds on the maximum end-to-end distance that allows the creation of an entangled state within the target rate using double-click MHEG protocol. Only photon loss is considered, assuming perfect quantum memories.

(a) $F_t = 0.8$ and $R_t = 1\,\text{Hz}$

Number of repeaters	**Distance** (km)	F_{lower}
0	129	0.8
1	239	0.89226
3	479	0.94404
7	958	0.97148

(b) $F_t = 0.9$ and $R_t = 0.1\,\text{Hz}$

Distance (km)	F_{lower}
171	0.9
319	0.94821
638	0.97364
1276	0.98670

strategy picked, as only those setups with lesser separation between nodes, $\leq 25\,\text{km}$, make use of EP with DEJMPS. The rest converged to SWAP-ASAP. Concretely, for 200 km, three repeaters running the SWAP-ASAP protocol was found optimal; for 400 km, seven QRs using one round of DEJMPS at the lowest level; and for 800 km, again seven but with SWAP-ASAP. The cost distribution is dissimilar, owing to the change of protocol. Comparing the two results with the same number of repeaters in (*iv*), we see that EP requires halving the two-qubit gate error as compared to SWAP-ASAP, where the gate error is 0.6%. Nonetheless, it helps at reducing the required elementary link fidelity, whose value of $f_{elem} = 0.9774$ is identical to the one found for 200 km. In fact, it is within the distillation range, showing that it is indeed advantageous. In contrast, the T_2 found in the setup for 400 km using distillation needs to be as large as the one for 800 km and SWAP-ASAP, about 11 s.

Next, fig. 5.5b presents the solutions with modified target values. In this case, no simulation with seven repeaters was executed on account of the impossibility of achieving the target fidelity, as explained in the previous section. Despite that, the desired effect of changing the targets is seen. In fig. 5.5a, the results for 200 km converged to SWAP-ASAP, but here, one iteration of DEJMPS is used because a higher fidelity is needed, and it is possible possible to regenerate elementary links in the required time in case an EP step fails. The cost for these solutions is higher than before, mostly due to T_2 and $p_{2,gate}$. Thus, the reduction on the target rate does not compensate the larger target fidelity, which could be expected because there are four parameters affecting the final fidelity against just one for the rate. The same parameters have to be largely increased for 400 km, even though it also uses SWAP-ASAP as network protocol. We will look again into them below, when we compare them with the optimisation over all gates.

Exactly like in section 5.3.1, the optimisation tasks will be repeated with the replacement of $p_{2,gate}$ by the parameter k_{gates}, which controls the improvement over the single and two qubit gate, measurement and initialisation errors. The results for the six possible configurations can be seen in fig. 5.6.

The change in the optimisation parameter does not modify the optimal strategy found in fig. 5.6a as compared to fig. 5.5a for each setup. It does, however, rearrange the optimal one that connects two nodes separated by 400 km. This was found to be the seven repeater scenario with DEJMPS, while now, three QRs with SWAP-ASAP minimise the cost function at this distance. Despite that, the cost between the two configurations is mostly the same, 40.26 against 39.40, so the viability of both solutions is equivalent. In terms of the parameters, the solution with three repeaters needs an elementary link fidelity and light-matter interface efficiency of 0.9891 and 66.09%, respectively; while with seven, those are decreased to 0.9684 and 54.13% thanks to EP and the smaller internode distance. In contrast, no improvement is needed on the gates in the first case, while the maximum tolerable two-qubit gate error is $\sim 0.5\%$ in the second. In both, a value of $T_2 \approx 10\,\text{s}$ is required in both cases, being a bit smaller in the latter. In the end, it all depends on the parameters that are easier to improve on a given physical realisation. Thus, one platform might find it harder to improve the interface efficiency than the gate errors, in which case the solution with seven QRs running DEJMPS at the lowest level can be better suited.

In any case, SWAP-ASAP is the chosen protocol for all distances, owing to the low elementary link success probability of DC, and the fact that DEJMPS only provides a little increase in the

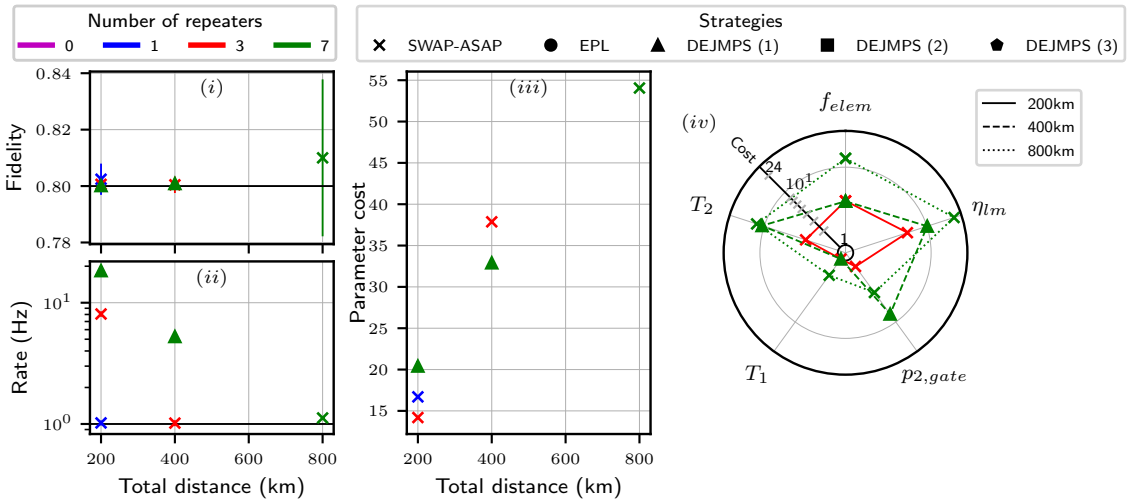

(a) $F_t = 0.8$ and $R_t = 1\,\text{Hz}$

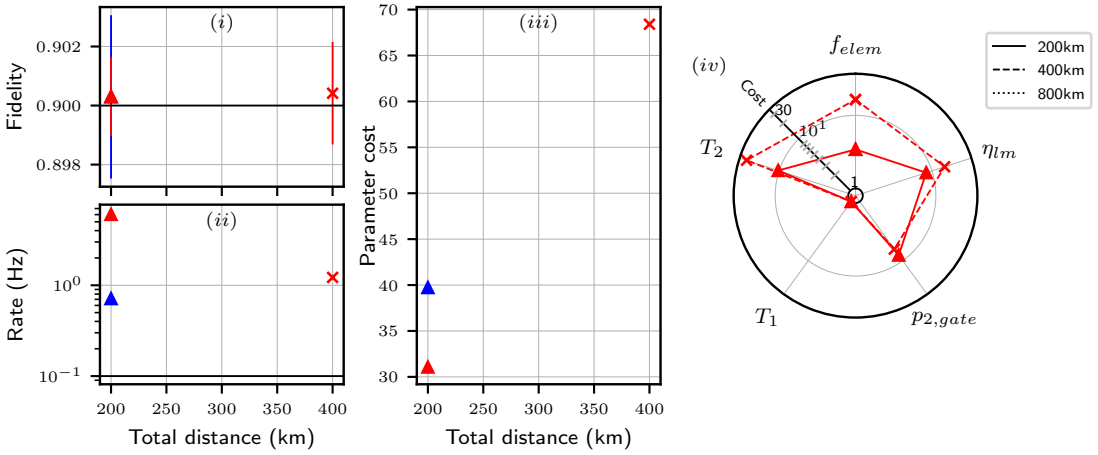

(b) $F_t = 0.8$ and $R_t = 1\,\text{Hz}$

Figure 5.5: Optimal solutions with a level dependent distillation strategy and double-click MHEG protocol optimising over $p_{2,gate}$ only. Each point shows the optimal protocol used (markers) for each of the possible combinations of number of repeaters (colours) and total distance between end nodes (x axis/line styles). $(i - ii)$ the end to end fidelity and entanglement generation rate respectively. (iii) the total parameter cost. (iv) the cost associated to each of the tunable hardware parameters individually, only the optimal solution per distance is shown.

fidelity. This strategy forces the improvement of the two elementary link properties by a similar amount. In the two situations with five repeaters, the dephasing time is the only noise parameter improved, leaving the gate errors at their baseline value. On the contrary, the use of seven QRs requires these to be enhanced, letting T_2 and f_{elem} remain at the same value found for 400 km.

Finally, the optimisation results for the second pair of target values are shown in fig. 5.6b. As in section 5.3.1, solutions with seven repeaters are found and this represents the optimal setup for 800 km. The optimal protocol corresponds to SWAP-ASAP, likewise for 200 km, while for 400 km it changes to one round of DEJMPS at the lowest level. The different protocol in the intermediate distance can be understood as a balance between fidelity and rate. That is, for 200 km, the cost of increasing all gates such that EP can be used is too high and thus, it is cheaper to attain the target fidelity by improving fewer quantities like f_{elem} and T_2. On the contrary, for 800 km, the nodes are far away from each other so it is not possible to achieve the target rate with EP. In between, the distance is such that distillation can be used without penalty on the rate, and SWAP-ASAP would

require such a high elementary link fidelity and dephasing time that it is reasonable to improve the other gates as to use DEJMPS.

The behaviour of the other optimal solutions for shorter distances is alike previous plots. For 400 km, the optimal setup corresponds to five nodes with SWAP-ASAP, just as in fig. 5.5a, the difference is in the reduction on f_{elem} and T_2 because other operations are improved. For 200 km, the optimal configuration changes from three to one QR, the reason being the cost associated to the extra gates, which do not have to be improved in the one repeater setup.

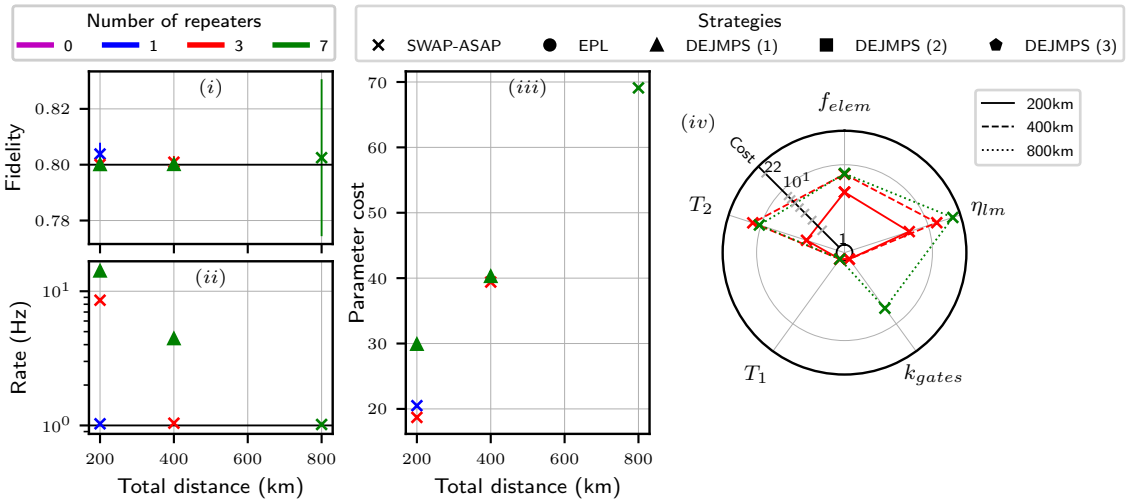

(a) $F_t = 0.8$ and $R_t = 1\,\text{Hz}$

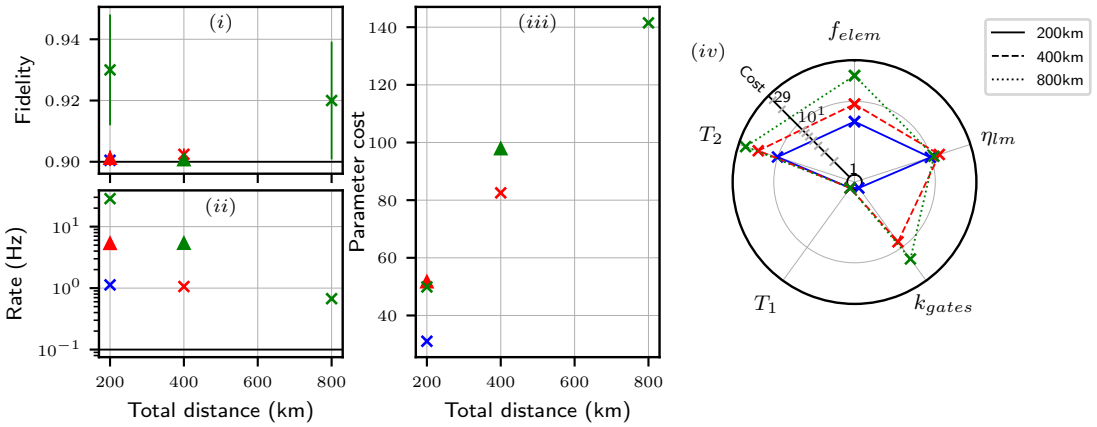

(b) $F_t = 0.9$ and $R_t = 0.1\,\text{Hz}$

Figure 5.6: Optimal solutions with a level dependent distillation strategy and double-click MHEG protocol optimising over all gate errors. Each point shows the optimal protocol used (markers) for each of the possible combinations of number of repeaters (colours) and total distance between end nodes (x axis/line styles). $(i - ii)$ the end to end fidelity and entanglement generation rate respectively. (iii) the total parameter cost. (iv) the cost associated to each of the tunable hardware parameters individually, only the optimal solution per distance is shown.

One can also note that all the optimal solutions converge to a similar value of the light-matter interface efficiency, approximately equal to 61.70%. All three solutions place the nodes at a distance of 100 km, so the elementary link success probability is similar. This was not seen with SC, even though the number of repeaters was also increased as the distance doubled, see fig. 5.3a or fig. 5.4a. There, the interface efficiency had to increase with the number of nodes too, a consequence of the existent trade-off between fidelity and rate. In order to achieve the same fidelity with more QRs – more noise – the bright-state parameter has to be reduced, and consequently, η_{lm} increased. Here,

without the trade-off, the same value can be maintained without affecting the fidelity.

The benefit of distillation is not as clear as with SC. We can in general assert that DEJMPS can only be used with setups whose internode distance is $\leq 50\,\text{km}$, although this does not represent a sufficient condition. The quadratic decrease in elementary link success probability forces the use of SWAP-ASAP for larger separations to attain the target rate. Moreover, the small improvement characteristic of DEJMPS (see fig. 3.4) does not allow to reduce the required elementary link fidelity to a large extent, which favours again SWAP-ASAP. Despite that, we can also see the ability of the GA to distinguish the state that is generated as to pick the optimal EP, EPL in case of SC (R-states) and DEJMPS with DC (Bell-diagonal).

5.4 Optimal Setups

The discussion on the results is not finished until the answer to what strategy is the best to connect two quantum devices at a certain distance is given. Here, for each distance, the two MHEG protocols will be compared, as well as the amount of repeaters. Hence, we consider the latter as a parameter that can be chosen in a practical situation, because it is part of the quantum implementation.

The analysis will be done with the results found in section 5.3 for the two pairs of target values separately. Besides, intermediate and longer distances will be considered to determine how does the total cost scale with it. Furthermore, simulations will be done with 17 QRs for distances $\geq 800\,\text{km}$ when optimising over all gate errors. This is not done with optimisation over $p_{2,gate}$ only, because it is not possible to achieve any of the target fidelities considered due to the other operational errors. From eq. (3.29), we can derive a maximum fidelity of 0.7168, even if a perfect state fidelity is assumed.

Then, in order to join the results from SC and DC, we will assume that we can compare their cost directly. In fact, in both there are five parameters affecting the total cost, being the parameter that controls the quality of the state the only one that differs. In SC this is given by the state efficiency, and in DC, it is the elementary link fidelity. Despite that, both arise from similar hardware parameters, like the beam splitter visibility or double excitations. Thus, we assume that the hardness of improving these quantities is comparable.

As said throughout the text, the viability of a particular solution depends to a large extent on the particular physical implementation that one wants to improve. We have presented the solutions obtained, but better solutions might exist that the GA could not find. Despite that, they clearly represent an upper bound to the global minimum. Another remark is that the values of distance given are valid for the fibre transmission loss considered, which corresponds to an attenuation length $L_0 \approx 20\,\text{km}$. The results cannot be directly mapped to other values, as quantities like the communication time will also be affected, but the simulations can be redone with other values to compare the results.

In general, we have seen the total hardware cost to increase exponentially with the distance. Yet, once the best setup and strategy is picked, we might expect to find a lesser scaling with distance. Accordingly, the cost of the optimal solutions will be fit with the functions*

$$C_{epx}(d) = \kappa_{exp} e^{d/\Delta_{exp}} \quad \text{and} \tag{5.8a}$$

$$C_{ln}(d) = \kappa_{ln} + \frac{D}{\Delta_{ln}} \ . \tag{5.8b}$$

The one that gives the higher correlation coefficient will be picked, being the one that better approximates the growth of the hardware cost. The parameter κ can be interpreted as the improvement or reduction over the baseline cost at 0 distance†, where this baseline cost κ_{base} is equal to the amount of optimised hardware quantities. Hence, if $\kappa_{base} \geq \kappa$ we conclude that it is

*The fit has been done using the `linregress` function in the `scipy` python library. It is necessary to take the base-2 logarithm on both sides beforehand when working with the exponential function.

†A null distance is nonphysical, what we mean is a distance such that any delay or noise arising from the node separation can be neglected. This typically occurs when the internode distance L_{node} is much smaller than the fibre attenuation length L_0, in our case, $L_{node} \ll 20\,\text{km}$.

possible to connect the two end nodes with state-of-the-art devices. In this case, we can estimate the maximum distance that could be connected with current technology, that is,

$$d_{exp}^{base} = \Delta_{exp} \ln \frac{k_{base}}{k_{exp}} \quad \text{and} \tag{5.9a}$$

$$d_{ln}^{base} = \Delta_{ln}(\kappa_{base} - \kappa_{ln}) \ , \tag{5.9b}$$

respectively. Else, a minimum improvement is needed even for short distance, which is given by κ. The values of k_{base} are: 5 in the optimisation over $p_{2,gate}$ only, and 9 with all gate errors. The second parameter, Δ, determines the slope of the curve, the rate at which the cost increases with the distance. Therefore, the larger Δ is, the better.

The optimal configurations to use per distance are shown in fig. 5.7, distinguished by the target values and the gate optimisation parameter. The same colours used in previous plots to identify the number of repeaters are employed, but they are divided into two groups. Lighter colours mark solutions implementing SC, while darker or brighter denote DC. The amount of strategies has been reduced to just four as the fifth one was never used. Yet, all simulations have been run including this last strategy as a possibility. The curve that better fits the data is shown in black, together with the corresponding parameters.

First of all, the upper plots condense all the results with optimisation over the two-qubit gate alone. There, we distinguish two scenarios for the different targets. In (i), the optimal MHEG protocol corresponds to SC for distances ≤ 400 km, and to DC after. The solutions using SC also distil the elementary link with EPL, whereas the others employ SWAP-ASAP as network protocol. The number of QRs rises progressively with the distance, from one repeater for the shortest separation, to three for 400 km, and to seven for the longest ones. In addition, the fit shows the linear growth of the total cost with the distance. This is not the case anymore in (ii), but we must remember that for this target fidelity no solution using seven repeaters can be found. In fact, from 400 km onwards, a setup consisting of three QRs is optimal, with varying protocols. Hence, when the number of repeaters is fixed, the cost follows an exponential function, in spite of using the optimal protocols. On the contrary, when the number of QRs can increase as to keep the internode length approximately constant, the hardware cost scales linearly. We must note that from the form of the cost function, the placing of more repeaters does not incur in a higher cost. Otherwise, the optimal solutions might differ, favouring those with fewer repeaters. Despite that, the number of repeaters implicitly affects parameters like the gate errors. In any case, $\kappa < \kappa_{base} = 5$ in both cases, allowing the connection up to a distance of 112(77) km without any improvement over current hardware.

Secondly, fig. 5.7b shows the optimal configurations with optimisation over all gates. The data for the two target pairs looks alike. Direct connection is the best method to use for 200 km, followed by three repeaters at 400 km, seven after that between $600 - 800$ km, and 15 thereafter up until 1600 km. Moreover, they both scale linearly with the distance. The differences are seen in the protocols used. In (i), all of them are found optimal with SWAP-ASAP, the MHEG protocol preferred is DC in the results with at least one repeater, and SC in the no repeater scenario. Instead, in (ii), BDCZ with entanglement purification outperforms SWAP-ASAP in some situations. Concretely, for 400 km the optimal protocols are SC and EPL, then for 1200 km these are DC with one round of DEJMPS, and finally for 1600 km SC with two iterations of DEJMPS. Again, we recall that the purification protocol is only employed at the lowest nesting level. The other solutions employ the same strategy as in (i).

The most remarkable feature is the linear growth of the cost with the distance. The only case in which it does not scale linearly is the same one for which it is not possible to increase the number of repeaters due to the fidelity threshold, that is, (ii) in fig. 5.7a. Similarly, we would expect that after 800 km in (i) the hardware cost starts growing exponentially, since neither it is possible to use a higher number of QRs. Going to the second set of solutions, fig. 5.7b, we find that the cost in (i) rises at a slower rate than in (ii), owing to the increased target fidelity. It fact, Δ is equal – within the uncertainty – to the one in fig. 5.7a (i), which tells us that, for separations ≤ 800 km, it is enough to improve the two-qubit gate alone. Even so, when one goes to larger lengths, it is necessary to make the other gates better, with the guarantee that the total cost will continue to increase linearly. The difference between them occurs in the variable k_{ln}, but few can be concluded from it due to its large uncertainty.

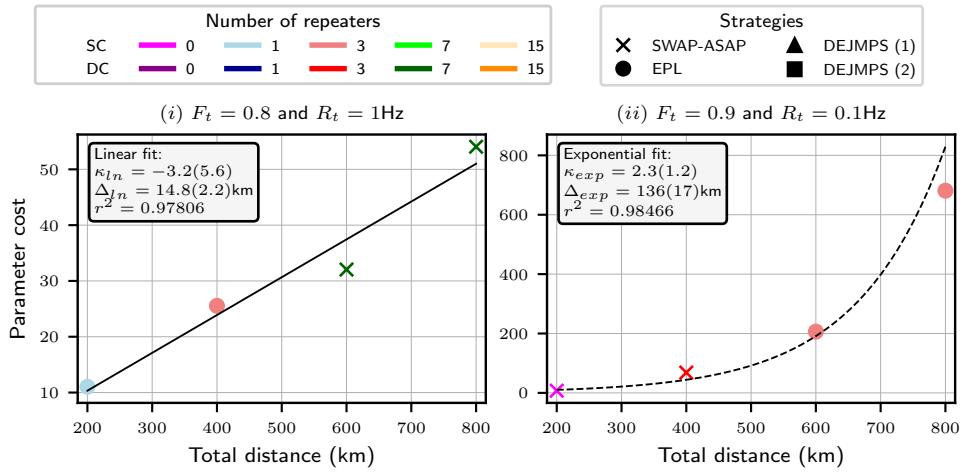

(a) Improvement over two-qubit gate only (note the different y axis limits).

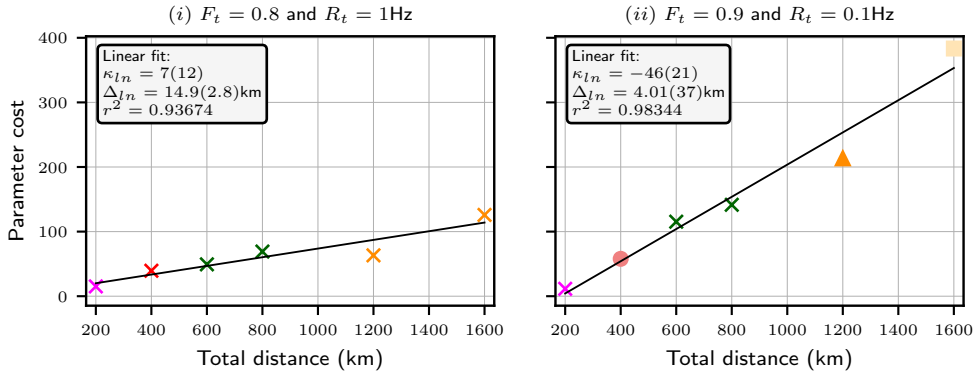

(b) Uniform improvement over all gate errors.

Figure 5.7: Optimal results for each of the distances considered with the two pairs of target values. The colours identify the number of repeaters while the MHEG protocol is distinguished by the lightness, darker colours are used for double-click and lighter for single-click. The markers identify the strategy that it is used in the lowest level. In black the fit, solid and dashed lines distinguish linear and exponential curves, respectively. The parameters for them are shown in the corresponding inner box.

The parameters that have been found for this last set of results are shown in fig. 5.8. Again, to better compare the two MHEG protocols, the elementary link fidelity is presented for both, which is determined by eq. (3.16) in SC. Let us go into the details for each of the individual parameters.

In (i) we have the required elementary link fidelity for which three different situations can be distinguished. First, when no QR is used, its value is equal to the target fidelity. No operations are done on the link, and the communication time is smaller than the baseline T_2, so few noise is induced. Then, we have the setups using DC and SWAP-ASAP, for which $f_{elem} \approx 0.99$. These do introduce noise in the system and no process is used to increase the quality of the links, therefore the initial fidelity must be large. No major difference is seen between the two targets. Last, in fig. 5.8b, there are two points using SC and EP at the lowest level. In those cases, the value of this parameter is much smaller, falling even below the target fidelity for 400 km.

The next parameter is the light-matter interface efficiency. Its baseline value is equal to 0.46% but all the results require at least an efficiency above 50% for the target rate of 1 Hz and above 10% for 0.1 Hz. This represents the most important stepping-stone in the generation of elementary links. In section 3.3, we commented that this parameter combines the emission and detection photon process and it arises from a combination of several independent processes. In order to attain these

minimum values, the efficiency of the processes should be above $\sim 85\%$ and $\sim 56\%$, respectively. The current value for the ZPL emission is $3-4\%$ for instance, far away from the requisite. Despite that, the coupling can be amplified using optical cavities [Riedel et al., 2017]. Nonetheless, there exist other diamond-based platforms like silicon-vacancy centres reaching a fibre coupling of 90% [Burek et al., 2017], which is enough for the solutions found. An alternative is to use multiplexing to abbreviate the waiting time of MHEG protocols [Dam et al., 2017]. The interface efficiency could then be reduced to η_{ln}/N_{qubit} in SC and to $\eta_{ln}/\sqrt{N_{qubit}}$ in DC, yielding values more manageable for the near-future.

We can proceed to the two-qubit gate error in (*iii*). Most of the values are found in the range $0.1-1\%$, which seems a reasonable aspiration for near-term devices. The two extreme points are found without a QR, with no improvement over the gates, and with 15 repeaters and two iterations of DEJMPS, with a value of $p_{2,gate} \approx 0.04\%$, this setup being the one that applies this gate the most. In general, the improvement is larger in fig. 5.8b because the target fidelity is larger too. In fact, we can see that the two configurations using seven repeaters in both targets, for which the same elementary link fidelity was found, have this parameter diminished from 0.3% to 0.1% for the target fidelity 0.8 and 0.9 respectively. Two-qubit gates with this error already exist in trapped-ions [Ballance et al., 2016] and superconducting qubits [Barends et al., 2014]. Furthermore, these quantities are expected to be achieved in the NISQ era [Preskill, 2018] and fall within the working regime of the first generation of QRs [Muralidharan et al., 2016]. Despite that, we must remember that these results are found considering an uniform improvement off all gates. Single-qubit gates with unit fidelity have been reached in NV-centres [Taminiau et al., 2014] and an average measurement error $\xi = (\xi_0 + \xi_1)/2 = 2.3 \times 10^{-3}$ in trapped-ions [Myerson et al., 2008]. Nonetheless, no physical implementation up to this date satisfies all the requirements.

Then, the T_1 relaxation time is the less improved parameter, showing that its current value is already high enough. There are just two configurations that require a longer time, but this is at most of 1.5 hours. At this point, it will be interesting to discuss the usefulness of the local search method explained in section 4.2. The GA has been found to converge successfully, we have given reasons to understand the solutions found as to prove that they indeed correspond to a minimum. In all cases, the local search method was executed to exploit the minimum, and mostly, it helped to take this parameter to the exact baseline. Other parameters were also minimised thanks to this method but its effect is clearly seen here.

Last but not least, we have the dephasing time T_2 in (*v*). The value reached by the GA has an approximately constant value of 10 s in fig. 5.8a owing to the almost constant light-matter interface efficiency. This is not the case in fig. 5.8b due to the change in the protocols. For instance, the solution for 400 km needs a coherence time larger than the solution for 600 km because it employs EP. Similarly, the solutions connecting larger distances also use EP and so require a $T_2 \approx 100$ s. Both these values have been achieved experimentally for NV-centers, Bradley et al. [2019] measured an average coherence time of the individual carbon qubits ≈ 10 s, with dynamical decoupling. This would already be sufficient to attain the target fidelity of 0.8. Moreover, a recent method was proposed by Bartling et al. [2021] to use carbon pairs instead of individual spins to encode the state, with which a 2 minute long coherence time was reached. The latter being sufficient for the results with target fidelity 0.9.

Obviously, as the quality of the hardware improves, the solutions will take different forms. For instance, they could prioritise more strategies with distillation if the light-matter interface efficiency was higher or the gate errors lower.

Overall, the results with current hardware emulating NV-centers show that DC can be beneficial when the internode distance is ≤ 100 km, because the cost of increasing the elementary link fidelity and success probability individually is smaller than the one required in SC due to the trade-off between them. Hence, the network protocol preferred is SWAP-ASAP as fewer operations and storage time is needed, lowering the necessary dephasing time and increasing the tolerable gate error. There are situations in which BDCZ with EP surpasses SWAP-ASAP and those mostly use SC as entanglement generation protocol. Generally, its use is more frequent when the target fidelity is 0.9, but cases with distillation have been found for the two targets.

Altogether, this dissertation has shown the possibility of reducing the total hardware cost by choosing the best combination of entanglement distribution protocols and number of quantum repeaters for each distance.

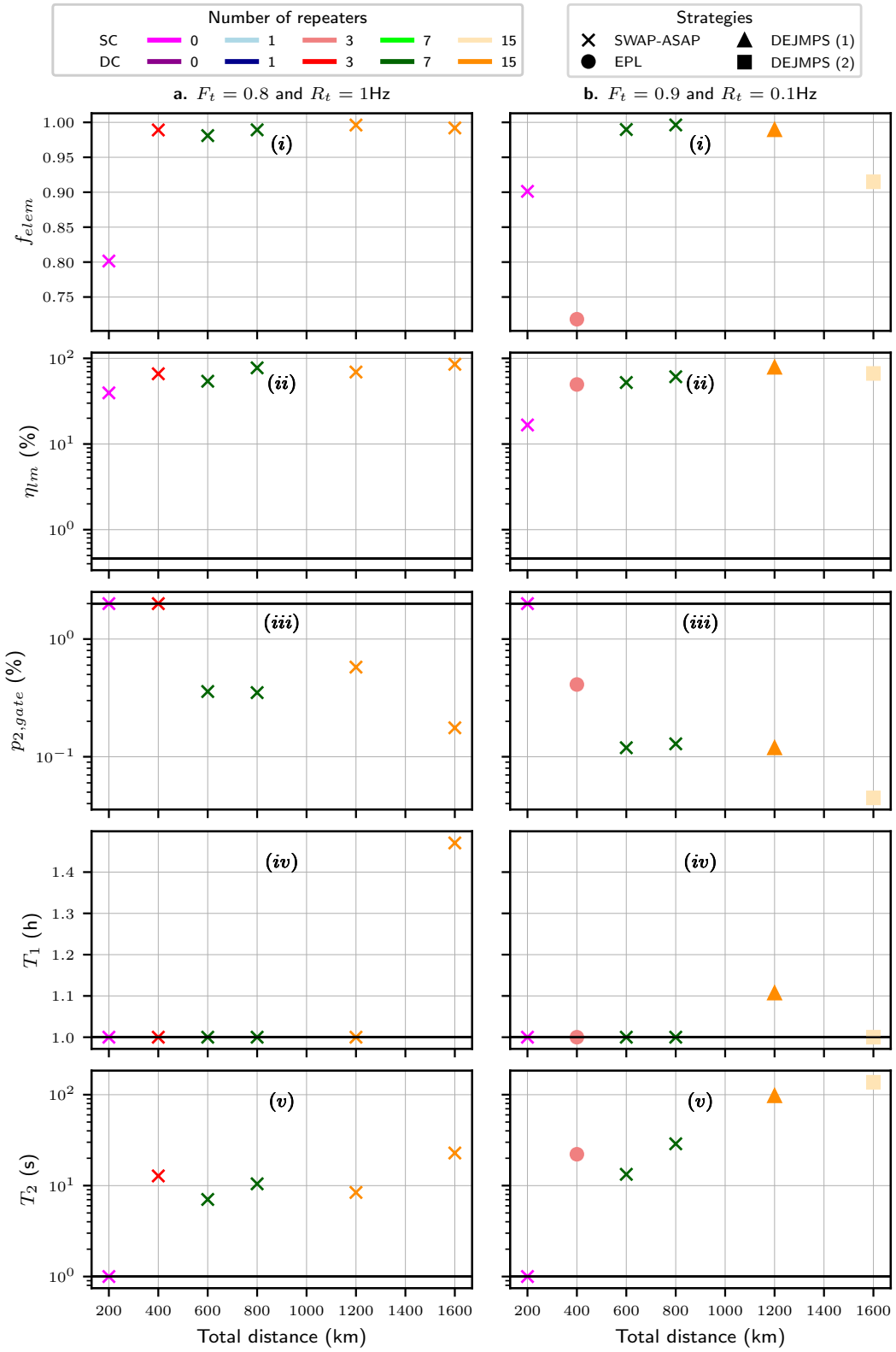

Figure 5.8: Parameters found with improvement over all gates, although only the two-qubit gate error is shown. An horizontal black line marks the baseline value for the parameters in $(ii - v)$. The elementary link fidelity has no baseline as it changes with the entanglement generation protocol.

6 Conclusions

> It is a mistake to confound strangeness with mystery.
>
> — Sherlock Holmes, *A Study in Scarlet*

The main results of thesis will be summarised in this chapter with an outlook on the applicability of this work and the prospect for future projects.

6.1 Summary

Throughout the thesis, the use of QRs has been explored to allow the connection of two distant quantum nodes. Numerical simulations have been used to model a realistic repeater chain, which was employed to find the optimal combination of quantum communication protocols and number of QRs that allowed the reliable connection of these nodes with minimal improvement from state-of-the-art devices.

The hardware modelling was kept abstract to generalise the methodology to multiple physical realisations as previously done by da Silva et al. [2020]. In section 5.1, this was compared to a hardware specific model simulating a repeater chain of NV-centers. The analysis showed the possibility of neglecting the restricted topology occurring in this realisation, as well as, other noise sources like dark counts for small internode distances. Despite that, current technology does not allow to simplify things further, forcing the use of a more complete model which includes beam splitter visibility besides phase path uncertainty and NV double excitations.

Using the validated model, several optimisation tasks where executed with the common goal of finding the optimal set of protocol and hardware parameters by employing different strategies, though. At first, a uniform distillation strategy was explored in section 5.2 which gave limited results due to the impossibility of reaching the target rate for distances larger than 200 km. Despite that, it let us identify the best method to use in following sections, proving the importance of keeping the trade-off in SC between entanglement generation quality and rate – arising from the bright-state population – during the optimisation.

In the next section 5.3, a level dependent strategy was explored which allowed to connect longer distances. The study was done separately for two different MHEG protocols, as well as considering only two-qubit gate errors, on the one hand, and an uniform improvement over all qubit operations, on the other. The results proved the viability of EP to reduce the hardware cost, specially with SC. This was found useful in the lowest level, right after elementary links are created, as a balance between increasing the fidelity of the states and keeping the rate above the threshold. Furthermore, the type of state created by the MHEG protocol conditions the EP protocol, EPL being preferred by SC and DEJMPS by DC. Nonetheless, the quadratic decrease in the elementary link success probability of DC made SWAP-ASAP more convenient when the internode distance exceeded 50 km.

All results were combined in section 5.4, where the linear growth of the total parameter cost with the distance was seen when the best possible setups are picked. The major contribution came

from the light-matter interface efficiency, two-qubit gate errors and T_2 dephasing time. The first one, important to achieve high entanglement generation rates, and the last two, to attain high fidelities. Furthermore, a uniform improvement over all gates shows the same scaling with distance than enhancing the two-qubit gate alone. The total cost is higher in the first, but the second permits the connection of longer distances.

6.2 Outlook and Future Work

This project has provided insights on the optimal way to connect two end nodes further away from each other that has been achieved so far. The specific results obtained are only applicable to NV-centres, but the methodology, as well as the model, is general and can therefore be applied to other physical realisations. One should provide a mapping from the particular implementation to the parameters in this abstract model, modify the baseline values, and finally, identify the key properties to optimise. Hence, experimentalists could use this technique to determine the best road map to improve their devices.

Unfortunately, we have also seen that a lot of work has to be done to accomplish a QI in the near future. Still, progress is being done in this direction with the recent realisation of a three node quantum network [Pompili et al., 2021], as an example. On the theoretical side, one can also expect to see improved protocols in the following years, which would permit to reduce even more the hardware cost.

In this work, several experiments have been set aside but could be interesting to look at in future projects. For instance,

- The study of other physical realisations. The results obtained here are not directly applicable to other platforms because the baseline values are different, therefore the solutions might not look alike. Despite that, the methodology is general so one could use it to compare different abstract mappings for other implementations.

- Similarly, one could apply the same methods to a hardware specific model. This will allow us to determine more accurately the advantages and drawbacks of the abstract model.

- The investigation of asymmetric setups using real map and fibre data. The complexity of the problem grows as the optimal bright-state population is different for each link, this depending on the internode distance and fibre transmission losses among others. Therefore, a method will be necessary to determine the value of this parameter efficiently from the hardware and protocol parameters without adding it to the actual optimisation.

- Obviously, other network protocols could be investigated, like the ones proposed by Duan et al. [2001] for atomic-ensembles or Childress et al. [2005] for solid-state repeaters. The actual implementation of Briegel et al. [1998] could also be extended to a number of nodes that is not a power of two, thus allowing for optimisation over the parameter L which determines the amount of links swapped without prior distillation in a given level (see section 3.6).

- A methodology to map the solutions from the abstract model to the hardware specific model. That is, some parameters in the abstract model are actually composed of several hardware properties like the light-matter interface (3.8) or state efficiency (5.1). Gradient-based methods could be used for this task, such that the minimal improvement over the individual hardware parameters is found while satisfying that the combined value is equal to the solution found in the abstract model.

- The implementation of a multiplexed MHEG protocol to reduce the requirement on the target rate [Dam et al., 2017]. This can benefit more distillation strategies, but at the same time, it can favour setups with fewer nodes and, consequently, longer internode lengths using SWAP-ASAP. A similar analysis to the one performed in this thesis could be done to determine the optimal setup.

Some of these items are part of the goals in the NL blueprint group for which the results presented in this thesis might prove useful.

7 References

M. H. Abobeih, J. Cramer, M. A. Bakker, N. Kalb, M. Markham, D. J. Twitchen, and T. H. Taminiau. One-second coherence for a single electron spin coupled to a multi-qubit nuclear-spin environment. *Nature communications*, 9(1):1–8, 2018.

G. Avis, T. Coopmans, A. Dahlberg, H. Jirovská, D. Maier, J. Rabbie, and M. Skrzypczyk. Netsquid magic, 2021. URL `https://gitlab.com/softwarequtech/netsquid-snippets/netsquid-magic/-/tree/master`.

C. Ballance, T. Harty, N. Linke, M. Sepiol, and D. Lucas. High-fidelity quantum logic gates using trapped-ion hyperfine qubits. *Physical review letters*, 117(6):060504, 2016.

R. Barends, J. Kelly, A. Megrant, A. Veitia, D. Sank, E. Jeffrey, T. White, J. Mutus, A. Fowler, B. Campbell, et al. Logic gates at the surface code threshold: Superconducting qubits poised for fault-tolerant quantum computing. *arXiv preprint arXiv:1402.4848*, 2014.

S. D. Barrett and P. Kok. Efficient high-fidelity quantum computation using matter qubits and linear optics. *Physical Review A*, 71(6):060310, 2005.

H. Bartling, M. Abobeih, B. Pingault, M. Degen, S. Loenen, C. Bradley, J. Randall, M. Markham, D. Twitchen, and T. Taminiau. Coherence and entanglement of inherently long-lived spin pairs in diamond. *arXiv preprint arXiv:2103.07961*, 2021.

J. Benhelm, G. Kirchmair, C. F. Roos, and R. Blatt. Towards fault-tolerant quantum computing with trapped ions. *Nature Physics*, 4(6):463–466, 2008.

C. H. Bennett and P. W. Shor. Quantum information theory. *IEEE transactions on information theory*, 44(6):2724–2742, 1998.

C. H. Bennett, G. Brassard, C. Crépeau, R. Jozsa, A. Peres, and W. K. Wootters. Teleporting an unknown quantum state via dual classical and einstein-podolsky-rosen channels. *Phys. Rev. Lett.*, 70:1895–1899, Mar 1993. doi: 10.1103/PhysRevLett.70.1895. URL `https://link.aps.org/doi/10.1103/PhysRevLett.70.1895`.

C. H. Bennett, G. Brassard, S. Popescu, B. Schumacher, J. A. Smolin, and W. K. Wootters. Purification of noisy entanglement and faithful teleportation via noisy channels. *Phys. Rev. Lett.*, 76:722–725, Jan 1996a. doi: 10.1103/PhysRevLett.76.722. URL `https://link.aps.org/doi/10.1103/PhysRevLett.76.722`.

C. H. Bennett, D. P. DiVincenzo, J. A. Smolin, and W. K. Wootters. Mixed-state entanglement and quantum error correction. *Physical Review A*, 54(5):3824, 1996b.

H. Bernien, B. Hensen, W. Pfaff, G. Koolstra, M. S. Blok, L. Robledo, T. Taminiau, M. Markham, D. J. Twitchen, L. Childress, et al. Heralded entanglement between solid-state qubits separated by three metres. *Nature*, 497(7447):86–90, 2013.

C. Bradley, J. Randall, M. Abobeih, R. Berrevoets, M. Degen, M. Bakker, M. Markham, D. Twitchen, and T. Taminiau. A ten-qubit solid-state spin register with quantum memory up to one minute. *Physical Review X*, 9(3):031045, 2019.

S. Brand, T. Coopmans, and D. Elkouss. Efficient computation of the waiting time and fidelity in quantum repeater chains. *IEEE Journal on Selected Areas in Communications*, 38(3):619–639, 2020.

H.-J. Briegel, W. Dür, J. I. Cirac, and P. Zoller. Quantum repeaters: the role of imperfect local operations in quantum communication. *Physical Review Letters*, 81(26):5932, 1998.

M. J. Burek, C. Meuwly, R. E. Evans, M. K. Bhaskar, A. Sipahigil, S. Meesala, B. Machielse, D. D. Sukachev, C. T. Nguyen, J. L. Pacheco, E. Bielejec, M. D. Lukin, and M. Lončar. Fiber-coupled diamond quantum nanophotonic interface. *Phys. Rev. Applied*, 8:024026, Aug 2017. doi: 10.1103/PhysRevApplied.8.024026. URL https://link.aps.org/doi/10.1103/PhysRevApplied.8.024026.

E. T. Campbell and S. C. Benjamin. Measurement-Based Entanglement under Conditions of Extreme Photon Loss. *Physical Review Letters*, 101(13):130502, Sept. 2008. ISSN 0031-9007, 1079-7114. doi: 10.1103/PhysRevLett.101.130502. URL https://link.aps.org/doi/10.1103/PhysRevLett.101.130502.

L. Childress and R. Hanson. Diamond NV centers for quantum computing and quantum networks. *MRS Bulletin*, 38(2):134–138, Feb. 2013. ISSN 0883-7694, 1938-1425. doi: 10.1557/mrs.2013.20. URL https://www.cambridge.org/core/product/identifier/S0883769413000201/type/journal_article.

L. Childress, J. M. Taylor, A. S. Sørensen, and M. D. Lukin. Fault-tolerant quantum repeaters with minimal physical resources and implementations based on single-photon emitters. *Phys. Rev. A*, 72:052330, Nov 2005. doi: 10.1103/PhysRevA.72.052330. URL https://link.aps.org/doi/10.1103/PhysRevA.72.052330.

M.-D. Choi. Completely positive linear maps on complex matrices. *Linear Algebra and its Applications*, 10(3):285 – 290, 1975. ISSN 0024-3795. doi: https://doi.org/10.1016/0024-3795(75)90075-0. URL http://www.sciencedirect.com/science/article/pii/0024379575900750.

J. Cirac, A. Ekert, S. Huelga, and C. Macchiavello. Distributed quantum computation over noisy channels. *Physical Review A*, 59(6):4249, 1999.

CISCO. Calculating the maximum attenuation for optical fiber links, 2021. URL https://www.cisco.com/c/en/us/support/docs/optical-networking/ons-15454-sonet-multiservice-provisioning-platform-mspp/27042-max-att-27042.html. Accessed February 22, 2021.

T. Coopmans, R. Knegjens, A. Dahlberg, D. Maier, L. Nijsten, J. Oliveira, M. Papendrecht, J. Rabbie, F. Rozpedek, M. Skrzypczyk, L. Wubben, W. de Jong, D. Podareanu, A. T. Knoop, D. Elkouss, and S. Wehner. NetSquid, a discrete-event simulation platform for quantum networks. *arXiv:2010.12535 [quant-ph]*, Oct. 2020. URL http://arxiv.org/abs/2010.12535. arXiv: 2010.12535.

T. Coopmans, S. Brand, and D. Elkouss. Improved analytical bounds on delivery times of long-distance entanglement. *arXiv preprint arXiv:2103.11454*, 2021.

F. F. da Silva, A. Torres-Knoop, T. Coopmans, D. Maier, and S. Wehner. Optimizing Entanglement Generation and Distribution Using Genetic Algorithms. *arXiv:2010.16373 [quant-ph]*, Nov. 2020. URL http://arxiv.org/abs/2010.16373. arXiv: 2010.16373.

S. B. v. Dam, P. C. Humphreys, F. Rozpedek, S. Wehner, and R. Hanson. Multiplexed entanglement generation over quantum networks using multi-qubit nodes. *Quantum Science and Technology*, 2(3):034002, June 2017. ISSN 2058-9565. doi: 10.1088/2058-9565/aa7446. URL https://doi.org/10.1088/2058-9565/aa7446. Publisher: IOP Publishing.

D. Deutsch, A. Ekert, R. Jozsa, C. Macchiavello, S. Popescu, and A. Sanpera. Quantum privacy amplification and the security of quantum cryptography over noisy channels. *Phys. Rev. Lett.*, 77:2818–2821, Sep 1996. doi: 10.1103/PhysRevLett.77.2818. URL https://link.aps.org/doi/10.1103/PhysRevLett.77.2818.

L.-M. Duan, M. D. Lukin, J. I. Cirac, and P. Zoller. Long-distance quantum communication with atomic ensembles and linear optics. *Nature*, 414(6862):413–418, 2001.

W. Dür and H. J. Briegel. Entanglement purification and quantum error correction. *Reports on Progress in Physics*, 70(8):1381, July 2007. ISSN 0034-4885. doi: 10.1088/0034-4885/70/8/R03. URL https://iopscience.iop.org/article/10.1088/0034-4885/70/8/R03/meta. Publisher: IOP Publishing.

W. Dür, H.-J. Briegel, J. I. Cirac, and P. Zoller. Quantum repeaters based on entanglement purification. *Physical Review A*, 59(1):169–181, Jan. 1999. ISSN 1050-2947, 1094-1622. doi: 10.1103/PhysRevA.59.169. URL http://arxiv.org/abs/quant-ph/9808065. arXiv: quant-ph/9808065.

A. Einstein, B. Podolsky, and N. Rosen. Can quantum-mechanical description of physical reality be considered complete? *Phys. Rev.*, 47:777–780, 5 1935. doi: 10.1103/PhysRev.47.777.

A. Ekert and D. Bouwmeester. *The Physics of Quantum Information: Quantum Cryptography, Quantum Teleportation, Quantum Computation*. Springer, 2000.

I. Esmaeil Zadeh, J. W. Los, R. B. Gourgues, J. Chang, A. W. Elshaari, J. R. Zichi, Y. J. van Staaden, J. P. Swens, N. Kalhor, A. Guardiani, et al. Efficient single-photon detection with 7.7 ps time resolution for photon-correlation measurements. *ACS Photonics*, 7(7):1780–1787, 2020.

C. A. Fuchs. Quantum mechanics as quantum information (and only a little more). *arXiv preprint quant-ph/0205039*, 2002.

N. Gisin. Quantum cloning without signaling. *Physics Letters A*, 242(1):1 – 3, 1998. ISSN 0375-9601. doi: https://doi.org/10.1016/S0375-9601(98)00170-4.

D. Goldberg and D. Edward. *Genetic Algorithms in Search, Optimization, and Machine Learning*. Artificial Intelligence. Addison-Wesley Publishing Company, 1989. ISBN 9780201157673. URL https://books.google.es/books?id=2IIJAAAACAAJ.

B. Hensen, H. Bernien, A. E. Dréau, A. Reiserer, N. Kalb, M. S. Blok, J. Ruitenberg, R. F. L. Vermeulen, R. N. Schouten, C. Abellán, W. Amaya, V. Pruneri, M. W. Mitchell, M. Markham, D. J. Twitchen, D. Elkouss, S. Wehner, T. H. Taminiau, and R. Hanson. Loophole-free Bell inequality violation using electron spins separated by 1.3 kilometres. *Nature*, 526(7575):682–686, Oct. 2015. ISSN 1476-4687. doi: 10.1038/nature15759. URL https://www.nature.com/articles/nature15759. Number: 7575 Publisher: Nature Publishing Group.

S. Hermans. Private communication, 2020. URL https://gitlab.com/softwarequtech/netsquid-snippets/netsquid-nv/-/blob/master/netsquid_nv/delft_nvs/delft_nv_2019_optimistic.py.

J. Hofmann, M. Krug, N. Ortegel, L. Gérard, M. Weber, W. Rosenfeld, and H. Weinfurter. Heralded entanglement between widely separated atoms. *Science*, 337(6090):72–75, 2012.

M. Horodecki, P. Horodecki, and R. Horodecki. Inseparable Two Spin- $\frac{1}{2}$ Density Matrices Can Be Distilled to a Singlet Form. *Physical Review Letters*, 78(4):574–577, Jan. 1997. doi: 10.1103/PhysRevLett.78.574. URL https://link.aps.org/doi/10.1103/PhysRevLett.78.574. Publisher: American Physical Society.

P. C. Humphreys, N. Kalb, J. P. J. Morits, R. N. Schouten, R. F. L. Vermeulen, D. J. Twitchen, M. Markham, and R. Hanson. Deterministic delivery of remote entanglement on a quantum network. *Nature*, 558(7709):268–273, June 2018. ISSN 0028-0836, 1476-4687. doi: 10.1038/s41586-018-0200-5. URL http://arxiv.org/abs/1712.07567. arXiv: 1712.07567.

N. Kalb, A. A. Reiserer, P. C. Humphreys, J. J. Bakermans, S. J. Kamerling, N. H. Nickerson, S. C. Benjamin, D. J. Twitchen, M. Markham, and R. Hanson. Entanglement distillation between solid-state quantum network nodes. *Science*, 356(6341):928–932, 2017.

N. Kalb, P. C. Humphreys, J. J. Slim, and R. Hanson. Dephasing mechanisms of diamond-based nuclear-spin memories for quantum networks. *Physical Review A*, 97(6):062330, June 2018. ISSN 2469-9926, 2469-9934. doi: 10.1103/PhysRevA.97.062330. URL `http://arxiv.org/abs/1802.05996`. arXiv: 1802.05996.

A. Kent. Entangled Mixed States and Local Purification. *Physical Review Letters*, 81(14):2839–2841, Oct. 1998. ISSN 0031-9007, 1079-7114. doi: 10.1103/PhysRevLett.81.2839. URL `https://link.aps.org/doi/10.1103/PhysRevLett.81.2839`.

W. Kozlowski and S. Wehner. Towards Large-Scale Quantum Networks. In *Proceedings of the Sixth Annual ACM International Conference on Nanoscale Computing and Communication*, pages 1–7, Dublin Ireland, Sept. 2019. ACM. ISBN 978-1-4503-6897-1. doi: 10.1145/3345312.3345497. URL `https://dl.acm.org/doi/10.1145/3345312.3345497`.

K. Kraus. *States, effects and operations: fundamental notions of quantum theory*. Springer, 1983.

N. Linden, S. Massar, and S. Popescu. Purifying Noisy Entanglement Requires Collective Measurements. *Physical Review Letters*, 81(15):3279–3282, Oct. 1998. ISSN 0031-9007, 1079-7114. doi: 10.1103/PhysRevLett.81.3279. URL `https://link.aps.org/doi/10.1103/PhysRevLett.81.3279`.

S. Luke. *Essentials of Metaheuristics*. Lulu, second edition, 2013. URL `http://cs.gmu.edu/~sean/book/metaheuristics/`.

C. Macchiavello. On the analytical convergence of the qpa procedure. *Physics Letters A*, 246(5):385–388, 1998.

A. G. J. MacFarlane, J. P. Dowling, and G. J. Milburn. Quantum technology: the second quantum revolution. *Philosophical Transactions of the Royal Society of London. Series A: Mathematical, Physical and Engineering Sciences*, 361(1809):1655–1674, Aug. 2003. doi: 10.1098/rsta.2003.1227. URL `https://royalsocietypublishing.org/doi/abs/10.1098/rsta.2003.1227`. Publisher: Royal Society.

W. J. Munro, K. Azuma, K. Tamaki, and K. Nemoto. Inside quantum repeaters. *IEEE Journal of Selected Topics in Quantum Electronics*, 21(3):78–90, 2015.

S. Muralidharan, L. Li, J. Kim, N. Lütkenhaus, M. D. Lukin, and L. Jiang. Optimal architectures for long distance quantum communication. *Scientific Reports*, 6(1):20463, Feb. 2016. ISSN 2045-2322. doi: 10.1038/srep20463. URL `https://www.nature.com/articles/srep20463`. Number: 1 Publisher: Nature Publishing Group.

A. Myerson, D. Szwer, S. Webster, D. Allcock, M. Curtis, G. Imreh, J. Sherman, D. Stacey, A. Steane, and D. Lucas. High-fidelity readout of trapped-ion qubits. *Physical Review Letters*, 100(20):200502, 2008.

M. Nielsen and I. Chuang. *Quantum Computation and Quantum Information*. Cambridge Series on Information and the Natural Sciences. Cambridge University Press, 2000. ISBN 9780521635035.

T. E. Northup and R. Blatt. Quantum information transfer using photons. *Nature Photonics*, 8(5):356–363, May 2014. ISSN 1749-4893. doi: 10.1038/nphoton.2014.53. URL `https://www.nature.com/articles/nphoton.2014.53`. Number: 5 Publisher: Nature Publishing Group.

A. Pirker, V. Dunjko, W. Dür, and H. J. Briegel. Entanglement generation secure against general attacks. *New Journal of Physics*, 19(11):113012, 2017.

M. Pompili, S. L. Hermans, S. Baier, H. K. Beukers, P. C. Humphreys, R. N. Schouten, R. F. Vermeulen, M. J. Tiggelman, L. dos Santos Martins, B. Dirkse, et al. Realization of a multinode quantum network of remote solid-state qubits. *Science*, 372(6539):259–264, 2021.

J. Preskill. Quantum Computing in the NISQ era and beyond. *Quantum*, 2:79, Aug. 2018. ISSN 2521-327X. doi: 10.22331/q-2018-08-06-79. URL http://arxiv.org/abs/1801.00862. arXiv: 1801.00862.

D. Riedel, I. Söllner, B. J. Shields, S. Starosielec, P. Appel, E. Neu, P. Maletinsky, and R. J. Warburton. Deterministic enhancement of coherent photon generation from a nitrogen-vacancy center in ultrapure diamond. *Physical Review X*, 7(3):031040, 2017.

F. Rozpedek, K. Goodenough, J. Ribeiro, N. Kalb, V. C. Vivoli, A. Reiserer, R. Hanson, S. Wehner, and D. Elkouss. Parameter regimes for a single sequential quantum repeater. *Quantum Science and Technology*, 3(3):034002, July 2018a. ISSN 2058-9565. doi: 10.1088/2058-9565/aab31b. URL https://iopscience.iop.org/article/10.1088/2058-9565/aab31b.

F. Rozpedek, T. Schiet, L. P. Thinh, D. Elkouss, A. C. Doherty, and S. Wehner. Optimizing practical entanglement distillation. *Physical Review A*, 97(6):062333, June 2018b. ISSN 2469-9926, 2469-9934. doi: 10.1103/PhysRevA.97.062333. URL https://link.aps.org/doi/10.1103/PhysRevA.97.062333.

F. Rozpedek, R. Yehia, K. Goodenough, M. Ruf, P. C. Humphreys, R. Hanson, S. Wehner, and D. Elkouss. Near-term quantum-repeater experiments with nitrogen-vacancy centers: Overcoming the limitations of direct transmission. *Physical Review A*, 99(5):052330, May 2019. ISSN 2469-9926, 2469-9934. doi: 10.1103/PhysRevA.99.052330. URL https://link.aps.org/doi/10.1103/PhysRevA.99.052330.

B. E. Saleh and M. C. Teich. *Fundamentals of photonics*. john Wiley & sons, 2019.

N. Sangouard, C. Simon, H. de Riedmatten, and N. Gisin. Quantum repeaters based on atomic ensembles and linear optics. *Reviews of Modern Physics*, 83(1):33–80, Mar. 2011. ISSN 0034-6861, 1539-0756. doi: 10.1103/RevModPhys.83.33. URL https://link.aps.org/doi/10.1103/RevModPhys.83.33.

P. W. Shor and J. Preskill. Simple proof of security of the bb84 quantum key distribution protocol. *Physical review letters*, 85(2):441, 2000.

J. S. Sidhu, S. K. Joshi, M. Gundogan, T. Brougham, D. Lowndes, L. Mazzarella, M. Krutzik, S. Mohapatra, D. Dequal, G. Vallone, P. Villoresi, A. Ling, T. Jennewein, M. Mohageg, J. Rarity, I. Fuentes, S. Pirandola, and D. K. L. Oi. Advances in space quantum communications, 2021.

C. Simon. Towards a global quantum network. *Nature Photonics*, 11(11):678–680, Nov. 2017. ISSN 1749-4893. doi: 10.1038/s41566-017-0032-0. URL https://www.nature.com/articles/s41566-017-0032-0. Number: 11 Publisher: Nature Publishing Group.

C. Simon and W. T. Irvine. Robust long-distance entanglement and a loophole-free bell test with ions and photons. *Physical review letters*, 91(11):110405, 2003.

SURFsara. Cartesius: the dutch supercomputer, 2021. URL https://userinfo.surfsara.nl/systems/cartesius. Accessed April 11, 2021.

T. H. Taminiau, J. Cramer, T. van der Sar, V. V. Dobrovitski, and R. Hanson. Universal control and error correction in multi-qubit spin registers in diamond. *Nature nanotechnology*, 9(3):171, 2014.

F. Verstraete, J. Dehaene, and B. DeMoor. Local filtering operations on two qubits. *Physical Review A*, 64(1):010101, June 2001. ISSN 1050-2947, 1094-1622. doi: 10.1103/PhysRevA.64.010101. URL https://link.aps.org/doi/10.1103/PhysRevA.64.010101.

J. von Neumann. *Mathematical Foundations of Quantum Mechanics*. Goldstine Printed Materials. Princeton University Press, 1955. ISBN 9780691028934.

J. Wallnöfer, A. A. Melnikov, W. Dür, and H. J. Briegel. Machine learning for long-distance quantum communication. *PRX Quantum*, 1(1):010301, 2020.

S. Wehner, D. Elkouss, and R. Hanson. Quantum internet: A vision for the road ahead. *Science*, 362(6412), 2018. ISSN 0036-8075. doi: 10.1126/science.aam9288. URL `https://science.sciencemag.org/content/362/6412/eaam9288`.

W. K. Wootters and W. H. Zurek. A single quantum cannot be cloned. *Nature*, 299(5886):802–803, Oct. 1982. ISSN 0028-0836, 1476-4687. doi: 10.1038/299802a0. URL `http://www.nature.com/articles/299802a0`.

S. Zaske, A. Lenhard, C. A. Keßler, J. Kettler, C. Hepp, C. Arend, R. Albrecht, W.-M. Schulz, M. Jetter, P. Michler, et al. Visible-to-telecom quantum frequency conversion of light from a single quantum emitter. *Physical review letters*, 109(14):147404, 2012.

M. Żukowski, A. Zeilinger, M. A. Horne, and A. K. Ekert. "event-ready-detectors" bell experiment via entanglement swapping. *Physical Review Letters*, 71(26):4287, 1993.

M. Zwerger, B. P. Lanyon, T. E. Northup, C. A. Muschik, W. Dür, and N. Sangouard. Quantum repeaters based on trapped ions with decoherence-free subspace encoding. *Quantum Science and Technology*, 2(4):044001, Dec. 2017. ISSN 2058-9565. doi: 10.1088/2058-9565/aa7983. URL `https://iopscience.iop.org/article/10.1088/2058-9565/aa7983`.

A Noisy Entanglement Purification

Give the equations for the expressions in the section but with p2 and measurement noise. Also, try to give an expression for entangleent swap with rstates if possible.

In section 3.5, the expression for the fidelity and success probability for both distillation protocols explained were given in the noiseless case. They do not model a realistic scenario in the NISQ era and thus expressions are needed that take into account the operational errors.

DEJMPS These expressions have been given in [Briegel et al., 1998; Dür and Briegel, 2007] for two equal Werner states and $\xi_0 = \xi_1$. The output state is a BD state [Deutsch et al., 1996] which can be brought back to a Werner form using the procedure in [Bennett et al., 1996a]. The previous state is not necessary as the virtue of this protocol is that it takes profit of the extra information to improve its performance.

EPL Similarly, EPL takes profit of the non BD component as to achieve a perfect Bell state in the absence of noise. Yet, in the presence of noise, the final state does not have a BD or R-state form. The state that is generate with $p_2 \equiv 1 - p_{2,gate}$ and $\xi \equiv 1 - \xi_0 = 1 - \xi_1$ is $F_{EPL} \left|\Phi_{01}\right\rangle\!\left\langle\Phi_{01}\right| + B \left|\Phi_{11}\right\rangle\!\left\langle\Phi_{11}\right| + C \left|00\right\rangle\!\left\langle 00\right| + D \left|11\right\rangle\!\left\langle 11\right|$ with

$$F_{EPL} = \frac{p_2^2\left(2f\left(4f(3(\xi-1)\xi+1)-4\xi^2+2\xi+1\right)+4\xi-3\right)+2(f-1)(2\xi-1)p_2+1}{4(2\xi-1)p_2\left(p_2(2(f-1)f(4\xi-3)+2\xi-1)+2(f-1)\right)+4} \tag{A.1a}$$

$$B = \frac{p_2^2(4f\xi(2f(\xi-1)-2\xi+1)+2f+4\xi-3)+2(f-1)(2\xi-1)p_2+1}{4(2\xi-1)p_2\left(p_2(2(f-1)f(4\xi-3)+2\xi-1)+2(f-1)\right)+4} \tag{A.1b}$$

$$C = \frac{p_2^2\left(2f^2(2\xi-1)(8\xi-7)-4f(3\xi-2)(4\xi-3)+(3-4\xi)^2\right)-2(f-1)p_2(2(f-2)\xi-f+3)+1}{4(2\xi-1)p_2\left(p_2(2(f-1)f(4\xi-3)+2\xi-1)+2(f-1)\right)+4} \tag{A.1c}$$

$$D = -\frac{(p_2-1)\left(p_2(2f(2(f-1)\xi-f+2)-1)+1\right)}{4(2\xi-1)p_2\left(p_2(2(f-1)f(4\xi-3)+2\xi-1)+2(f-1)\right)+4} \tag{A.1d}$$

For small errors, $D \ll C$ so the state can be brought back to a noisy R-state form with $p[q\left|\Phi_{01}\right\rangle\!\left\langle\Phi_{01}\right| + (1-q)\left|\Phi_{11}\right\rangle\!\left\langle\Phi_{11}\right|] + (1-p)\left|00\right\rangle\!\left\langle 00\right|$ using $p = 1 - C$ and $q = F/(1-C)$.

B. NV to Abstract Mapping

Throughout the thesis, several characteristics of NV-centres have been mentioned and briefly explained. Let us give a more detailed explanation about the differences with the abstract model and the way to map the parameters from an NV platform. More elaborate explanations are given in [Childress and Hanson, 2013; Coopmans et al., 2020; Rozpedek et al., 2019].

NV-centres are envisioned as a possible candidate to constitute in the near future a QR, satisfying all the necessary requirements given in section 3.3. This realisation has spin degrees-of-freedom coming from the outermost nitrogen electron and the nearby carbon nuclear spins. The electron spin can be manipulated, measured, and used to communicate with the outside world. In contrast, the nuclear spins can only be used to store quantum states and perform rotations around the z axis. Despite that, the latter have longer coherence times.

The distinction between the two types of qubits is not done in the abstract model. For this reason, properties that are common in both types of spin are mapped to the corresponding parameter using the worst-case-scenario. That is, the maximum value between electron and carbon spins is taken for single-qubit and initialisation errors, and similarly for their gate duration. On the other hand, the minimum relaxation and dephasing time is taken. Error parameters dealing with measurements are taken directly from the electron as have no analogue in the carbon. This worst-case-scenario was used because it would allow us to determine whether the lowest value of the two is enough to attain the targets, and if not, whether the improvement needed is above the highest.

All gate error probabilities (first four in table B.1) have to be mapped to efficiencies to evaluate their cost. This is done through the function $x = 1 - p$, such that the improved value by a cost k is (from eq. (4.1))

$$p^{(k)} = 1 - (1 - p)^{1/k} \ . \tag{B.1}$$

Coherence times are mapped as said in the main text as $x = 1 - T^{-1}$, then the improved value is given by

$$T^{(k)} = \frac{1}{1 - (1 - T^{-1})^{1/k}} \ . \tag{B.2}$$

Also, the abstract model disregards the induced dephasing T_2^* that is introduced in the carbons for each entanglement generation attempt. This error plays an important role in the SWAP-ASAP protocol [da Silva et al., 2020] but we will assume that it can be neglected when using distillation as it has a much more important role than entanglement generation.

Other parameters related to the duration of an operation will be kept fixed in all cases. The reason is that these times are related to a physical process which can not be shortened infinitesimally. For instance, the intrinsic cycle time duration comes from the time that is needed to excite the electron spin and wait for the decay.

Finally, the elementary link parameters are derived from the respective MHEG protocol. However, both the elementary link fidelity and success probability are within the range $[0, 1]$ and satisfy that the perfect value is 1 so no mapping is needed. These parameters are derived from other hardware properties given in table B.1. The expression in eq. (3.16) is derived by applying two dephasing

Table B.1: Parameters used in validation plots, same as those in [Coopmans et al., 2020]. In case of duplicate value between electron and carbon, the most pessimistic parameter is chosen.

Parameter	**NV equivalent**	**Near-term**	**Improved x10**
$p_{1,gate}$	Carbon single qubit gate error	(4/3)0.001	(4/3)0.0001
$p_{2,gate}$	Electron-Carbon (EC) controlled R_X gate error	0.02	0.002
$\xi_0,\ \xi_1$	Electron readout error	0.05, 0.005	0.005, 0.0005
p_{init}	Electron initialisation error	0.02	0.002
T_1	Electron relaxation time	1 h	10 h
T_2	Carbon dephasing time	1 s	10 s
T^*_{cycle}	Photon emission delay	3.8 μs	
$t_{1,gate}$	Carbon single qubit gate duration	20 μs	
$t_{2,gate}$	EC controlled R_X gate duration	500 μs	
t_{init}	Carbon initialisation duration	310 μs	
t_{meas}	Electron read-out duration	3.7 μs	
N_{qubit}	Number of qubits per node	4	
γ	Transmission loss	0.2 dB/km	
c	Velocity of light in fiber ($n = 1.44$)	208 189.207 km/s	
η_{lm}	Detector efficiency	0.0046	0.58
V	Photon visibility	0.9	0.99
p_d	Probability of double excitation	0.06	0.003
p_ϕ	Interferometric phase uncertainty	0.35 rad	0.11 rad

channels with probability p_d – one for each qubit – to the state in eq. (3.14) and a single dephasing channel with probability p_ϕ to one of the qubits [Coopmans et al., 2020].

In section 5.1, the parameters used for both near-term and improved hardware are found in table B.1. During the optimisation tasks, section 5.2 and beyond, some of the previous parameters are updated, these are shown in table B.2. Even though we take the worst-case value between electron and carbon, the values that are used for the optimisation are the best ones that have been achieved experimentally up to the date of this thesis. These can have been achieved or measured independently from each other. In particular, measurement and initialisation errors have been improved, as well as the intrinsic cycle time. Nonetheless, the transmission loss in fibre has been increased as to represent a more realistic scenario.

Table B.2: Modified baseline values from table B.1 near-term data with up-to-date best measured values.

Parameter	**Baseline value**
$\xi_0,\ \xi_1$	0.01, 0.005 [Humphreys et al., 2018]
p_{init}	0.006 [Bradley et al., 2019]
T^*_{cycle}	3.5 μs [Hermans, 2020]
N_{qubit}	10 [Bradley et al., 2019]
γ	0.22 dB/km [CISCO, 2021]

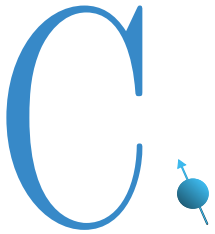

Optimisation Results

The numerical results that go together with the figures in chapter 5 are presented in this chapter. The simulations that did not converge are also shown and they are marked with an "x" in the cost.

The uncertainty in the fidelity and rate is of one sigma. Typically, without repeaters, the uncertainty in the fidelity falls below 10^{-10} because no random process happens. This uncertainty comes from errors due to the computer floating-point precision rounding.

As explained in the main text, the perfect value of the parameters is limited by $1-\epsilon$, where $\epsilon = 10^{-6}$, such that the cost function (4.1) is always finite. This also limits the upper bound of the coherence times, but a more restrictive bound is chosen for them. This is because experimentally we have seen that the baseline T_1 is enough in the majority of the situations, so we can reduce the search space. In consequence, the search space for T_2 is limited because they have to satisfy that $T_2 < T_1$. Thus, the upper limit for T_1 is set at 1×10^3 h and for T_2 at 1×10^5 s $< 1 \times 10^3$ h.

The bright-state population does not have any associated cost and should not have to be lower bounded by ϵ (see table C.1c e.g.). Despite that, a value of 0 would imply a null elementary link success probability, and therefore, no elementary link will be created. Hence, we set the minimum to ϵ because from eq. (3.21), ignoring the communication time and considering perfect transmittivity, the waiting time is $\propto T^*_{cycle}/\epsilon \approx 1$ s. This already gives rates below 1 Hz and so no solution could be found with a lower value of α.

Table C.1: Optimisation parameters with a uniform strategy.

(a) Unrestricted method.

Parameter	Baseline	Range
f_{elem}	$f_{elem,b}$	$[f_{elem,b}, 1-\epsilon]$
p_{elem}	$p_{elem,b}$	$[p_{elem,b}, 0.5-\epsilon]$
$p_{2,gate}$	0.02	$[\epsilon, 0.02]$
T_1	1 h	$[1\,\text{h}, 1\times10^3\,\text{h}]$
T_2	1 s	$[1\,\text{s}, 1\times10^5\,\text{s}]$
Uniform strategy	–	$[0, 5)$

(b) Restricted method with $\eta_f = 1$.

Parameter	Baseline	Range
α	–	$[\epsilon, 0.5]$
η_{lm}	0.0046	$[0.0046, 1-\epsilon]$
$p_{2,gate}$	0.02	$[\epsilon, 0.02]$
T_1	1 h	$[1\,\text{h}, 1\times10^3\,\text{h}]$
T_2	1 s	$[1\,\text{s}, 1\times10^5\,\text{s}]$
Uniform strategy	–	$[0, 5)$

(c) Restricted method optimising over η_f too.

Parameter	Baseline	Range
α	–	$[\epsilon, 0.5]$
η_f	0.9196	$[0.9196, 1-\epsilon]$
η_{lm}	0.0046	$[0.0046, 1-\epsilon]$
$p_{2,gate}$	0.02	$[\epsilon, 0.02]$
T_1	1 h	$[1\,\text{h}, 1\times10^3\,\text{h}]$
T_2	1 s	$[1\,\text{s}, 1\times10^5\,\text{s}]$
Uniform strategy	–	$[0, 5)$

Table C.2: Optimisation results with the unrestricted method considering a uniform distillation strategy corresponding to fig. 5.2a. The target values are $F_t = 0.8$ and $R_t = 1\,\text{Hz}$.

(a) 200km

	Number of repeaters			
	0	1	3	7
f_{elem}	0.9204	0.9585	0.9659	0.9953
p_{elem}	0.0011	0.0147	0.0743	0.0293
$p_{2,gate}$	0.0200	0.0200	0.0087	0.0041
T_1 (h)	1	1	1	1.321
T_2 (s)	1	1	1.934	37.36
Uniform Strategy	–	DEJMPS (1)	DEJMPS (1)	SWAP
Cost	8.589	6.048	9.358	52.38
Fidelity	0.919 529 627 635 7(57)	0.8012(34)	0.800 82(98)	0.860(25)
Rate (Hz)	1.107(76)	6.80(25)	15.19(33)	59.0(1.6)

(b) 400km

	0	1	3	7
f_{elem}	0.8017	0.9204	0.9585	0.9938
p_{elem}	0.0020	0.0297	0.0983	0.0026
$p_{2,gate}$	0.0200	0.0200	0.0078	0.0073
T_1 (h)	1	1	1	1
T_2 (s)	1	1.3	2.757	50.26
Uniform Strategy	–	DEJMPS (1)	DEJMPS (1)	SWAP
Cost	10.93	7.756	11.79	60.76
Fidelity	0.800 204 487 099 2(52)	0.8043(27)	0.8009(12)	0.805(40)
Rate (Hz)	1.103(79)	6.49(21)	9.67(23)	5.79(24)

(c) 800km

	0	1	3	7
f_{elem}	0.8032	0.7434	0.9496	0.9918
p_{elem}	0.0037	0.0464	0.1689	0.0437
$p_{2,gate}$	0.0200	0.0122	0.0069	0.0053
T_1 (h)	1	1	1	1
T_2 (s)	1	2.781	3.721	43.02
Uniform Strategy	–	EPL	DEJMPS (1)	SWAP
Cost	12.56	13.28	18.23	55.97
Fidelity	0.800 171 594 473 1(50)	0.8004(43)	0.8023(10)	0.822(27)
Rate (Hz)	1.045(69)	1.468(68)	6.82(16)	22.22(52)

Table C.3: Optimisation results with the restricted method with $\eta_f = 1$ considering a uniform distillation strategy corresponding to fig. 5.2b. The target values are $F_t = 0.8$ and $R_t = 1\,\text{Hz}$.

(a) 200km

	Number of repeaters			
	0	1	3	7
α	0.1991	0.2832	0.1113	0.0052
η_{lm}	0.3450	0.2539	0.3276	0.0891
$p_{2,gate}$	0.0184	0.0137	0.0042	0.0068
T_1 (h)	1	1	1	1
T_2 (s)	1	3.012	5.23	46.32
Uniform Strategy	–	EPL	DEJMPS (1)	SWAP
Cost	11.14	9.408	15.9	x
Fidelity	0.800 087 901 132 0(36)	0.8008(29)	0.8009(59)	0.747(31)
Rate (Hz)	1.016(47)	1.473(47)	1.34(63)	1.039(33)

(b) 400km

	0	1	3	7
α	0.4001	0.2473	0.1081	0.0064
η_{lm}	0.9818	0.9848	0.5752	0.3073
$p_{2,gate}$	0.0056	0.0006	0.0033	0.0064
T_1 (h)	66.44	877.3	1	1
T_2 (s)	1454	8895	17.43	53.35
Uniform Strategy	–	DEJMPS (1)	DEJMPS (1)	SWAP
Cost	x	x	34.26	x
Fidelity	0.599 888 937 725 20(16)	0.8029(74)	0.8008(19)	0.765(30)
Rate (Hz)	0.0164(10)	0.508(23)	1.027(26)	1.249(37)

(c) 800km

	0	1	3	7
α	0.2146	0.3695	0.0377	0.0135
η_{lm}	0.6782	0.9631	0.9261	0.2342
$p_{2,gate}$	0.0190	0.0016	0.0009	0.0031
T_1 (h)	816.7	743	1.557	1
T_2 (s)	236.3	3496	478.7	62.8
Uniform Strategy	–	SWAP	SWAP	SWAP
Cost	x	x	x	x
Fidelity	0.785 410 58(17)	0.452 38(76)	0.808 74(64)	0.735(31)
Rate (Hz)	$1.328(90) \times 10^{-7}$	0.007 28(36)	0.1543(60)	0.2781(74)

Table C.4: Optimisation results with the restricted method with $\eta_f < 1$ considering a uniform distillation strategy corresponding to fig. 5.2c. The target values are $F_t = 0.8$ and $R_t = 1\,\text{Hz}$.

(a) 200km

	Number of repeaters			
	0	1	3	7
α	0.1606	0.2693	0.0733	0.0012
η_f	0.9580	0.9237	0.9468	0.9961
η_{lm}	0.4238	0.3057	0.3479	0.1796
$p_{2,gate}$	0.0200	0.0117	0.0049	0.0041
T_1 (h)	1	1	1	1
T_2 (s)	1	2.765	8.341	57.06
Uniform Strategy	–	EPL	DEJMPS (1)	SWAP
Cost	14.22	11.08	20.07	x
Fidelity	0.803 395 343 549 7(39)	0.8019(30)	0.8010(59)	0.730(45)
Rate (Hz)	1.004(48)	1.607(52)	1.03(47)	0.505(23)

(b) 400km

	0	1	3	7
α	0.3691	0.2345	0.0961	0.0026
η_f	0.9843	0.9976	0.9652	0.9919
η_{lm}	0.9255	0.9908	0.6664	0.2940
$p_{2,gate}$	0.0051	0.0001	0.0119	0.0077
T_1 (h)	4.148	135	1.286	3.069
T_2 (s)	65.3	1.548×10^4	135.4	93.04
Uniform Strategy	–	DEJMPS (1)	DEJMPS (1)	SWAP
Cost	x	x	x	x
Fidelity	0.620 919 699 126 9(46)	0.8251(69)	0.755(14)	0.825(27)
Rate (Hz)	0.013 58(88)	0.499(20)	0.084(22)	0.472(14)

(c) 800km

	0	1	3	7
α	0.2629	0.5000	0.0362	0.0063
η_f	0.9898	0.9400	0.9982	0.9911
η_{lm}	0.6679	0.9854	0.9351	0.6432
$p_{2,gate}$	0.0011	0.0200	0.0018	0.0071
T_1 (h)	303.5	7.988	1	2.331
T_2 (s)	37328	1.424×10^4	495.5	67.22
Uniform Strategy	–	SWAP	SWAP	SWAP
Cost	x	x	x	x
Fidelity	0.729 530 588 76(97)	0.3586(21)	0.806 34(87)	0.715(45)
Rate (Hz)	$1.59(12) \times 10^{-7}$	0.009 66(34)	0.1606(90)	0.401(19)

Table C.5: Optimisation parameters with a level dependent strategy, single-click entanglement generation protocol and optimisation $p_{2,gate}$ only on a chain with $2^n + 1$ nodes.

Parameter	Baseline	Range
α	–	$[\epsilon, 0.5]$
η_f	0.9196	$[0.9196, 1 - \epsilon]$
η_{lm}	0.0046	$[0.0046, 1 - \epsilon]$
$p_{2,gate}$	0.02	$[\epsilon, 0.02]$
T_1	1 h	$[1\,\text{h}, 1 \times 10^3\,\text{h}]$
T_2	1 s	$[1\,\text{s}, 1 \times 10^5\,\text{s}]$
Global Strategy (S)	–	$[0, 5^n)$

Table C.6: Optimisation results with single-click entanglement generation, level dependent strategy and optimisation over $p_{2,gate}$ only; corresponding to fig. 5.3a. The target values are $F_t = 0.8$ and $R_t = 1\,\text{Hz}$.

(a) 200km

	Number of repeaters			
	0	1	3	7
α	0.1532	0.2597	0.1807	0.0979
η_f	0.9462	0.9196	0.9224	0.9593
η_{lm}	0.4503	0.2328	0.2657	0.3987
$p_{2,gate}$	0.0200	0.0121	0.0058	0.0022
T_1 (h)	1	1	1	1
T_2 (s)	1	3.68	3.926	6.723
Strategy ($n = 0$)	–	EPL	EPL	EPL
Cost	14.26	11.03	13.5	24.83
Fidelity	0.800 520 490 857 7(38)	0.8014(30)	0.8008(21)	0.800 77(78)
Rate (Hz)	1.034(51)	1.175(42)	4.38(16)	11.48(30)

(b) 400km

	0	1	3	7
α	0.3599	0.2222	0.2094	0.0978
η_f	0.9962	0.9980	0.9485	0.9634
η_{lm}	0.9202	0.9987	0.4729	0.4803
$p_{2,gate}$	0.0164	0.0027	0.0045	0.0018
T_1 (h)	590.5	2.543	1	1
T_2 (s)	14.32	2253	11.26	14.72
Strategy ($n = 0$)	–	DEJMPS (1)	EPL	EPL
Cost	x	x	25.54	36.53
Fidelity	0.637 571 317 753(17)	0.8219(41)	0.8018(21)	0.8011(11)
Rate (Hz)	0.014 11(75)	0.466(14)	1.306(45)	4.02(14)

(c) 800km

	0	1	3	7
α	0.2218	0.5000	0.1603	0.0887
η_f	0.9617	0.9591	0.9994	0.9852
η_{lm}	0.5422	0.9762	0.9971	0.6748
$p_{2,gate}$	0.0085	0.0025	0.0011	0.0012
T_1 (h)	2.295	40.28	396.3	1
T_2 (s)	5516	23764	89934	51.4
Strategy ($n = 0$)	–	SWAP	DEJMPS (1)	DEJMPS (2)
Cost	x	x	x	89.06
Fidelity	0.748 419 214 8(84)	0.3635(20)	0.8040(47)	0.8001(10)
Rate (Hz)	$9.91(46) \times 10^{-8}$	0.011 05(39)	0.2076(76)	1.085(22)

Table C.7: Optimisation results with single-click entanglement generation, level dependent strategy and optimisation over $p_{2,gate}$ only; corresponding to fig. 5.3b. The target values are $F_t = 0.9$ and $R_t = 0.1\,\text{Hz}$.

(a) 200km

	Number of repeaters			
	0	1	3	7
α	0.0567	0.1882	0.0986	0.0032
η_f	0.9556	0.9466	0.9623	0.9975
η_{lm}	0.1293	0.4244	0.4869	0.6469
$p_{2,gate}$	0.0200	0.0050	0.0022	0.0001
T_1 (h)	1	1	1	101.2
T_2 (s)	1	6.666	13.97	2508
Strategy ($n = 0$)	–	EPL	EPL	DEJMPS (1)
Cost	10.48	19.47	33.84	x
Fidelity	0.900 563 473 648(43)	0.9007(15)	0.900 33(66)	0.8848(90)
Rate (Hz)	0.1041(52)	1.948(66)	5.97(20)	0.30(25)

(b) 400km

	0	1	3	7
α	0.2676	0.2296	0.1251	0.0042
η_f	0.9961	0.9642	0.9724	0.9986
η_{lm}	0.9989	0.6814	0.6180	0.9586
$p_{2,gate}$	0.0152	0.0024	0.0011	0.0000
T_1 (h)	44.15	1.064	1.137	5.468
T_2 (s)	1099	70.53	42.02	2229
Strategy ($n = 0$)	–	EPL	EPL	DEJMPS (1)
Cost	x	96.4	75.19	x
Fidelity	0.729 597 773 441 07(28)	0.9000(18)	0.900 44(89)	0.894 09(77)
Rate (Hz)	0.011 86(59)	0.1431(49)	1.346(45)	0.835(25)

(c) 800km

	0	1	3	7
α	0.1789	0.3208	0.1816	0.0055
η_f	0.9908	0.9816	0.9925	0.9999
η_{lm}	0.5543	0.9982	0.8608	0.9536
$p_{2,gate}$	0.0079	0.0082	0.0006	0.0001
T_1 (h)	147.4	29.38	1	9.73
T_2 (s)	429.3	2.169×10^4	664.7	1.418×10^4
Strategy ($n = 0$)	–	SWAP	EPL	DEJMPS (1)
Cost	x	x	748.2	x
Fidelity	0.813 502 65(11)	0.489 55(16)	0.901 26(79)	0.893 03(74)
Rate (Hz)	$8.88(45) \times 10^{-8}$	0.006 08(21)	0.1020(36)	0.1648(47)

Table C.8: Optimisation parameters with a level dependent strategy, single-click entanglement generation protocol and optimisation over all gate errors.

Parameter	Baseline	Range
α	–	$[\epsilon, 0.5]$
η_f	0.9196	$[0.9196, 1-\epsilon]$
η_{lm}	0.0046	$[0.0046, 1-\epsilon]$
k_{gates}	1	$[1, 10^4]$
T_1	1 h	$[1\,\text{h}, 1\times10^3\,\text{h}]$
T_2	1 s	$[1\,\text{s}, 1\times10^5\,\text{s}]$
Strategy ($n=0$)	–	$[0, 5)$

Table C.9: Optimisation results with single-click entanglement generation, level dependent strategy and optimisation over all gate errors; corresponding to fig. 5.4a. The target values are $F_t = 0.8$ and $R_t = 1\,\text{Hz}$.

(a) 200km

	Number of repeaters			
	0	1	3	7
α	0.1695	0.2294	0.2179	0.2169
η_f	0.9651	0.9196	0.9196	0.9209
η_{lm}	0.3955	0.2665	0.2310	0.1911
k_{gates}	1	1	2.412	10.5
T_1 (h)	1	1	1	1.123
T_2 (s)	1	5.064	3.517	1.811
Strategy ($n = 0$)	–	EPL	EPL	EPL
Cost	18.16	16.14	21.25	59.68
Fidelity	0.800 743 939 113 6(40)	0.8009(35)	0.8011(23)	0.8024(50)
Rate (Hz)	1.002(50)	1.339(71)	4.12(14)	8.50(40)

(b) 400km

	0	1	3	7
α	0.1980	0.2407	0.3187	0.2618
η_f	0.9997	0.9881	0.9271	0.9196
η_{lm}	0.9722	0.9880	0.3833	0.3561
k_{gates}	1225	7962	6.102	11.83
T_1 (h)	188.5	2.008	1	1
T_2 (s)	28.94	498.1	6.79	3.562
Strategy ($n = 0$)	–	DEJMPS (1)	EPL	EPL
Cost	x	x	45.03	69.9
Fidelity	0.801 759 713 666(30)	0.809(16)	0.8045(41)	0.8053(49)
Rate (Hz)	0.007 09(54)	0.506(40)	1.141(42)	1.33(93)

(c) 800km

	0	1	3	7
α	0.5000	0.5000	0.1816	0.3046
η_f	0.9196	0.9464	0.9983	0.9363
η_{lm}	0.0046	0.9638	0.9675	0.4797
k_{gates}	1	10000	1181	13.67
T_1 (h)	1	78.52	689.9	1.024
T_2 (s)	1	570.4	45201	14.29
Strategy ($n = 0$)	–	SWAP	DEJMPS (1)	EPL
Cost	x	x	x	92.25
Fidelity	0.0(0)	0.015(10)	0.829(11)	0.8181(40)
Rate (Hz)	0.001(0)	0.001 051(37)	0.238(13)	1.125(42)

Table C.10: Optimisation results with single-click entanglement generation, level dependent strategy and optimisation over all gate errors; corresponding to fig. 5.4b. The target values are $F_t = 0.9$ and $R_t = 0.1\,\mathrm{Hz}$.

(a) 200km

	Number of repeaters			
	0	1	3	7
α	0.0454	0.2889	0.2635	0.1837
η_f	0.9441	0.9196	0.9202	0.9360
η_{lm}	0.1668	0.3066	0.2548	0.2711
k_{gates}	1	4.141	7.583	12.13
T_1 (h)	1	1	1	1
T_2 (s)	1	5.445	4.859	5.1
Strategy ($n = 0$)	–	EPL	EPL	EPL
Cost	14.46	32.7	48.72	72.13
Fidelity	0.900 388 021 956(40)	0.9010(21)	0.9014(31)	0.9005(46)
Rate (Hz)	0.1121(56)	1.558(51)	4.78(28)	4.0(2.5)

(b) 400km

	0	1	3	7
α	0.0948	0.3585	0.2574	0.2506
η_f	0.9952	0.9503	0.9672	0.9280
η_{lm}	0.9993	0.5750	0.4956	0.3406
k_{gates}	1907	7.188	4.906	16.09
T_1 (h)	6.732	1	1	1
T_2 (s)	5263	46.41	22.13	9.686
Strategy ($n = 0$)	–	EPL	EPL	EPL
Cost	x	94.74	57.85	97.27
Fidelity	0.900 791 547 569 17(37)	0.9011(42)	0.9014(22)	0.9003(20)
Rate (Hz)	0.003 72(27)	0.1333(65)	1.58(10)	4.42(18)

(c) 800km

	0	1	3	7
α	0.2960	0.3296	0.3447	0.2769
η_f	0.9196	0.9976	0.9542	0.9409
η_{lm}	0.0046	0.9995	0.8164	0.6208
k_{gates}	1	2335	12.11	30.07
T_1 (h)	1	322.6	1.937	1.2
T_2 (s)	1	1.526×10^4	172.3	53.09
Strategy ($n = 0$)	–	SWAP	EPL	EPL
Cost	x	x	263.2	217.3
Fidelity	0.0(0)	0.329(37)	0.9002(24)	0.9185(95)
Rate (Hz)	0.0001(0)	0.000 287(61)	0.1053(38)	0.126(57)

Table C.11: Optimisation parameters with a level dependent strategy, double-click entanglement generation protocol and optimisation over $p_{2,gate}$ only.

Parameter	Baseline	Range
α	–	$[\epsilon, 0.5]$
f_{elem}	0.92	$[0.92, 1-\epsilon]$
η_{lm}	0.0046	$[0.0046, 1-\epsilon]$
$p_{2,gate}$	0.02	$[\epsilon, 0.02]$
T_1	1 h	$[1\,\text{h}, 1\times10^3\,\text{h}]$
T_2	1 s	$[1\,\text{s}, 1\times10^5\,\text{s}]$
Strategy ($n=0$)	–	$[0, 5)$

Table C.12: Optimisation results with double-click entanglement generation, level dependent strategy and optimisation over $p_{2,gate}$ only; corresponding to fig. 5.5a. The target values are $F_t = 0.8$ and $R_t = 1\,\text{Hz}$.

(a) 200km

	Number of repeaters			
	0	1	3	7
f_{elem}	0.9788	0.9683	0.9776	0.9649
η_{lm}	0.9995	0.5484	0.3722	0.4326
$p_{2,gate}$	0.0031	0.0200	0.0153	0.0031
T_1 (h)	152.5	1.06	1	1
T_2 (s)	300.1	3.09	2.749	4.227
Strategy ($n = 0$)	–	SWAP	SWAP	DEJMPS (1)
Cost	x	16.7	14.19	20.41
Fidelity	0.978 761 859 384 0(11)	0.8024(55)	0.8006(20)	0.8001(10)
Rate (Hz)	0.0215(15)	1.021(48)	8.07(42)	18.35(53)

(b) 400km

	0	1	3	7
f_{elem}	0.9200	0.9200	0.9794	0.9774
η_{lm}	0.9427	0.9977	0.6650	0.5866
$p_{2,gate}$	0.0108	0.0200	0.0141	0.0027
T_1 (h)	4.19	169.1	1	1
T_2 (s)	11.14	3815	18.24	10.65
Strategy ($n = 0$)	–	SWAP	SWAP	DEJMPS (1)
Cost	x	x	37.87	32.9
Fidelity	0.919 814 8(21)	0.810 86(74)	0.8004(29)	0.8009(16)
Rate (Hz)	$3.14(25) \times 10^{-7}$	0.009 69(52)	1.017(58)	5.25(17)

(c) 800km

	0	1	3	7
f_{elem}	–	0.9200	0.9463	0.9936
η_{lm}	–	0.0046	0.9275	0.7932
$p_{2,gate}$	–	0.0200	0.0080	0.0059
T_1 (h)	–	1	2.925	1.807
T_2 (s)	–	1	869.7	12.61
Strategy ($n = 0$)	–	EPL	SWAP	SWAP
Cost	–	x	x	54.06
Fidelity	–	0.0(0)	0.0(0)	0.810(28)
Rate (Hz)	–	0.001(0)	0.001(0)	1.121(33)

Table C.13: Optimisation results with double-click entanglement generation, level dependent strategy and optimisation over $p_{2,gate}$ only; corresponding to fig. 5.5b. The target values are $F_t = 0.9$ and $R_t = 0.1\,\text{Hz}$.

(a) 200km

	Number of repeaters			
	0	1	3	7
f_{elem}	0.9789	0.9657	0.9759	0.9994
η_{lm}	0.9977	0.6698	0.5216	0.9057
$p_{2,gate}$	0.0198	0.0036	0.0025	0.0001
T_1 (h)	1.574	1	1	5.283
T_2 (s)	8.371	17.27	10.31	422.9
Strategy ($n = 0$)	–	DEJMPS (1)	DEJMPS (1)	EPL
Cost	x	39.72	31.06	x
Fidelity	0.978 830 121 457(42)	0.9003(28)	0.9003(13)	0.8949(13)
Rate (Hz)	0.0202(15)	0.712(28)	6.03(25)	32.9(1.3)

(b) 400km

	0	1	3	7
f_{elem}	0.9342	0.9620	0.9949	0.9998
η_{lm}	0.8056	0.9978	0.7021	0.7740
$p_{2,gate}$	0.0140	0.0090	0.0032	0.0001
T_1 (h)	1.04	12.75	1	51
T_2 (s)	1.561	2.505×10^4	29.38	781.4
Strategy ($n = 0$)	–	SWAP	SWAP	DEJMPS (1)
Cost	x	x	68.41	x
Fidelity	0.932 880(14)	0.902 08(27)	0.9004(17)	0.895 07(79)
Rate (Hz)	$2.91(20) \times 10^{-7}$	0.010 06(50)	1.221(61)	8.63(27)

(c) 800km

	0	1	3	7
f_{elem}	–	0.9200	0.9850	0.9990
η_{lm}	–	0.0046	0.9985	0.9102
$p_{2,gate}$	–	0.0200	0.0007	0.0000
T_1 (h)	–	1	383	52.14
T_2 (s)	–	1	24238	3043
Strategy ($n = 0$)	–	DEJMPS (3)	DEJMPS (1)	DEJMPS (1)
Cost	–	x	x	x
Fidelity	–	0.0(0)	0.9167(14)	0.894 33(72)
Rate (Hz)	–	0.0001(0)	0.002 69(11)	0.549(19)

Table C.14: Optimisation parameters with a level dependent strategy, double-click entanglement generation protocol and optimisation over all gate errors.

Parameter	Baseline	Range
α	–	$[\epsilon, 0.5]$
f_{elem}	0.92	$[0.92, 1-\epsilon]$
η_{lm}	0.0046	$[0.0046, 1-\epsilon]$
k_{gates}	1	$[1, 10^4]$
T_1	1 h	$[1\,\text{h}, 1\times10^3\,\text{h}]$
T_2	1 s	$[1\,\text{s}, 1\times10^5\,\text{s}]$
Strategy ($n=0$)	–	$[0, 5)$

Table C.15: Optimisation results with double-click entanglement generation, level dependent strategy and optimisation over all gate errors; corresponding to fig. 5.6a. The target values are $F_t = 0.8$ and $R_t = 1\,\text{Hz}$.

(a) 200km

	Number of repeaters			
	0	1	3	7
f_{elem}	0.9621	0.9686	0.9818	0.9563
η_{lm}	0.9934	0.5370	0.3855	0.3811
k_{gates}	8289	1	1	3.625
T_1 (h)	1	1	1	1
T_2 (s)	3.396	3.224	2.513	3.312
Strategy ($n = 0$)	–	SWAP	SWAP	DEJMPS (1)
Cost	x	20.49	18.7	29.88
Fidelity	0.961 826 295 496(69)	0.8038(40)	0.8001(16)	0.8000(18)
Rate (Hz)	0.0202(10)	1.029(36)	8.57(33)	14.15(47)

(b) 400km

	0	1	3	7
f_{elem}	0.9569	0.9516	0.9891	0.9684
η_{lm}	0.9613	0.9907	0.6609	0.5413
k_{gates}	1	2570	1	3.847
T_1 (h)	1.135	86.04	1	1.249
T_2 (s)	1	1101	12.78	8.407
Strategy ($n = 0$)	–	SWAP	SWAP	DEJMPS (1)
Cost	x	x	39.4	40.26
Fidelity	0.954 806(14)	0.8684(18)	0.8009(22)	0.8001(23)
Rate (Hz)	$3.59(18) \times 10^{-7}$	0.010 22(35)	1.039(38)	4.43(15)

(c) 800km

	0	1	3	7
f_{elem}	–	0.9200	0.9842	0.9893
η_{lm}	–	0.0046	0.9961	0.7751
k_{gates}	–	1	3172	5.751
T_1 (h)	–	1	56.3	1
T_2 (s)	–	1	3681	10.47
Strategy ($n = 0$)	–	DEJMPS (1)	SWAP	SWAP
Cost	–	x	x	69.1
Fidelity	–	0.0(0)	0.9018(17)	0.802(28)
Rate (Hz)	–	0.001(0)	0.007 56(29)	1.016(27)

Table C.16: Optimisation results with double-click entanglement generation, level dependent strategy and optimisation over all gate errors; corresponding to fig. 5.6b. The target values are $F_t = 0.9$ and $R_t = 0.1\,\mathrm{Hz}$.

(a) 200km

	Number of repeaters			
	0	1	3	7
f_{elem}	0.9543	0.9844	0.9646	0.9903
η_{lm}	0.9980	0.5740	0.5043	0.3152
k_{gates}	4177	1	6.973	6.669
T_1 (h)	1.352	1	1	1
T_2 (s)	47.8	10.08	5.617	2.312
Strategy ($n = 0$)	–	SWAP	DEJMPS (1)	SWAP
Cost	x	31.06	51.66	49.89
Fidelity	0.954 241 432 670 9(49)	0.9005(17)	0.9011(25)	0.930(18)
Rate (Hz)	0.020 18(99)	1.128(39)	5.32(21)	28.51(76)

(b) 400km

	0	1	3	7
f_{elem}	0.9276	0.9920	0.9909	0.9715
η_{lm}	0.8394	0.9489	0.6613	0.5939
k_{gates}	1	7227	8.07	14.67
T_1 (h)	1.427	733	1	1
T_2 (s)	1.488	3869	19.03	10.28
Strategy ($n = 0$)	–	SWAP	SWAP	DEJMPS (1)
Cost	x	x	82.54	97.83
Fidelity	0.926 141(11)	0.708(34)	0.9024(19)	0.9007(17)
Rate (Hz)	$2.84(15) \times 10^{-7}$	0.000 364(46)	1.061(37)	5.35(16)

(c) 800km

	0	1	3	7
f_{elem}	–	0.9200	0.9999	0.9963
η_{lm}	–	0.0046	0.9965	0.6099
k_{gates}	–	1	10000	15.68
T_1 (h)	–	1	981.5	1
T_2 (s)	–	1	3389	28.84
Strategy ($n = 0$)	–	DEJMPS (3)	SWAP	SWAP
Cost	–	x	x	141.5
Fidelity	–	0.0(0)	0.574(44)	0.920(19)
Rate (Hz)	–	0.0001(0)	0.000 76(21)	0.673(19)